Ultrasound-mediated microbubble drug delivery to the injured lung in Acute Respiratory Distress Syndrome

By

Victoria Mintsopoulos

A thesis submitted in conformity with the requirements
for the degree of Master of Science
Institute of Medical Science
University of Toronto

ABSTRACT

Ultrasound-mediated microbubble drug delivery to the injured lung in Acute Respiratory Distress Syndrome

Victoria Mintsopoulos

Master of Science
Institute of Medical Science
University of Toronto
2019

Acute respiratory distress syndrome (ARDS) is a common diagnosis in ICUs and has a mortality rate approaching 40%. This disease is characterized by a build-up of fluid in the alveolar sacs. Most patients exhibit heterogeneous injury, with relatively normal-appearing areas abutting densely consolidated regions. This heterogeneity makes treatment difficult. Ultrasound-destruction of microbubbles (USMB) has been demonstrated to increase drug uptake by tissues but has never been attempted in the lung. We hypothesized that USMB would only increase drug uptake in edematous lung regions, since air scatters ultrasound waves. USMB increased the deposition and efficacy of low dose gentamicin in the lungs of an *E. coli*-induced ARDS mouse model. Further, we validated the use of USMB drug delivery to the injured lung in a porcine pneumonia model, suggesting feasibility in humans. USMB may therefore allow for targeted delivery of therapies – antibiotics, antivirals, genes – to the injured lung in ARDS.

ACKNOWLEDGEMENTS

“Our deepest fear is not that we are inadequate. Our deepest fear is that we are powerful beyond measure. It is our Light, not our Darkness, that most frightens us.” – Marianne Williamson.

A quote from a powerful speech, delivered by a woman who inspires me. I remember reading this quote at my grade 8 graduation and it has stuck with me ever since.

These two years came with many ups, some downs, and lots of fun in between. My accomplishments could not have been possible without the support from a number of outstanding individuals.

Most importantly, thank you to my supervisor and mentor, Dr. Warren Lee. Your passion and dedication to research and medicine inspires me daily and your support and immediate feedback to your students is unheard of. Thank you for seeing the potential in me. I would not be where I am today if it was not for your perseverance and guidance.

Thank you to my committee members, Dr. Arthur Slutsky and Dr. Tara Moriarty, for all of your support and guidance throughout my MSc journey and for seeing my potential in research.

To the Lee lab - you have all contributed to creating a space that is welcoming and supportive. Each and every one of you has made a huge impact on me.

To Changsen – your smile and kindness made every day in the lab better. Thank you for all of your help with my experiments, especially the HMGB1 mouse breeding, and for all of your stories in between.

To Sia – thank you for welcoming me into the lab as soon as I arrived, for delivering excellent advice, and for imaging all of my slides.

To Rajiv – Markham to the 6ix. From all the inside jokes to all the troubleshooting talk, we have been there for each other since we started. Your presence made me feel a lot less stressed during very stressful times – and I thank you for that.

To Elyse, Erika, Negar, and Misha (+ Jaryd who may as well be part of the Lee lab) – the succeeding MSc students - you have created a space here that feels like a community and a home to me. From Wednesday half price wings, to weekends in the lab, to karaoke – you have made my last year of my MSc so enjoyable. I will miss you guys.

To Judy, Julie, Maz, Yanbo, Sahil, and the rest of the 6th floor - thank you for your entertaining conversations and advice, I sincerely enjoyed the time I've spent with you all.

To those of you who have contributed not only your presence, but also your expertise:

Most importantly, to Dr. Alberto Goffi – who is an exceptional teacher and an all-round wonderful human being. Without your dedication to my project, none of the pig experiments would have been possible. Thank you for taking the time out of your busy schedule to conduct and trouble shoot through this project with me. Your presence always made pig experiment days my favourite learning experiences.

To Michael Kuliszewski for making cationic microbubbles at any time of the day and for all of your help with the Sonos 5500 ultrasound machine.

To Dr. Caterina Di Ciano-Oliveira, thank you for teaching me how to use a microscope and for all of your funny stories that always kept imaging interesting.

To every single one of the St. Michael's vivarium staff, thank you for always being helpful and for running the facility so smoothly. Especially to Danielle and Amanda, your help with the pig experiments was fantastic and we could not have attained our results without your help.

To Dr. Michael Sugiyama for training me in all mouse experimental techniques when I arrived at the lab and for starting and trouble-shooting the USMB project. I was fortunate to have carried on your fantastic work when you graduated.

To Hira Raheel for welcoming me into the lab, assisting me with all my first experiments, and for reminding me to never lose sight of my biggest goals.

To Victoria Tokarz, who although only worked in the lab with me for a couple months ended up being my gym buddy and managed to be the best advice giver throughout my entire MSc.

To those outside of science:

My childhood best friends - Nicole P, Nicole S, and Michelle – from girls' nights, to concerts, to phone calls, thank you for always supporting me through my endeavours and for being there whenever I needed you.

To my partner, Matthew, for being my rock during these two years and for always encouraging me to follow my dreams. Thank you for all your support during my MSc; from attending my research day oral presentations, to coming into the lab with me on the weekends and for driving through rush hour to pick me up. Your love and constant humor keep me going.

Most importantly, a gigantic thank you to my favourite people, my parents. You have always been and continue to be my biggest fans. Your support throughout all of my

schooling is indescribable. Thank you for always believing me and for seeing my potential in everything I do. I hope to make you two proud!

CONTRIBUTIONS

Unless otherwise indicated all experiments were done by Victoria Mintsopoulos

Dr. Michael Sugiyama created F**igure 3.1(A)** and executed experiments in **Figure 3.1(B)**

Danny Ma assisted in lung homogenization, bacterial plating, and CFU counts in **Figure 3.2(A)**

Dr. Alberto Goffi assisted in the experiments of **Figures 4.3, 4.4,** and **Supplemental Figure 5.7**

Misha Ditmans assisted in the experiments of **Figures 4.4** and **Supplemental Figure 5.2**

Dr. Siavash Ghaffari imaged and quantified **Supplemental Figures 5.1** and **5.3**

Negar Khosraviani assisted with the immunofluorescence staining in **Supplemental Figures 5.1** and **5.3**

Dr. Caterina Di Ciano-Oliveira executed the imaging in **Supplemental Figure 5.4**

Changsen Wang executed the experiments in **Supplemental Figure 5.5**

Shawn Veitch conducted the RNA extraction and qPCR analysis in **Supplemental Figure 5.7**

TABLE OF CONTENTS

LIST OF ABBREVIATIONS

ARDS	Acute respiratory distress syndrome
ICU	Intensive care unit
PaO_2/ FiO_2	Arterial oxygen partial pressure/Fractional inspired oxygen
PEEP	Positive end-expiratory pressure (alveolar pressure at the end of expiration)
AECC	American-European Consensus Conference
ALI	Acute lung injury
CT	Computed tomography
HAP	Hospital-acquired pneumonia
VAP	Ventilator-associated pneumonia
DARC	Duffy antigen receptor for chemokines
IL	Interleukin
VILI	Ventilator-induced lung injury
NMBA	Neuromuscular blocking agents
NO	Nitric oxide
iNO	Inhaled nitric oxide
V_A	Alveolar ventilation
Q	Perfusion
V_A/Q	Alveolar ventilation-to-perfusion ratio
BALF	Bronchoalveolar lavage fluid
ICAM-1	Intracellular adhesion molecule-1
LTB4	Leukotriene B4
PMNs	Polymorphonuclear leukocytes
NETs	Neutrophil extracellular traps
PRRs	Pattern recognition receptors
PAMPs	Pathogen-associated molecular patterns
DAMPs	Danger-associated molecular patterns
TLRs	Toll-like receptors
HMGB1	High mobility group box-1
RAGE	Receptor for advanced glycation end products

VEGF	Vascular endothelial growth factor
Tie2	Tyrosine kinase receptor 2
Ang-1,2	Angiopoietin 1,2
miRNA	MicroRNA
SPRED-1	Sprouty-related protein-1
PIK3R2	Phosphoinositide-3-kinase regulator subunit 2
MAP	Mitogen-activated protein
ERK	Extracellular signal–regulated kinase
PI3	Phosphoinositide-3
EPC	Endothelial progenitor cell
JAMs	Junctional adhesion molecules
PKC	Protein kinase C
INFs	Interferons
NF-κB	Nuclear factor-κB
MIP-2	Macrophage inflammatory protein-2
TNF-α	Tumor necrosis factor-α
FOXO1	Forkhead Box O1
ZO-1	Zonula occludens-1
HUVECs	Human umbilical vein endothelial cells
oxLDL	Oxidized low-density lipoprotein
HDMEC	Human dermal microvascular endothelial cells
PAF	Platelet-activating factor
S1P	Sphingosine-1-phosphate
NOS	Nitric oxide synthase
eNO	Endothelial nitric oxide synthase
Rap1	Ras-related protein 1
MAC-1	Macrophage-1 antigen
PECAM	Platelet and endothelial cell adhesion molecule
PSGL-1	P-selectin glycoprotein ligand-1
ESL-1	E-selectin ligand-1
HO-1	Heme oxygenase-1

MRI	Magnetic resonance imaging
FDA	Food and Drug Administration
GFP	Green fluorescent protein
DNA	Deoxyribonucleic acid
RNA	Ribonucleic acid
PEG	Polyethylene glycol
CBLuc	Click beetle luciferase
CFUs	Colony-forming units
IT	intratracheally
EBD	Evan's blue dye
PFUs	Plaque-forming units
LB	Lysogeny broth

LIST OF FIGURES

Supplemental Figure 5.7. USMB increases the deposition of miRNA-126 in the lungs of influenza-infected mice**.**

CHAPTER 1: LITERATURE REVIEW

1.1 ARDS

Acute respiratory distress syndrome (ARDS) is a common diagnosis in the intensive care unit (ICU). It is characterized by a build-up of fluid in the alveolar sacs, resulting in non-cardiogenic pulmonary edema, hypoxemia, and a loss of lung compliance. A number of primary insults that either induce direct lung injury or indirect lung injury can lead to ARDS however, the most common include bacterial or viral pneumonia and sepsis. The pathophysiology of the disease involves numerous factors and pathways. In general, there is increased permeability of the pulmonary endothelium and disruption of the alveolar epithelial junctional proteins. An inflammatory response is present which induces pro-inflammatory cytokine production and recruits neutrophils and immune cells to the lung. This excessive fluid and inflammation results in impaired gas exchange and decreased respiratory compliance, demanding the need for mechanical ventilation.

The incidence of ARDS differs quite drastically between the USA and Europe. For example, in 1972, the National Heart and Lung Institute indicated an incidence of 75 cases/100 000 population in the USA (*National Heart and Lung Institutes: Respiratory diseases: task force on problems, research approaches, needs.*, 1972), whereas in Europe most studies indicated 5-8 cases/100 000 individuals (Villar et al., 2014). This inconsistency could be due to a number of factors such as differences in demographics, culture, and healthcare systems and in diagnosing ARDS. Despite the difference in incidence, the mortality rate for ARDS is typically high at 40%, with about 75% of patients exhibiting moderate or severe cases of the syndrome (Villar et al., 2014). Currently there are no effective treatments for ARDS. Patients with ARDS are typically managed in the ICU by the application of mechanical ventilation, prone positioning, and occasionally the administration of other agents such as anti-inflammatories, diuretics, and bronchodilators. Although a number of potential therapeutics have been tested, none have consistently improved mortality in ARDS patients in clinic. One of the main reasons why most therapies lack significant benefit is due to the heterogeneity in the presentation and progression of ARDS among patients. Another factor to consider is the heterogeneity in an ARDS lung, with injured and edematous regions interspersed

among healthy and aerated areas (Maundern et al., 1986). It is challenging for therapies to direct themselves to these injured areas, even if they are inhaled, as they preferentially travel to uninjured and non-edematous lung regions. A delivery system that targets therapies specifically to the injured lung regions may lead to improved clinical outcomes and mortality in ARDS patients.

1.1.1 Historical and Current Definitions of ARDS

ARDS was first identified in 1821, as 'idiopathic pulmonary edema' (Sakula, 1981) however, the first systematic definition of this disease arose in 1967, by Ashbaugh and his colleagues (Ashbaugh et al., 1967). These first criteria focused on hypoxia, pulmonary edema, and responses to mechanical ventilation.

In 1988, John Murray developed a lung injury score known as the Murray Score, which served as a definition for ARDS (Murray et al., 1988). The Murray Score encompassed 4 criteria each which were given a score of 0 to 4. The first criterion included the chest roentgenogram, where each quadrant containing alveolar consolidation contributed one point to the score. The other principles included the classification of hypoxemia based the ratio of arterial oxygen partial pressure (PaO_2) to fractional inspired oxygen (FiO_2), the level of positive end-expiratory pressure (PEEP) under ventilation, and the degree of lung compliance. The summed value was divided by the number of criteria considered to obtain the final Murray Score. A score of 0 indicated no lung injury, values between 1-2.5 suggested mild to moderate lung injury, and a score higher than 2.5 determined the presence of ARDS (Murray et al., 1988). Further, Murray and his team acknowledged epithelial and endothelial lung damage as a potential cause of ARDS (Murray et al., 1988). This definition of ARDS was useful because it considered reliable indicators of lung injury such as PEEP and lung compliance however, it could not distinguish ARDS from cardiac pulmonary edema (Raghavendran & Napolitano, 2011).

Finally, in 1994, a unanimous definition of ARDS was established by the American-European Consensus Conference (AECC) (Bernard et al., 1994). ARDS was defined by bilateral infiltrates present on a chest radiograph, no signs of cardiogenic edema, and a PaO_2/FiO_2 less than 200 mmHg (Bernard et al., 1994). The AECC also

termed acute lung injury (ALI) as having similar features to ARDS but with a PaO_2/FiO_2 ratio between 200 and 300 mmHg (Bernard et al., 1994). The AEEC definition was widely accepted however, it did generate confusion among physicians due to a number of limitations (Amin & Amanda, 2017). Firstly, the term 'acute' was not clearly defined. The AECC definition also lacked the ability to distinguish between ARDS and pulmonary hydrostatic edema due to similar observations in chest x-rays and gas exchange (Amin & Amanda, 2017). Further, although PEEP was recognized to affect oxygenation, it was not included into the definition because of irregularities in patient responses (Costa & Amato, 2013). This indicates that PaO_2/FiO_2 will change as the level of PEEP changes. For example, a patient who has a PaO_2/FiO_2 ratio of 200 mmHg or less may not attain the same range at an increased PEEP and therefore may no longer meet the AECC criteria for ARDS diagnosis (Villar et al., 1999). These issues were addressed and updated in the current definition of ARDS known as the Berlin Definition.

In 2011, the European Society of Intensive Care Medicine identified a panel of diverse individuals who were regarded as experts in the field of ARDS. The Berlin definition that they established proved to be feasible, reliable, and valid by the assessment of a large cohort of patients with the syndrome (defined by the 1994 definition). The Berlin definition has four main criteria for ARDS diagnosis which are described below (ARDS Definition Task Force et al., 2012).

1. The onset of ARDS should be within 1 week of a known insult or worsening respiratory symptoms (Gajic et al., 2011).
2. Chest imaging (radiography or computed tomography (CT) scans) should demonstrate bilateral opacities. This should not be entirely the result of lung effusions, lung collapses, or masses (Meade et al., 2000; Rubenfeld et al., 1999).
3. Patients will have respiratory failure that cannot be fully explained by cardiac failure or fluid overload (ARDS Definition Task Force et al., 2012).
4. Three sub-groups were established based on the severity of the disease which is determined by the level of oxygenation (ARDS Definition Task Force et al., 2012). This is measured by the ratio of PaO_2/FiO_2 at a minimum PEEP of 5 cm of H_2O (Rice et al., 2007). This PEEP value was chosen because it is the minimum

value required to diagnose ARDS and it excludes atelectasis-induced hypoxemia (Amin & Amanda, 2017).

a. Mild: $200 < PaO_2/FiO_2 \leq 300$
b. Moderate: $100 < PaO_2/FiO_2 \leq 200$
c. Severe: $100 \leq PaO_2/FiO_2$

The Berlin definition of ARDS improved on the previous AECC definition by incorporating the timing of onset, a minimum PEEP value, an expanded imaging criterion, and classifications of ARDS severity (Amin & Amanda, 2017). The Berlin definition has supported clinicians in appropriately diagnosing patients with ARDS and recognizing suitable management and treatment options based on the severity of the disease. This systematic criterion is expected to be edited and adjusted in the future as breakthroughs in research and advances in practice become available.

1.1.2 Clinical Causes of and Risk Factors for ARDS

ARDS is a complicated syndrome. It is associated with a list of clinical causes and its development and outcomes can be influenced by a number of potential risk factors. These numerous considerations may partially explain why the appearance and progression of ARDS is often heterogenous among patients that fit the Berlin definition. Attention to the primary cause and other individual risk factors must be considered to ensure the best management and care of the patient.

The clinical disorders often correlated to ARDS development are typically categorized as a direct lung insult or an indirect lung insult. Overall, the most common cause of ARDS is direct lung injury from bacterial or viral induced pneumonia (Piantadosi & Schwartz, 2004). This can either be classified as community-acquired pneumonia or nosocomial pneumonia, the latter of which is further denoted as hospital-acquired pneumonia (HAP) or ventilator-associated pneumonia (VAP) (Kalil et al., 2016). Other less common direct lung insults that may lead to ARDS include drowning, aspiration, injury from inhalation, and pulmonary vasculitis (Ferguson et al., 2012). The second most common cause of ARDS is sepsis which can be associated with pneumonia, however it may also result from non-pulmonary infections or conditions

(Matthay & Zemans, 2011). Other non-direct lung injury causes can include trauma, burns, drug overdose, pancreatitis, or blood transfusions (Ferguson et al., 2012).

An international, multicenter study involving 459 ICUs across 50 countries evaluated the incidence and outcomes in ARDS patients fulfilling the ARDS Berlin definition. This 4-week study, known as the LUNG-SAFE study, found 10.4% of ICU patients met the ARDS criteria, and more than half of them developed ARDS from pneumonia (59%) (Bellani et al., 2016). Other primary causes included non-pulmonary sepsis (16%), gastric aspiration (14%), non-cardiogenic shock (8%), and trauma and transfusions (< 5%) (Bellani et al., 2016).

In addition to the various clinical disorders, there are a number of lifestyle risk factors that associate with ARDS. Factors such as environmental pollution (Ware et al., 2016), cigarette smoking (Calfee et al., 2011), chronic alcohol abuse (Thakur et al., 2009), biological sex (Lemos-Filho et al., 2013; Moss & Mannino, 2002; Heffernan et al., 2011), and race (Kangelaris et al., 2012) may influence the prevalence and outcomes of ARDS. In terms of biological sex, the literature seems to be inconsistent. In one study it was demonstrated that men were more likely to develop ALI ($p<0.001$) and stayed in the ICU for a longer duration ($p=0.002$) compared to women, however both sexes had similar rates of mortality (Lemos-Filho et al., 2013). In another study, rates of death from ARDS were doubled in men compared to women ($p<0.05$) (Moss & Mannino, 2002). In contrast, Heffernan and colleagues found that females were significantly more likely to develop ARDS than males, however there were no mortality differences (Heffernan et al., 2011). These findings suggest more research must be done to confirm the effect of biological sex on ARDS susceptibility and outcome.

Further, African Americans with ARDS were found to have a higher chance of death compared to white individuals with ARDS. This was explained by a 17% increase in mortality in patients with a polymorphism in the duffy antigen receptor for chemokines (DARC) gene promoter leading to DARC deficiency, which is present almost exclusively in African Americans (Kangelaris et al., 2012). DARC has a role in binding pro-inflammatory cytokines when they are high and releasing them when they are low. It has been suggested that this increase in mortality from ARDS in the DARC null

population is due to increased plasma levels of interleukin (IL)-8 (Kangelaris et al., 2012).

Lifestyle factors that one may be able to control are also of interest. Focusing on environmental pollution, a study observing 1558 critically ill patients who lived less than 50 km away from an air quality monitor and had an ARDS clinical risk factor were monitored. The incidence of ARDS increased with increasing ozone exposure with 42% incidence in the highest ozone exposure quartile (Ware et al., 2016). This was also particularly increased in patients with trauma as their clinical risk factor and in current smoking adults (Ware et al., 2016). Another study found that higher levels of cotinine, a metabolite of nicotine, were independently associated with the development of ALI following severe trauma, with moderate to severe passive smoking having a similar association as active smoking (Calfee et al., 2011). In regard to alcohol consumption, a population-based study observed that 13% of patients with significant alcohol consumption history developed ARDS compared to only 5% of patients who consumed less than 14 drinks/week (Thakur et al., 2009). Thus, avoiding passive and active smoking, excessive alcohol consumption, and living in high ozone exposed areas may decrease one's risk of developing ARDS and/or mortality from ARDS.

ARDS by definition is a syndrome not a disease. This syndrome can be induced by a range of various insults that can either be classified as a direct or non-direct lung insult, and the severity and outcome of the disease can be influenced by a number of different risk factors. Furthering the complexity, diffuse lung injury has a heterogenous effect on the lung and its extent of injury can vary between patients. Considering the variance in diagnosis, clinicians must be wise and resourceful in their therapeutic approach.

1.1.3 Treatments for ARDS

There are currently no effective treatments for ARDS, which is one of the reasons why the mortality rate is high. Therapeutics used today are mainly supportive and include both pharmacological and non-pharmacological interventions.

Mechanical Ventilation

One of the most common supportive care methods in ARDS patients is mechanical ventilation. Mechanical ventilation is a process that ensures sufficient oxygenation and gas exchange and can be performed either non-invasively or invasively. The non-invasive route reduces the effort required for breathing without heavily sedating the patient (Umbrello et al., 2016), whereas invasive mechanical ventilation will reduce respiratory muscle activity while providing adequate gas exchange by both increasing PaO_2 and removing CO_2 (Gattinoni, 2016). This increase in oxygenation is due to increasing FiO_2 and opening collapsed pulmonary units. The issue in regard to mechanical ventilation is the risk of ventilator-induced lung injury (VILI) as well as the potential of pulmonary units collapsing during expiration (Pelosi et al., 2001). In order to avoid these concerns, mechanical ventilation must be appropriately tailored to each patient.

PEEP and Recruitment Maneuvers

In order to appropriately gear mechanical ventilation to each ARDS patient, a number of factors must be considered. One of these is PEEP, which is the pressure in the lungs following expiration. Increasing PEEP may be beneficial in avoiding alveolar opening and closing, recruiting lung units, and overall improving oxygenation. However, PEEP that is too high can cause lung over-distension. PEEP is often accompanied by a recruitment maneuver, which is a sustained increase in pressure that will open alveoli that have been collapsed. This would be followed by the application of PEEP to maintain the opening of these lung units. Numerous studies have aimed to identify a level of PEEP that leads to better outcomes in ARDS patients. A group performed a meta-analysis on clinical trials that compared the use of higher PEEP levels versus lower PEEP levels in ARDS patients (Walkey et al., 2017), hypothesizing that higher PEEP would lead to improved outcomes as theoretically it should result in enhance alveolar recruitment. However, in 6 clinical trials there was no difference in mortality between the groups, although the higher PEEP group did demonstrate improved oxygenation (Walkey et al., 2017). Considering the heterogeneity of ARDS lungs and the variability between patients, it was proposed to adjust the PEEP to each patient.

This process was termed PEEP titration, where the PEEP level would start high and then would be incrementally decreased by 2 cm H_2O. At each step, lung recruitment would be measured typically by lung compliance or oxygenation (Hess & Faarc, 2015). Once lung recruitment is not maintained, the level of PEEP is adjusted 2 cm H_2O higher. A study determined if a lung recruitment maneuver plus titration of PEEP would benefit patients with moderate to severe ARDS compared to the conventional low-PEEP application (Investigators et al., 2017). About 1000 patients were recruited in this multi-center study. Patients who received titrated PEEP and lung recruitment had a significantly increased 28-day and 6-month mortality compared to the control group, potentially as a result of increased barotrauma from a higher PEEP (Investigators et al., 2017). Post hoc analysis of randomized clinical trials have suggested to alter the PEEP based on the severity of ARDS. These findings propose mild, moderate, and severe ARDS patients should be put on PEEP levels of 5-10 cm H_2O, 10-15 cm H_2O, and 15-20 cm H_2O, respectively (Gattinoni et al.i, 2015).

Tidal Volume

In addition to PEEP, the tidal volume must also be considered when mechanically ventilating patients. Applying high pressures and volumes has the potential to induce VILI. Especially with the heterogeneity of the ARDS lung, it is not uncommon to see hyperinflation in normal areas of the lung. The use of high tidal volumes in mechanically ventilated patients was associated with increased risk of ARDS development and mortality in ARDS patients (Acute Respiratory Distress Syndrome Network et al., 2000). Patients with ARDS who were ventilated with 6mL/kg tidal volume had significantly reduced mortality rates ($p=0.007$) and increased days without ventilation over 28-days ($p=0.007$) compared to ARDS patients given a traditional higher tidal volume of 12mL/kg (Acute Respiratory Distress Syndrome Network et al., 2000). The use of low tidal volumes in mechanical ventilation has become routine practice in the management of ARDS patients.

Prone Positioning

Another non-pharmacological intervention that is important to consider in ARDS management is prone positioning. This stance allows for a more uniform distribution of stress on the body, is more efficient at recruiting dorsal regions of the lung, and has shown to protect the lung from VILI (Gattinoni et al., 2013). In supine position, the dorsal regions of the lung are poorly expanded resulting in inadequate oxygenation. This is due to both gravitational forces as well as pressure from the heart and abdominal organs. In contrast, prone positioning results in less compliance of the anterior chest wall, allows a greater expansion of the dependent dorsal regions of the lung, and reduces gravitational-induced pressure on the lungs. In addition, prone positioning in ARDS patients has demonstrated more homogenous inflation of dependent lung regions (Koulouras et al., 2016). A multi-center randomized control trial in 2001, compared the effect of prone positioning versus the conventional supine position in over 300 patients with ARDS or ALI (Gattinoni et al., 2001). Patients in the prone position group were kept in a prone position for six or more hours per day for 10 consecutive days. Although the prone position group demonstrated significantly improved oxygenation, there was no difference in mortality between the two groups (Gattinoni et al., 2001). Further, the study indicated that the number of new or worsening pressure sores per patient was higher in the prone group however, the number of days with pressure sores per patient was not different between the two groups (Gattinoni et al., 2001). A few years later, another group compared prone versus supine positioning in approximately 800 patients with acute respiratory failure (Guérin et al., 2004). In this study, patients in the treatment group were placed in a prone position for at least 8 hours per day for 28 days. Similar to the previous study, there was no difference in mortality between groups however, the prone positioned group did have significantly improved PaO_2/FiO_2 compared to the supine group (Guérin et al., 2004). Considering these trials failed to show a mortality benefit from prone positioning, a study in 2013 aimed to evaluate this strategy again in 466 patients with specifically severe ARDS where about half were placed in a prone position for at least 16 hours a day and the other half remained in supine position (Guérin et al., 2013). Researchers found the prone position group had a significant reduction in 28-day and 90-day mortality

compared to the supine position group (Guérin et al., 2013). Further, the only complication that differed between groups was a higher incidence of cardiac arrests in the supine group. Therefore, prone positioning has become a standard management strategy in patients with severe ARDS.

Pharmacological Therapeutics

Pharmacological interventions, including those administered intranasally, orally, and systemically, have also been pursued. Many of these agents attempt to dampen the overbearing inflammatory response during ARDS however, many have been found to be ineffective and their administration remains controversial in ARDS patients.

For example, glucocorticoids have been proposed to be beneficial in ARDS if dosed and timed appropriately and combined with other common management strategies like mechanical ventilation (Marik et al., 2011). A number of studies and reviews have aimed to determine the best practices for glucocorticoid use in ARDS. A meta-analysis showed that prolonged administration of low-dose methylprednisolone treatment (Days 1-28) in ARDS patients increased the duration without mechanical ventilation ($p<0.001$), reduced days in the ICU ($p<0.001$) and hospital ($p<0.001$) and reduced the development of shock ($p<0.001$) and infections ($p<0.001$) (Meduri et al., 2018). Another clinical study compared the effect of methylprednisolone discontinuation following extubation. They found patients who were discontinued off methylprednisolone were more likely to require mechanical ventilation and had a higher risk of mortality compared to patients discontinued from placebo treatment (Meduri et al., 2018). Another meta-analysis reviewed 8 randomized control trials and 10 cohort studies that compared the use of corticosteroids, all of which demonstrated no significant difference in ICU mortality and 60-day mortality (Ruan et al., 2014). However, in a subgroup analysis the use of corticosteroids in influenza-induced ARDS was shown to increase mortality in 3 cohort studies (Ruan et al., 2014). A study in the New England Journal of Medicine observed the effects of corticosteroid administration to patients with persistent ARDS. They took 180 patients who were diagnosed with ARDS for at least 7 days and provided methylprednisolone or placebo treatment. There was no difference in 60-day or 180-day mortality between groups however, the treatment group experienced

increased days without ventilation and shock (Steinberg et al., 2006). Despite the physiological improvements, since there was no mortality benefit the researchers discouraged the use of corticosteroids in ARDS patients (Steinberg et al., 2006). Due to this controversy, a team of critical care experts aimed to develop a consensus for the use of corticosteroids in ARDS management. This group recommended that a moderate dose of glucocorticoids should be considered when managing patients with early and severe ARDS and administered before Day 14 in patients with persistent ARDS (Marik et al., 2008). Experts made this decision based on 5 randomized control trials. Although these studies differed in dose and treatment duration, they all revealed that glucocorticoid treatment significantly improved PaO_2/FiO_2, reduced mechanical ventilation duration, and decreased days in the ICU, and 4 out of the 5 studies demonstrated a reduction in mortality (Marik et al., 2008).

Neuromuscular blocking agents (NMBA) are often used in ARDS to abolish spontaneous patient breathing during ventilation, an incident that could worsen lung damage. A meta-analysis showed that use of NMBA in the early phase of ARDS improves 28-day survival, increases ventilator free days, and improves PaO_2/FiO_2 (Serpa Neto et al., 2012). However, later findings suggested that spontaneous breathing may be beneficial in mild to moderate cases of ARDS. Thus, early use of NMBAs is suggested only in patients with severe ARDS (Umbrello et al., 2016).

Considering ARDS is primarily a lung disease, inhaled therapeutics, specifically bronchodilators and pulmonary vasodilators, were proposed. Nitric oxide (NO) is an endogenous compound that can also be administered through the inhaled route where is can pass alveolar barriers to promote smooth muscle relaxation and vascular dilation (Griffiths & Evans, 2005). A systematic review indicated that inhaled NO (iNO) improved arterial oxygenation in patients with ARDS but did not have an effect on the mortality rate (Monsalve-Naharro et al., 2017). Thus, iNO treatment is not recommended, except for patients with severe and persistent hypoxemia (Monsalve-Naharro et al., 2017). Additionally, β2-agonists which are bronchodilators and are also involved in alveolar fluid clearance (Artigas et al., 2017), were tested as an inhaled therapy for ARDS patients in two clinical trials. In one multi-center randomized control trial, patients who were given aerosolized albuterol, a β2-agonist, spent more days in the ICU, and

although not significant, had less ventilator free days compared to patients that were given placebo (National Heart, Lung, and Blood Institute Acute Respiratory Distress Syndrome (ARDS) Clinical Trials Network et al., 2011). Despite worse clinical outcomes, there was no difference in mortality (National Heart, Lung, and Blood Institute Acute Respiratory Distress Syndrome (ARDS) Clinical Trials Network et al., 2011). In another clinical study the intravenous administration of the β2-agonist, salbutamol, increased 28-day mortality in ARDS and reduced ventilator-free days and organ failure-free days (Gao Smith et al., 2012). In addition, the intravenous injection of salbutamol was associated with tachycardia, arrhythmias, and lactic acidosis (Gao Smith et al., 2012). This study confirmed that β2-agonist should not be intravenously administered to patients with ARDS.

In conclusion, there are currently no universally effective treatments for ARDS. The proposed methods described above (e.g. lung protective ventilation, neuromuscular blockade) attempt to limit VILI and are not always successful. In order to offer the most effective resolution, treatments or management methods are often individualized to suit each patient's needs. Additional to the complexity of ARDS, one main reason why many therapies are ineffective is due to the nature of the lung in this disease. CT scans have identified that the lungs of patients with ARDS are heterogenous, revealing areas with dense-consolidation, indicating edema and fluid buildup, interspersed among regions that look relatively normal **(Figure 1.1)** (Maunder et al., 1986). This introduces a challenge when treating or managing the lung. For example, mechanical ventilation will preferentially inflate normal regions of the lung where it can cause over distension and lung damage (Murray & Nadel's Textbook of Respiratory Medicine, 2-Volume Set, 6th Edition, US Elsevier Health Bookshop, 2006). Inhaled drugs will also direct themselves to the healthy regions of the lung instead of the injured areas, potentially causing adverse effects (Sugiyama et al., 2018). Further, orally or systemically administered therapeutics are likely to cause off-target effects as they will interact with all tissues and organs in the body (Gao Smith et al., 2012). Therefore, a drug delivery system that targets treatments specifically to the injured lung must be considered.

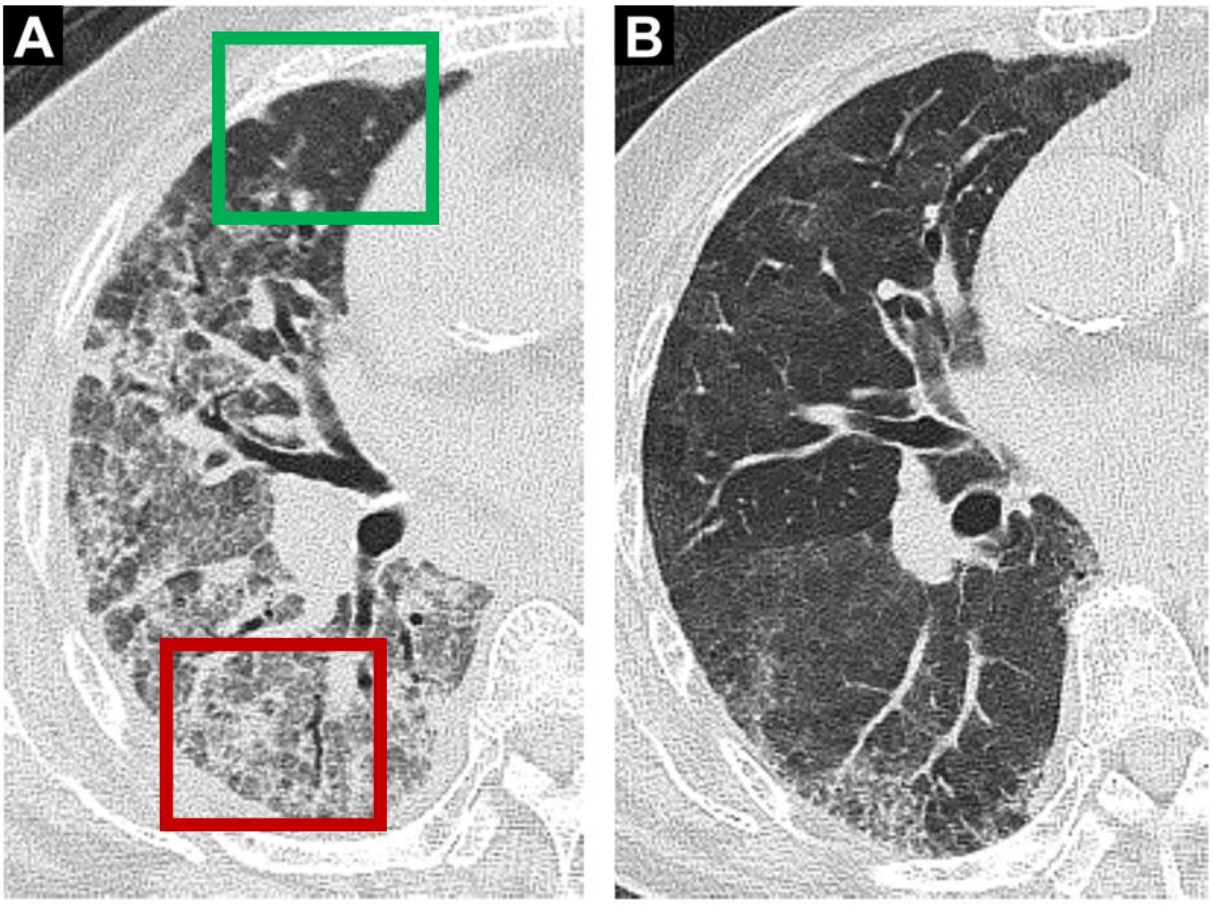

Figure 1.1. Lung computed tomography scan of a patient with ARDS (A) verses a healthy individual (B). The CT scan of the ARDS patient (A) indicates that the lung is heterogenous; with edematous or consolidated areas (outlined in red) interspersed among regions that appear healthy and aerated (outlined in green). Figure adapted with permission from Anan K. *et al BMJ Open* 2017.

1.1.3.1 Pneumonia-induced ARDS

As previously mentioned, the most common cause of ARDS is primary pneumonia. This disease can be induced by a number of microorganisms although the most common are bacteria or viruses (Bellani et al., 2016). In 2013, pneumonia was the second leading cause of death worldwide. Although everyone can contract this disease, the most susceptible include children under the age of 5 and adults over 65 years old, as well as individuals who are immunocompromised. For example, in 2015, pneumonia accounted for 16% of deaths in children under the age of 5, making it the leading cause

of death in that age group. Considering pneumonia is the primary cause of ARDS, it is essential to investigate both viral and bacterial-pneumonia induced ARDS development and management.

Community-acquired pneumonia involves a number of symptoms such as a fever, cough and fatigue, and also encompasses a lower respiratory tract infection which is confirmed by the presence of infiltrates on a chest radiograph. The most common pathogen to induce community-acquired pneumonia is *Streptococcus pneumoniae*, whereas viruses, mainly influenza, induce a third of pneumonia cases (Prina et al., 2015). The pathogen however, is only detected in half of pneumonia cases (Uyeki et al., 2018), typically in at risk populations such as young children, the immunosuppressed, those with severe pneumonia, or after a failed treatment (Prina et al., 2015). Molecular testing for respiratory pathogens reduces the failure of treatments and the overuse of antibiotics, which can contribute to antibiotic resistance (Prina et al., 2015). The treatment provided is mostly dependent on the specific pathogen however, individual risk factors must also be taken into account. Additionally, it is important to note that recommended treatment regimens differ world-wide. In North America, most patients with bacterial-induced pneumonia are administered a β-lactam with a macrolide. However, monotherapy with a β-lacatam in hospitalized patients with moderate to severe community-acquired pneumonia had similar outcomes to dual therapy of β-lacatam with macrolide (Garin et al., 2014). Despite this finding, the dual approach is still recommended.

Nosocomial pneumonia can occur in patients who have been hospitalized for 48 hours or longer. The infection is further designated into either VAP, which can occur in patients receiving mechanical ventilation for at least 48 hours, or HAP in patients that do not undergo mechanical ventilation. Further, late nosocomial pneumonia, which occurs 5 days after admission, typically involves multi-drug resistant pathogens, resulting in a case that is more dangerous and difficult to treat. Despite numerous antibiotics and combination therapies, gram-negative bacteria are especially problematic because of their high resistance to antibiotics. Over the years of antibiotic usage, many bacteria have developed resistance to certain antibiotic classes through mechanisms such as altering the drug binding site, constructing efflux pumps, and producing enzymes that

can alter or bind to the antibiotic (Munita & Arias, 2016). For example, β-lactams can be degraded by the presence of β-lactamases, which are produced by resistant bacteria (Munita & Arias, 2016). Such resistance led to the development of broad-spectrum antibiotics. In late nosocomial pneumonia, it is recommended to administer broad-spectrum antibiotics or a combination of them in high risk patients (Frantzeskaki & Orfanos, 2018) to avoid inadequate therapy due to drug-resistance. Interestingly, most gram-negative lung pathogens remain sensitive to aminoglycosides. However, clinical infectious disease guidelines suggest avoiding the use of aminoglycosides, in gram-negative induced pneumonia or ARDS when other agents are available (Kalil et al., 2016) due to poor lung penetration; furthermore their use increases the risk of nephrotoxicity and ototoxicity even at therapeutic doses (Kalil et al., 2016). If aminoglycosides could be specifically targeted to the injured lung in patients with gram-negative pneumonia or ARDS these two issues could be tackled. First, there would be higher penetration of the drug to the target regions, thus increasing lung deposition and efficacy. Secondly, considering the drug is being targeted to the region of interest, a smaller therapeutic dose would be required. Thus, a lower dose and increased lung deposition would result in less drug available systemically and decrease the potential of adverse effects and toxicities.

In addition to bacterial-induced pneumonia, influenza viruses can cause major seasonal outbreaks and pandemics. For example, in the 2017-2018 flu season, approximately 80,000 individuals in the United States died from influenza infection (*Estimated Influenza Illnesses, Medical visits, Hospitalizations, and Deaths in the United States — 2017–2018 influenza season* | *CDC*). Influenza-induced pneumonia can develop into a more serious respiratory infection such as ALI or ARDS, which is a challenge to treat due to the lack of effective anti-viral therapies and the difficulty of targeting drugs to the injured lung areas.

Influenza A and B typically cause seasonal outbreaks, whereas influenza C induces less serious infections. Influenza viruses contain haemagglutinin (HA) and neuraminidase (NA) membrane proteins, and influenza A subtypes are determined by the antigenicity of these proteins. HA proteins binds to sialic acid receptors on host cells, which allows the virus to enter the cell. Human influenza viruses typically bind α-

2,6-linked sialosaccharides and often induce upper respiratory tract infections, whereas avian influenza viruses prefer binding to α-2,3-linked sialosaccharides and induce lower respiratory infections, which are generally more dangerous. The NA proteins release the virus from the cell via cleaving the sialic acid receptor from HA. Then, the M2 viral protein assists in the replication and spread of the virus. As viral particles increase, the epithelial and endothelial lung barriers become damaged and the progression of ARDS is initiated.

For patients with severe influenza infection, the standard dose of oseltamivir, 75 mg, is given twice daily for 5 days or longer if symptoms progress, with an antibiotic (Choi et al., 2014). Unlike bacteria-pneumonia, combination anti-viral therapy is not recommended in these patients. If this infection develops into ARDS, antiviral therapy is usually no longer effective. In ARDS, the lung barrier is damaged, there is extensive pulmonary edema, and the patient is hypoxic. Antiviral therapy cannot effectively treat these serious conditions thus supportive management strategies like mechanical ventilation are provided. Further, the heterogeneity of the ARDS lung imposes a challenge for antivirals and other potential therapeutics as they have difficulty penetrating the injured areas of the lung. Similar to aminoglycosides, a drug delivery system that could target specifically the injured lung in ARDS or pneumonia patients could improve the efficacy of antivirals and other therapies in influenza-induced ARDS.

1.1.4 Pathophysiology of ARDS

ARDS is a complicated syndrome that is often heterogenous in appearance between patients. There are a number of different factors that influence the pathophysiology of ARDS and its resolution **(Figure 1.2)**. The primary element to consider is the reduced capacity of gas exchange in patients with ARDS due to abnormalities in either the ventilation or the perfusion of alveoli, which is typically the result of pulmonary edema and excessive inflammation. Various external and endogenous factors induce an inflammatory response that involves cytokine and chemokine production, neutrophil recruitment, cell junctional remodelling, cell death, and stimulation of downstream pathways. The mechanisms contributing to the pathophysiology of ARDS will be described in detail below.

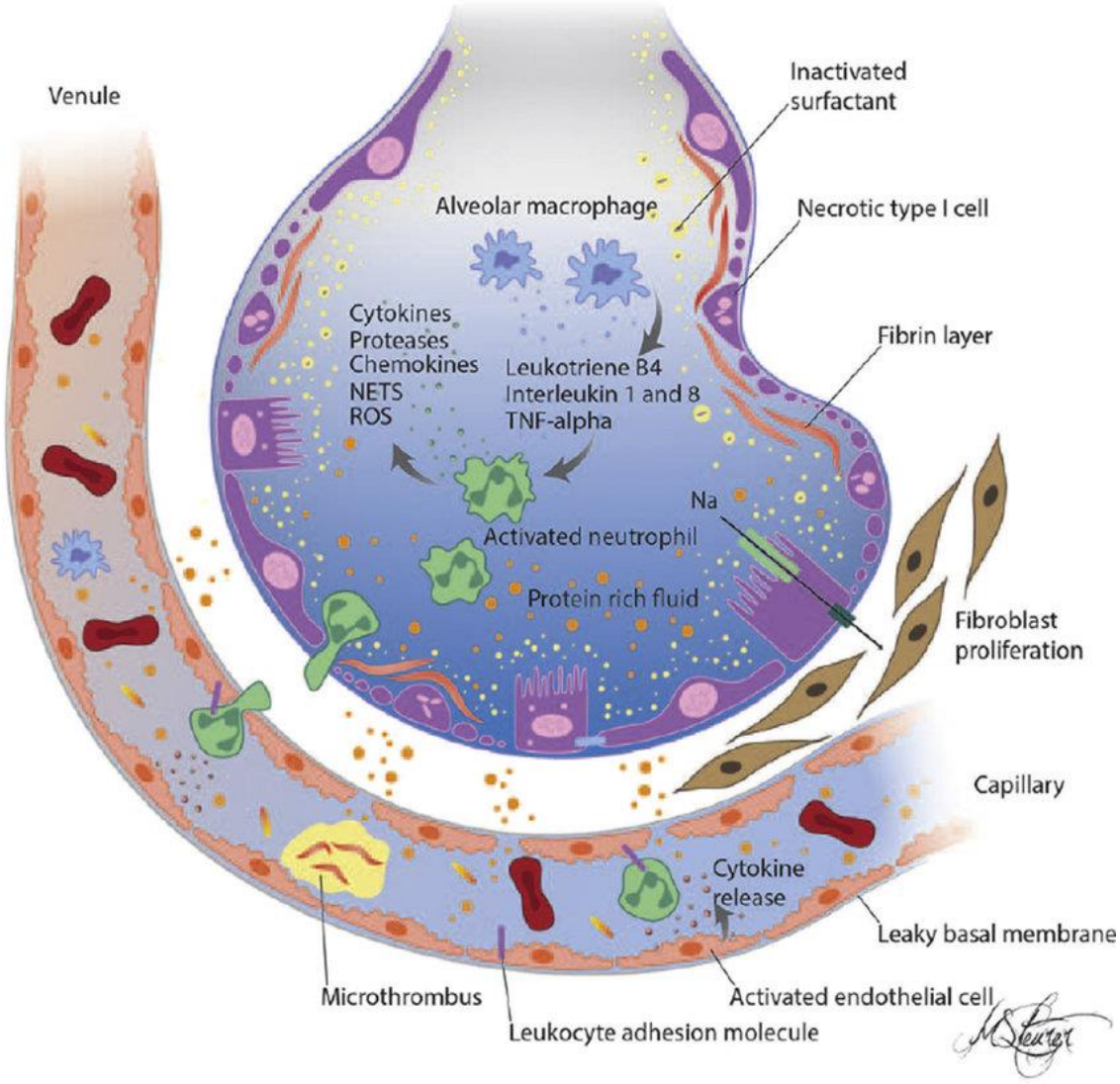

Figure 1.2. Pathophysiology of ARDS. The pathophysiology of ARDS involves the interplay of numerous immune cells such as macrophages and neutrophils and their release and response to various cytokines, chemokines, and ROS. These inflammatory factors increase the lung endothelial and epithelial barrier, allowing protein-rich fluid to escape the vessels and invade the lung. Increased lung edema will propagate additional inflammation and lead to poor gas exchange in ARDS patients. Figure adapted with permission from Heidemann S. *et al Pediatr Clin N Am*, 2017(Heidemann et al., 2017).

Gas Exchange

One of the most crucial abnormalities in ARDS involves gas exchange. Interestingly, the impairment of gas diffusion between alveoli and blood is not the main cause. Instead this flaw in gas exchange in ARDS is the result of alterations in alveolar ventilation (V_A) and perfusion (Q) (Henderson et al., 2017). The alveolar ventilation-to-perfusion ratio, V_A/Q, indicates that an optimal ratio will generate ideal gas exchange. Alterations in this ratio can induce effects often observed in ARDS. A low V_A/Q ratio, indicating good perfusion but insufficient ventilation, will typically lead to hypoxemia (Henderson et al., 2017); a high V_A/Q ratio induces hypercapnia as a result of efficient ventilation but inadequate perfusion (Henderson et al., 2017). In extreme cases there is no ventilation of alveoli, thus V_A/Q equals 0. Typically, pulmonary blood flow includes a component that is called shunt, which includes regions of flow that are not involved in gas exchange like bronchial veins and regions of alveoli that are not ventilated (Riley & Cournand, 1949). The latter, often referred to as physiological shunt, is considered wasted perfusion. This region is frequently increased in patients with ARDS and can result in hypoxemia (Henderson et al., 2017). In order to partially correct this, FiO_2 should be increased to enhance oxygenation of arterial blood (Dantzker et al., 1979). In contrast, when there is no alveolar perfusion, the V_A/Q ratio can reach a maximal value. This occurrence is due to the presence of dead space, which designates the regions of the lung that do not participate in gas exchange (Henderson et al., 2017). These areas include the airways and regions of alveoli that are either not perfused well or over-ventilated. Patients with ARDS often have increased dead space within the lung, causing an impairment of CO_2 clearance which later can result in hypercapnia (Riley & Cournand, 1949). One idea in ARDS management is to reduce the amount of dead space in order to reverse this issue.

It is important to note that the ARDS lung is often heterogenous resulting in variations of V_A/Q ratios among lung regions (Henderson et al., 2017). While some areas of the lung are well perfused but not ventilated, other areas lack blood flow and are over-ventilated. The heterogeneity in the lung and between patients may be partially explained by the level of diffuse alveolar damage present in ARDS. Diffuse alveolar damage is indicated by pulmonary endothelial and epithelial cell injury which leads to

edema and can result in fibrosis. Interestingly, only one half of patients with ARDS have diffuse alveolar damage. Patients who were diagnosed with ARDS and had diffuse alveolar damage had a lower PaO_2/FiO_2 ratio, reduced lung compliance, and were more likely to die from hypoxemia compared to ARDS patients who did not have diffuse alveolar damage (Lorente et al., 2015). Variations of V_A/Q ratios and alveolar damage within each ARDS patient and between ARDS patients make managing ARDS a challenge.

Neutrophils

The lung is a unique area for neutrophil recruitment due to the large surface area of the pulmonary microvasculature. Neutrophils rapidly respond to inflammation and can cross the endothelium in less than 2 minutes by a multi-step process known as emigration or diapedesis. The first is the rolling step, which is where neutrophils begin to interact with the endothelium. The initial capture involves P-selectin glycoprotein ligand-1 (PSGL-1) and E-selectin ligand-1 (ESL-1) molecules on the neutrophil villi (Hidalgo et al., 2007). PSGL-1 interacts with P-selectin and E-selectin on the endothelium, where ESL-1 interacts with solely E-selectin. The rolling of neutrophils is arrested by the activation of the integrin, lymphocyte function-associated antigen-1 (LFA-1), which initiates the adhesion step. This step is also induced by the redistribution and clustering of PSGL-1 and ESL-1 on the neutrophil. Further, during the transition from rolling to adhesion, neutrophils will become polarized to form a front and back end, which is mainly achieved through the phosphoinositide-3 kinase (PI3K) signalling pathway (Hind et al., 2016). The activation of PIP3 by PI3K signalling will induce the reformation of F-actin, which is responsible for the differentiation of the front end of the neutrophil. In contrast, at the back end of the neutrophil, PIK3 signalling is antagonized and actin and myosin interactions regulate the formation of this end.

The adhesion of neutrophils to endothelial cells is critical for the induction of lung injury such as in ARDS. There are a number of adhesion molecules involved including P-selectin, E-selectin, intracellular adhesion molecule-1 (ICAM-1), and many others. The presence of integrins LFA-1 and macrophage-1 antigen (Mac-1) on neutrophils are crucial for adhesion onto the endothelium. When neutrophils are partially active, these

integrins can be involved with slow rolling of the neutrophils however, once neutrophils are fully activated, they instigate a full stop. LFA-1 will first bind to ICAM-1 on the endothelium, which is required for a strong adhesive hold. Next, Mac-1 and ICAM-1 interact and this is crucial for the beginning of trans-endothelial migration. A study explored the role of P-selectin and ICAM-1 in lung injury. They found that neutrophil sequestration was decreased by 57% and 78% and edema was decreased by 60% and 88% when wild-type mice were given anti-P-selectin and anti-ICAM-1 antibodies, respectively (Jones et al., 2019). *In vitro*, ICAM-1 levels were significantly increased in human pulmonary endothelial cells after exposure to influenza however, P-selectin levels did not change (Sugiyama et al., 2016). Similarly, in human airway epithelial cells, ICAM-1 was increased following parainfluenza virus type-2 insult (Tosi et al., 1992). This increase in ICAM-1 expression observed *in vitro* would likely lead to elevated neutrophil adhesion in lung injury *in vivo* models.

Following a strong attachment to adhesion molecules on the endothelial cells, neutrophils reorganize their cytoskeleton to spread out across the endothelium. In this position, neutrophils escape the endothelium through intercellular movement with the help of PECAM-1. After transmigration, neutrophils can release a number of factors that can defend against pathogens however, an excess will contribute to lung tissue damage. Neutrophils hold prestored soluble factors that are released in the lung and have shown to be involved with lung injury. One of these factors, neutrophil elastase, was found to be elevated in the plasma of patients with ARDS (Donnelly et al., 1995). It was observed that higher levels of elastase correlated with the need for mechanical ventilation and low oxygenation levels (Donnelly et al., 1995). Further, various animal models demonstrated a reduction in lung injury when neutrophil elastase was inhibited (Williams & Chambers, 2014) however, when mice were deficient in this protein they had an impaired immune response to gram-negative bacteria insult (Belaaouaj et al., 1998). Another neutrophil component that is important in ARDS is the release of neutrophil extracellular traps (NETs), which induce the death of various microbes through the process known as netosis. In the BALF of patients with ARDS, the formation of NETs was significantly elevated compared to healthy volunteers (Grégoire et al., 2018). Moreover, the engulfment of NETs and apoptotic cells by macrophages

was absent in ARDS patients (Grégoire et al., 2018). Despite the importance of neutrophils in the development of ARDS, patients with severe neutropenia have presented with ARDS. Thus, pulmonary neutrophil infiltration is not mandatory for the development of ARDS suggesting that other immune factors must be involved (Ognibene et al., 1986).

The effect of neutrophil recruitment on microvascular permeability was assessed in an LPS-induced ARDS mouse model. When neutrophils were depleted in mice, protein accumulation in the BALF was inhibited at 3-hours post-infection, indicating a neutrophil-dependent role on microvascular permeability at this time point (Chignard & Balloy, 2000). However, protein concentration in the BALF was comparable at 24, 48 and 72-hours following LPS-instillation in neutropenic mice and control mice, suggesting a neutrophil-independent permeability mechanism at these time points (Chignard & Balloy, 2000). Overall, neutrophils may play a role in microvascular permeability during the early phase of the disease however, their involvement decreases as the disease progresses. Further, a study observed the effect on neutrophil recruitment in the BALF following the administration of leukotriene B4 (LTB4), a potent neutrophil attractant, in a section of the right middle lobe in healthy human volunteers. Four hours later, there was a large increase in polymorphonuclear leukocytes (PMNs) in the BALF however, only a small increase in protein levels, suggesting that neutrophils can be recruited to the lung without inducing a significant increase in protein permeability (Martin et al., 1989).

Acute inflammation in the lung is consistently observed in ARDS patients and has been attributed to neutrophil influx into the lung. A study by Steinberg *et al* demonstrated increased leukocytes in the bronchoalveolar lavage fluid (BALF) on all days following diagnosis in patients with ARDS who died compared to those who lived (Steinberg et al., 1994). Thus, neutrophilia in the lung is considered an indicator of ARDS mortality. The first step in neutrophil influx is neutrophil migration to the site of inflammation, in this case the lung. The leukocyte chemokine, CXCL8 (IL-8), is shown to play the most significant role in this step. It was demonstrated that CXCL8 and neutrophil recruitment levels in the BALF of ARDS patients correlated with disease severity (Hashemian et al., 2014). Further, in LPS-challenged mice, the blockade of chemokines, CCL2 and CCL7, significantly reduced neutrophil recruitment to the lungs

(Mercer et al., 2013). It was later demonstrated that CCL2 and CCL7 play a synergistic role with CXCL8 in neutrophil migration in patients with ARDS (Williams et al., 2017).

PRRs, PAMPs, and DAMPs

Pattern recognition receptors (PRRs) are important in the innate immune response in ARDS. These receptors, which are present in most immune cells, can be membrane bound or cytosolic. They are activated by both pathogen-associated molecular patterns (PAMPs) and danger-associated molecular patterns (DAMPs), the latter composed of endogenously constructed or secreted factors from cells. PRRs can respond to DAMPs and PAMPs via signalling through intracellular pathways that activate nuclear factor-κB (NF-κB), which can then trigger the transcription of various pro-inflammatory cytokines. The cause of ARDS will determine exactly which PRRs are involved and what ligands will activate specific receptors. A number of studies have shown the importance of toll-like receptors (TLRs), a group of PRRs, in viral and bacterial pneumonia. In this case, TLRs bind to PAMPs derived from the insult pathogen and signal through downstream molecules to induce an inflammatory response. In ARDS cases where PAMPs are present and in cases where they are not, such as when ARDS is provoked by drowning or trauma, PRRs respond to endogenous DAMPs to initiate inflammation (Nakamura et al., 2011; Ueno et al., 2004). One specific DAMP, known as the high mobility group box-1 (HMGB1) protein, was found elevated in the plasma and BALF of humans with ALI and in mice instilled with LPS (Ueno et al., 2004). Furthermore, HMGB1 levels and the soluble form of one of its main receptors, the receptor for advanced glycation end products (RAGE), were significantly higher in ARDS patients who did not survive (Nakamura et al., 2011).

1.1.4.1 The Alveolar-Capillary membrane

The smallest unit of the lung is known as the alveolus, which is where gas exchange takes place. The many alveoli in the lungs, comprising about 99% of lung volume, span a surface area of approximately 150 square meters (Guillot et al., 2013) and are each lined with alveolar epithelial cells. Surrounding the alveoli is a network of capillaries. These capillaries are lined by a monolayer of endothelial cells, as are all

blood and lymphatic vessels in the body. Pulmonary endothelial cells and alveolar epithelial cells are bound by their basement membranes by an interstitium comprised of an extracellular network of fibers. Having the epithelial and endothelial cells share a basal membrane allows for a thin barrier for gas exchange that is only 1 μm thick (Guillot et al., 2013).

Alveolar Epithelial Cells

The alveolar epithelial barrier is composed of both type I and type II alveolar epithelial cells, and although similar in number make up 96% and 4% of the surface, respectively (Guillot et al., 2013). Type I cells are thin, squamous, and are found overlying capillaries, thus they have an important role in gas exchange. The depth of type I alveolar epithelial cells is small and minimizes the cytoplasm which contains few organelles (Weibel, 2017). Further, each alveolus has two capillaries surrounding it to ensure efficient gas exchange (Guillot et al., 2013). Type II alveolar epithelial cells are cuboidal shaped and are mainly found in the corners of alveoli. They are responsible for secreting surfactant which is a factor that ensures alveolar stability during collapsing pressures. These cells have an abundance of endoplasmic reticulum and golgi apparatus that help with the synthesis, packing, and storing of surfactant (Weibel, 2017). The large volume and location of type II cells renders them less suitable for gas exchange compared to type I cells.

The epithelium also plays an important barrier function in the lung, protecting the body from pathogens and inhaled substances and preventing leakage from vessels into the alveolar space. They enforce this barrier through intercellular junctions including tight junctions, adhesion junctions, and desmosomes, which play a role in regulating the movement of fluids and solutes across the barrier.

The tight junctions, mainly occludin, claudins, and junctional adhesion molecules (JAMs), are connected to the cytoskeleton through zona occludin proteins. There are two categories of claudins, one group that forms pores and that other group that does not. Lung epithelial cells contain mainly non-pore forming claudins to form a tight alveolar barrier. One splice variant of claudin-18 is specifically expressed in alveolar epithelial cells. Claudin-18 deficient mice were observed to have high paracellular

permeability between the blood and alveoli however, these mice also exhibited increased fluid clearance which was thought to explain why they were immune to VILI (G. Li et al., 2014). Another tight junctional protein highly abundant in alveolar epithelial cells is claudin-4. Human lungs that were perfused *ex vivo* had a positive correlation between claudin-4 expression and fluid clearance in the alveoli, however there was no relationship with lung injury (Rokkam et al., 2011). Moreover, higher claudin-4 expression in the lungs was associated with lower clinical respiratory impairment (Rokkam et al., 2011). In addition, occludins demonstrate an important role in VILI, as rats administered high tidal ventilation showed increased lung edema that was associated with significantly reduced levels of occludins (Liu et al., 2014). When a protein kinase C (PKC) inhibitor was given as a pre-treatment, rats in the high tidal ventilation group experienced less edema and increased occludin levels compared to the non-inhibitor, high tidal group (Liu et al., 2014). This data suggested a relationship between PKC activation and occludin protein loss.

E-cadherin is a junctional protein classified under the adherens family. In addition to maintaining the alveolar epithelial barrier, it also has an important role in supporting epithelial structure and in lung development and function. At 4 weeks old, lung epithelial specific E-cadherin knockout mice displayed less overall airway epithelial and ciliated cell numbers, epithelial denudation, and spontaneous hypersecretion of mucus and increased pro-inflammatory cytokines and chemokines compared to control littermates (Post et al., 2018). These lung phenotypes were similar to those observed in patients with asthma.

In addition to barrier function, alveolar epithelial cells are also involved in innate immunity. Lung epithelial cells are typically the first cells exposed to inhaled pathogens that may trigger a respiratory infection. Viruses such as influenza can bind to epithelial cells via sialic acid residues which induces viral endocytosis and results in viral replication. In bacterial respiratory infections, the pathogen will colonize and invade epithelial cells where they can grow and produce. A number of stimuli can trigger PRRs to activate transcription factor NF-κB, which leads to the production of a number of pro-inflammatory cytokines, chemokines, anti-microbial peptides, and type 1 interferons (IFNs). A mouse model that inhibited NF-κB activation solely in airway epithelial cells

had significantly reduced neutrophil influx into the lungs and reduced macrophage inflammatory protein-2 (MIP-2) and tumor necrosis factor-α (TNF-α) levels in the BALF compared to littermate controls following intranasal exposure of LPS (Poynter et al., 2003). This suggested an important inflammatory role in response to LPS. Furthermore, alveolar epithelial cells are involved in linking the innate and adaptive immune systems during certain infections. A prominent example is when alveolar epithelial cells release cytokines IL-25, IL-33, and thymic stromal lymphopoietin (TSLP). This cytokine expression favours a T helper cell-2 (Th2) response which is commonly observed in allergic reactions (Hallstrand et al., 2014). The production of TSLP by epithelial cells induced CD4+ T cell proliferation *in vitro*, which were stimulated to produce a typical Th2 allergic response involving the production of IL-4, IL-5 and IL-13 (Soumelis et al., 2002). Further, administration of IL-33 induced mRNA levels of IL-13, IL-5, and IL-4 in the lungs of mice (Schmitz et al., 2005). These mice also experienced enhanced lung epithelial hypertrophy, increased presence of mucus on the epithelial lining, and recruitment of neutrophils and eosinophils into the alveoli (Schmitz et al., 2005). IL-25 is produced by mouse and human lung epithelial cells in response to ragweed allergen *in vitro* (Angkasekwinai et al., 2007). When T cells were stimulated with IL-25 they induced a predominant Th2 response characterized by increased IL-4, IL-5, and IL-13 cytokine production (Angkasekwinai et al., 2007).

In response to pro-inflammatory stimuli, alveolar epithelial cells produce the CCL20 chemokine, responsible for recruiting dendritic cells to the lung epithelium. This was demonstrated in mice where the only receptor for CCL20, CCR6, was knocked out in mice. These CC6R deficient mice were unable to promote dendritic cell accumulation in the lung epithelium and could not induce CD8+ T cells (Le Borgne et al., 2006). Moreover, TSLP production by lung epithelial cells increased the expression of major histocompatibility complex (MHC)-II on dendritic cells to promote the activation of the adaptive immune system (Hallstrand et al., 2014).

Lastly, E-cadherin is not only involved in epithelial structure and function, but also in immunity. E-cadherin has been identified to interact with immune cells such as dendritic cells, natural killer cells and adaptive immune cells like CD8+ T cells, CD4+ T cells and Tregs (Hallstrand et al., 2014). For example, it was suggested that CD103

plays a role in the local control of Tregs during *Leishmania major* infection in mice. CD103 knockout mice were found to be resistant to *Leishmania major* infection however, when wild-type Tregs were administered to knockout mice the infected phenotype was restored (Suffia et al., 2005). Further it was found that CD103+ dendritic cells were responsible for the generation of CD8+ T cell responses after pulmonary poxvirus infection (Beauchamp et al., 2010).

Pulmonary Endothelial Cells

Endothelial cells form a continuous monolayer that lines all the blood vessels in the body and play a critical role in the maintenance of vascular homeostasis. Specifically, the pulmonary vasculature is made up of pulmonary endothelial cells, which are squamous in shape, mesenchyme-derived, and are non-fenestrated (Millar et al., 2016). In the 1970s, pulmonary endothelial cells were simply thought to act as a semi-permeable barrier that regulated the traffic of fluids and solutes into and out of the bloodstream (Hurley, 1978). However, today we know that these cells are highly metabolically active and perform a number of important functions.

In addition to its barrier function, pulmonary endothelial cells are involved in regulating vascular tone, coagulation and thrombosis, immune responses, and a number of others. At the time of infection in the lung, neutrophils are recruited to the capillaries where they are able to undergo transmigration (Grommes & Soehnlein, 2011). This process is suggested to not increase vascular permeability due to endothelial domes that are formed by ICAM-1 and LFA-1, which seal the barrier during diapedesis (Carman & Springer, 2004). However, neutrophils are able to secrete substances like TNF-α (Petrache et al., 2003; Petrache et al., 2001) and reactive oxygen species (ROS) (Gao et al., 2007), both which can induce vascular permeability through various signalling mechanisms. Platelets on the other hand are stimulated by TNF-α to secrete thromboxane, which is a protein required for the formation of neutrophil-platelet complexes which also induce vascular permeability during inflammation (Clark et al., 2007).

Although endothelial cells have many functions, the one most relevant to the development and progression of ARDS is endothelial permeability. The factors and

pathways that are involved in the maintenance and regulation of endothelial permeability will be described in detail below.

Endothelial Cell Junctions

The homeostasis of endothelium integrity is generally maintained by junctional proteins known as adherens junctions, tight junctions and desmosomes, which contribute important functions to maintain the integrity of endothelial cells **(Figure 1.3)**. These junctional proteins are essential in regulating vascular permeability and are also involved in responding to mechanical stressors through intracellular signalling pathways.

Tight junctions are mainly made up of claudins, occludins and JAMs, making up about 20% of the junctional proteins in endothelial cells. Although having many roles, this family mainly regulates the paracellular movement of fluids and solutes. Claudins are transmembrane proteins with 2 extracellular loops and 2 cytosolic termini (Bazzoni & Dejana, 2004). There are 27 different claudin proteins however, claudin-5 is enriched in endothelial cells. Its levels are established by the interaction of PI3K, AKT, and the forkhead Box O1 (FOXO1) transcription factor. When PI3K is activated, it will phosphorylate AKT which in turn will phosphorylate FOXO1. This removes FOXO1 from the nucleus and results in less claudin-5 transcription. In contrast, when this pathway is not activated, FOXO1 is nuclear and claudin-5 levels are increased. Claudin-5 and the PI3K-AKT-FOXO1 pathway have been demonstrated to play an important role in the maintenance of endothelial permeability (Geng et al., 2018).

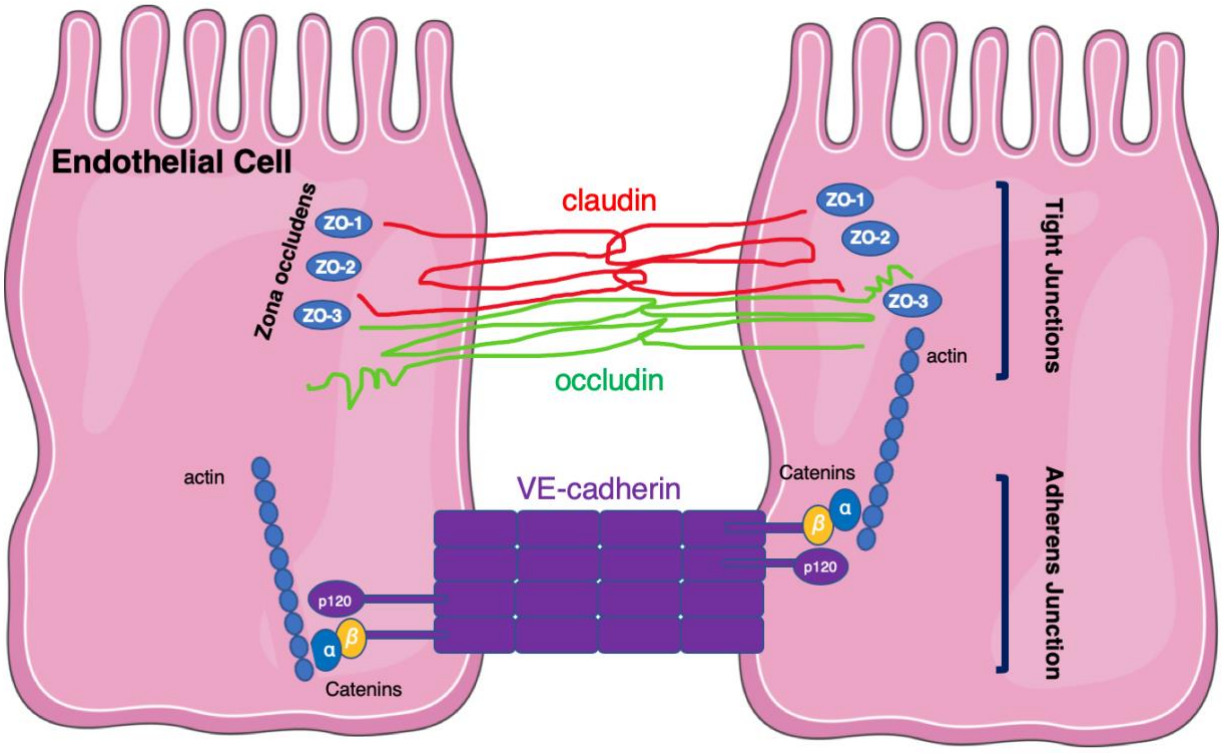

Figure 1.3. Endothelial intercellular junctions. In this figure, two main types of endothelial cell junctions are shown – tight junctions and adherens junctions. The two tight junctions mainly expressed between pulmonary endothelial cells are claudin and occludin, which are both stabilized by interactions with ZO-1,2,3 proteins. In contrast, VE-cadherin interacts with actin proteins via its attached catenin components.

In a brain microvascular endothelial cell line, PLL3.7, the overexpression of claudin-5 caused significantly more cells to be in the S-phase and resulted in less cell migration, while knockdown of claudin-5 led to more cells in the Go/G1 phase and increased cell migration (Ma et al., 2017). Further, this group showed that overexpression of claudin-5 in PLL3.7 cells allowed significantly fewer A459 cells to invade compared to PLL3.7 cells without treatment and PP3.7 with claudin-5 knockdown, suggesting its role in maintaining endothelial paracellular permeability (Ma et al., 2017). The role of claudin-5 in maintaining specifically pulmonary endothelial permeability has been explored further both *in vitro* and *in vivo*. Exposure of human lung endothelial cells to poly(I:C), a synthetic molecule that mimics viral nucleic acid, induced increased endothelial monolayer permeability with a decrease of claudin-5 (Huang et

al., 2016). Similarly, in a rat acute lung injury model, claudin-5 levels in the lung were significantly decreased at 12 and 24-hours after insult (Geng et al., 2018). Moreover, a group of researchers showed that 129X1/Svj mice exhibited significantly enhanced survival compared to BALB/cByJ mice following acrolein-induced acute lung injury (Jang et al., 2011). It was proposed that the BALB/cByJ were more sensitive due to increased vascular permeability observed by enhanced perivascular edema and more protein in the BALF, which was further explained by significantly higher levels of claudin-5 mRNA and protein levels in the resistant strain compared to the sensitive strain 12-hours after insult (Jang et al., 2011).

Occludin is a transmembrane protein with two extracellular loops with both the carboxyl and amino terminals facing the cytosol. This protein is heavily expressed in the brain endothelial cells however, is still present on other endothelial cells (Bazzoni & Dejana, 2004). Occludin binds zonula occludins-1 (ZO-1), which is necessary for its localization to tight junction areas however, ZO-1 does not require occludin for its tight junction localization (Bazzoni & Dejana, 2004). Occludins are well studied in epithelial cells and brain endothelial cells however, their role in vascular endothelial cells is limited. One study using a rat endothelial cell line observed that the presence of occludin at cell junctions was abolished when actin was depolymerized (Kuwabara et al., 2001). They also demonstrated that the overexpression of occludin *in vitro* did not alter endothelial paracellular permeability measured by TER and the influx of small molecules (Kuwabara et al., 2001). Although quite important in epithelial cells, occludin does not appear to have as significant a function in vascular endothelial cell integrity.

The final intercellular tight junction protein, JAMs, include three main classes JAM-A, B, and C, which are all expressed on vascular endothelial cells. Healthy endothelial cells contain JAMs primarily at tight junction areas, typically on the lateral membranes. However, when endothelial cells are stimulated with inflammatory insults, JAMs are relocated from the lateral membrane to the luminal membrane. This shift increases endothelial permeability and allows JAM interaction with leukocytes. When human umbilical vein endothelial cells (HUVECs) were stimulated with oxidized low-density lipoprotein (oxLDL) there was increased expression of JAM-C, which appeared to be re-localized from inter-endothelial junctions to the endothelial cell surface (Keiper

et al., 2005). When ICAM-1 was inhibited on HUVECs, monocyte migration was decreased however, when ICAM-1 and JAM-C were inhibited, monocyte migration was abolished (Keiper et al., 2005). In contrast, when human dermal microvascular endothelial cells (HDMECs) were stimulated with VEGF and histamine, JAM-C that was originally intracellular, rapidly accumulated into the cell junction and colocalized with ZO-1 (Orlova et al., 2006). When JAM-C was knocked down, VEGF- and histamine-induced endothelial permeability was abolished through increased VE-cadherin expression between adjacent endothelial cells, suggesting JAM-C increases endothelium permeability during inflammation (Orlova et al., 2006).

Adherens junctions are mainly made up of VE-cadherin, also known as cadherin-5 or CD144, which is highly expressed in endothelial cells and is considered one of the most important junctional proteins in the regulation of the endothelial barrier function and endothelial permeability (Sukriti et al., 2014). In terms of structure, VE-cadherin is composed of 5-extracellular cadherin-like domains which are linked together by calcium ions (Leckband & Sivasankar, 2000). This junctional protein is affiliated with proteins known as catenins, such as p-120 and β-catenin, which are involved in physically linking VE-cadherin to the actin cytoskeleton (Yagi & Takeichi, 2000). When VE-cadherin interacts with actin bundles, they are said to be in a stable and linear form, which exhibits a strong barrier. Transgenic mice that replaced VE-cadherin with VE-cadherin-α-catenin (a fusion protein) were strongly resistant to VEGF and histamine-induced vascular permeability measured by intradermal Evan's blue dye (Schulte et al., 2011). These transgenic mice further blocked the infiltration of leukocytes and neutrophils into the skin and lung following LPS challenge (Schulte et al., 2011). Although maintaining strong endothelium integrity is preferred, VE-cadherin must be dynamic in order to allow the invasion of immune cells to induce an appropriate inflammatory response. To achieve this, VE-cadherin becomes more discontinuous when triggered by inflammatory insults. In HUVECs, stimulation with TNF-α increased the presence of stress fibers which were demonstrated to attach to VE-cadherin (Millán et al., 2010). These stress fibers are key factors in paracellular permeability and leukocyte migrations. Further other agents that increase vascular permeability such as VEGF and histamine phosphorylates the cytoplasmic domain of VE-cadherin which induces its dissociation

with catenin and induces VE-cadherin internalization, resulting in enhanced endothelial permeability (Rho et al., 2017).

Furthermore, VE-cadherin controls leukocyte infiltration and vascular permeability through different tyrosine residues. This finding was demonstrated through the development of two mutant knock-in mice, one with the VE-cadherin mutation Y685F and the other Y731F. VEGF and histamine increased vascular permeability in wild-type and Y731F mutant mice however, this was not observed in the Y685F mutant mouse, suggesting that phosphorylation of Tyr685 on VE-cadherin is necessary for inducing vascular permeability (Wessel et al., 2014). Further, Y731F mutant mice had significantly less transmigration of leukocytes following IL-1β injection compared to Y685F mutant and wild-type mice, despite similar levels of rolling and adherent leukocytes (Wessel et al., 2014). This finding determined that de-phosphorylation of Tyr731 on VE-cadherin is required for leukocyte extravasation *in vivo*. The functional separation of leukocyte extravasation from vascular leakage has potential translational implications, as it implies that treatment of edema does not have to impair the innate immune response (Heemskerk et al., 2016).

Another role of VE-cadherin is vessel development. VE-cadherin deficiency and the truncation of its β-catenin binding domain in mice causes death approximately 9.5 days into embryogenesis (Carmeliet et al., 1999). Lethality was not due to initial vascular endothelial formation but instead in their development and maturation, which was associated with increased endothelial apoptosis in both models from a lack of VEGF signalling through β-catenin (Carmeliet et al., 1999).

VE-cadherin expression in confluent endothelial cells increased the expression of claudin-5 *in vitro* and *ex vivo*, which was via the inhibition of FOXO1 activity via PI3K and AKT signalling (Taddei et al., 2008). Further, the absence of VE-cadherin is associated with claudin-5 loss, whereas enhanced expression of VE-cadherin directly increases claudin-5 levels (Taddei et al., 2008). These studies suggest that VE-cadherin plays an upstream regulatory role in endothelial or vascular integrity. Thus, increased endothelial permeability may not only be due to the loss of VE-cadherin but also in result of changes in other junctional proteins affected by this decrease. Overall, both

tight junctions and adherens junctions work together to provide endothelial cell and barrier integrity, while nevertheless maintaining their individual functions.

1.1.4.2 Regulation of Endothelial Permeability

Endothelial permeability is coordinated by paracellular and transcellular pathways, which regulate the movement of fluids and solutes across the vasculature. The transcellular pathway is involved in the transport of albumin from the luminal to the basal surface through vesicular structures called caveolae. Paracellular permeability is regulated by intercellular junctional proteins previously described. A number of insults such as histamine (Shasby et al., 2002), TNF-alpha (Angelini et al., 2006), and platelet-activating factor (PAF) (Hudry-Clergeon et al., 2005), and a number of pathways such as the VEGF pathway (Koch et al., 2011), the sphingosine-1-phosphate (S1P) pathways (Mehta et al., 2005) and the Slit-Robo system (London et al., 2010) can modulate vascular permeability by acting on VE-cadherin and the affiliated actin cytoskeleton.

VEGF

Lung endothelial cells possess abundant VEGF, an important angiogenic and permeability factor in the pulmonary endothelium. When various cell lines are exposed to hypoxic conditions, VEGF mRNA is significantly enhanced but then goes back to baseline once oxygen is supplied (Shweiki et al., 1992). VEGF has two main receptors, VEGFR1 and VEGFR2 however, VEGFR2 has been linked to most VEGF functions including its involvement in regulating endothelial permeability. When VEGF binds to VEGFR2, it activates downstream signalling Src tyrosine kinases, which lead to enhanced vascular permeability. The role of specific Src family kinases (SFKs), including src, yes, and fyn, were observed in relation to VEGF-induced vascular permeability. Mice that were deficient in SFKs, src and yes, demonstrated a lack of VEGF-induced vascular permeabilization however, fyn -/- mice displayed a normal response (Eliceiri et al., 1999). In contrast, src -/- mice showed a normal vascular permeability response to the inflammation inducer, allyl isothiocyanate (Eliceiri et al., 1999). This finding suggests that VEGF-induced vascular permeability requires the SFKs, src and yes (Eliceiri et al., 1999).

In addition, NO plays an important role in regulating VEGF-induced endothelial permeability. VEGF stimulates the activation of NO synthases (NOS), endothelial NOS (eNOS) and iNOS, which are responsible for producing NO. The role of eNOS and iNOS in VEGF induced vascular permeability was observed in mice. Following VEGF infusion, vascular permeability was significantly increased in wild-type mice and in iNOS deficient mice however, not in eNOS deficient mice (Fukumura et al., 2001). This data suggested that VEGF-induced vascular permeability was regulated by eNOS.

There are a number of proposed mechanisms for how VEGF can directly influence vascular permeability. One proposal is via interacting with endothelial junctional proteins. In endothelial cells, the GTPase, Ras-related protein 1 (Rap1), strengthened the endothelial barrier through enforcing VE-cadherin junctional integrity however, its regulation *in vivo* is more complicated. Both Rap1 isoforms Rap1A and Rap1B were considered. Following VEGF administration, Rap1A deficient mice and wild-type mice had significantly increased endothelial permeability however, Rap1B deficient mice did not, suggesting that the Rap1B isoform is required for VEGF-induced permeability (Lakshmikanthan et al., 2018). Another mechanism is through the activation of c-Src which phosphorylates VE-cadherin and results in the internalization and degradation or recycling of this junctional protein, thus increasing vascular permeability (Eliceiri et al., 1999b).

Since VEGF increases vascular permeability (Medford & Millar, 2006), one would assume that VEGF levels would increase during ARDS as it induces endothelial permeability, however, a wealth of scientific evidence suggests the opposite. ARDS patients have significantly lower levels of VEGF in the epithelial lining fluid and their alveolar macrophages produced significantly less VEGF in culture compared to patients who were at risk of developing ARDS (Thickett et al., 2002). A similar study found less VEGF levels in lung tissue of ARDS patients compared to healthy controls, which correlated with increased cellular apoptosis (Abadie et al., 2005). Further, plasma VEGF levels were low during the early phase of ARDS however, returned to normal levels during the recovery process.

A similar phenotype was observed in ALI mouse models. VEGF treatment in an LPS-induced ALI mouse model reduced lung wet-to-dry ratio, neutrophil infiltration into

the lung, and apoptotic cells as well as increased the pulmonary vasculature compared to the control group (Song et al., 2015). Another group compared the effects of exogenous VEGF and an anti-VEGF monoclonal antibody on the vasculature in an LPS-induced ALI mouse model. Mice given supplemental VEGF presented decreased LPS-induced albumin leakage, edema, and apoptosis, whereas anti-VEGF delivery following LPS-instillation increased lung edema and neutrophil migration to the lung (Koh et al., 2007).

In contrast to ALI mouse models and patients with ARDS, VEGF levels are high in patients with severe sepsis (van der Flier et al., 2005). The administration of an anti-VEGF antibody known as Bevacizumab reduced mortality in mice with sepsis induced by endotoxemia or cecal ligature puncture (Jeong et al., 2013). The Bevacizumab group also decreased leakage in the lung, spleen, and kidney compared to the placebo group (Jeong et al., 2013). A clinical trial was planned to administer Bevacizumab to severe sepsis patients to prevent ARDS however, it was withdrawn due to lack of funding. Another group repeated the study described above however, found no difference in mortality between the Bevacizumab and control groups in a cecal ligature puncture-induced sepsis mouse model (Besnier et al., 2017).

Tie2 and Angiopoietins

Tie2 is a tyrosine kinase protein that is highly expressed on vascular endothelial cells and is also essential for regulating vascular permeability. It has four ligands known as angiopoietins (Ang) 1-4, however Ang-1 and Ang-2 are the most studied. Ang-1 is secreted by pericytes and platelets and can bind to Tie2 to induce downstream signalling pathways which promote vessel maturation and angiogenesis and is also regularly involved in maintaining the endothelial barrier (Hashimoto & Pittet, 2006). It was demonstrated that Ang-1 protects mice against endotoxin shock by means of reducing lung injury (Witzenbichler et al., 2005), and avoids VEGF-induced vascular leakage by preventing cytosolic Ca^{2+} build-up in cells (Jho et al., 2005). Ang-1 mediates these functions by promoting the junctional accumulation of VE-cadherin (Lee et al., 2014) and inhibiting actin-stress fiber formation (Mammoto et al., 2007). On the other hand, Ang-2 is known to enhance vascular permeability, as its administration induces

pulmonary edema in healthy mice (Hashimoto & Pittet, 2006). Ang-2, which is typically stored in Weibel-Palade bodies in endothelial cells, is transcriptionally and post-transcriptionally regulated by hypoxia and VEGF (Pichiule et al., 2004). It is also rapidly secreted in the presence of histamine and thrombin, indicating its role in responding to vascular inflammation and changes in hemodynamics (Fiedler et al., 2004).

Tie2 is usually found in either the junctional protein area or localized to the extracellular matrix. When associated with the extracellular matrix, Tie2 regularly promotes cell migration through extracellular signal–regulated kinase (ERK) signalling (Saharinen et al., 2008). Conversely when Tie2 is translocated to the junctional regions between endothelial cells by Ang-1, it will preferentially signal through the PI3K or AKT pathways to induce endothelial survival and enhance barrier function (Fukuhara et al., 2008). Further, endothelial permeability is affected by the decline in Tie2 abundance and activation. Tie2 protein abundance and activation levels were decreased in mouse lungs 16-hours following LPS-infection (David et al., 2011). Similarly, Tie2 levels were also shown to decrease in mouse lung 4 days post-influenza infection (Sugiyama et al., 2015).

COMP-Ang1 is a soluble and stable Ang-1 variant that can be used for therapeutic applications. COMP-Ang1 has demonstrated an angiogenic effect while avoiding vessel leakage *in vivo* (Cho et al., 2004). The application of COMP-Ang1 in endotoxemia, a disease that involves increased vascular permeability and edema, was observed in mice. Mice that received COMP-Ang1 treatment displayed decreased LPS-induced vascular leakage, measured by Evan's blue dye accumulation, in the lungs, heart, kidney and small intestine compared to mice that received placebo (J.-A. Hwang et al., 2009). Further, COMP-Ang1 reduced leukocyte infiltration by decreasing the expression of vascular cell adhesion molecule-1 (VCAM-1) and Mac-1 and enhanced the expression of the tight junctional protein, platelet and endothelial cell adhesion molecule-1 (PECAM-1) (J.-A. Hwang et al., 2009).

Koh's group generated an anti-angiopoietin 2 antibody that was able to bind to Ang-2 and activate Tie2, which they termed ABTAA (Han et al., 2016). The delivery of ABTAA to a cecal ligature puncture sepsis mouse model enhanced survival by 40% in the first week compared to mice that received the Fc control. However, ABTAA was not

able to improve mortality from sepsis in Tie2 deficient mice and Ang-2 deficient mice, suggesting that ABTAA relies on both of these structures to induce its effects. ABTAA appears to reduce mortality in mice with sepsis by preventing ALI, reducing vascular leakage and neutrophil infiltration, improving vascular function, and decreasing cytokine and Ang-2 circulating levels.

Vasculotide (VT) is a tetrameric peptide that is a Tie2-agonist. Daily delivery of VT to influenza-infected mice significantly improved survival when administration began at the time of infection or at 24, 48, or 72 hours post-infection (Sugiyama et al., 2015). It was shown that VT did not alter viral replication, alveolar neutrophil infiltration or lung injury however, oxygenation was improved. VT also improved survival in a septic mouse model induced by cecal ligature puncture (Kümpers et al., 2011). In this model, the administration of VT reduced capillary leakage and inflammatory cell count in the peritoneal lavage fluid, ameliorated the upregulation of VCAM-1 and reduced pro-inflammatory and chemotactic cytokines in the serum.

In a healthy state, Ang-1 binds Tie2, induces its phosphorylation, which in turn promotes barrier function. However, during ARDS, levels of Ang-2 are upregulated causing vascular leakage and inflammation (Medford & Millar, 2006). In regard to clinical ARDS, a study demonstrated that Ang-2 levels were significantly higher in ARDS patients who did not survive, compared to those who did, suggesting Ang-2 levels to correlate with a poor outcome (Gallagher et al., 2007). Further, Tie2 expression and Tie2 phosphorylation were decreased in mouse lungs 4 days post-influenza infection (Sugiyama et al., 2015). In this study, mice that were administered vasculotide, a Tie2 agonist, showed enhanced survival post-influenza infection compared to mice that received placebo. The importance of Tie2 in ARDS is also exemplified by a group that administered intratracheal endotoxin to Tie2 heterozygote mice, which presented with enhanced lung injury and an increased mortality rate compared to infected wild-type mice (McCarter et al., 2007).

microRNAs

MicroRNAs (miRNAs) are non-coding RNA strands that are about 22 nucleotides in length and control target gene expression at either the translational or post-translational levels. Commonly, miRNAs will bind the 3'-untranslated regions (3'UTR) of its target gene and will either degrade the mRNA or inhibit its protein translation. A number of pathways are regulated by miRNAs, and many of these are involved in the pathogenesis of ARDS and other lung diseases.

A study identified 27 miRNAs and 37 mRNAs that were significantly changed in a rat model of ARDS. miRNA-126, which is a regulator of vascular integrity and angiogenesis, has demonstrated involvement in ARDS and ALI. Interestingly, miRNA-126 is one of the only endothelial-specific miRNAs. Prior to excision, the pre-miRNA-126 is made up of both miRNA-126-3p (typically referred to as miRNA-126) and miRNA-126-5p (referred to as miRNA-126*). Recently it has been shown that miRNA-126* (miRNA-126-5p) has a biological effect, as it can induce endothelial proliferation and attenuate atherosclerosis (Schober et al., 2014). However, the majority of the literature focuses on the effects of miRNA-126 (miRNA-126-3p), which will be discussed further.

One of the main functions of miRNA-126 is regulating VEGF signalling. miRNA-126 has been identified to repress sprouty-related protein-1 (SPRED-1) and phosphoinositide-3-kinase regulator subunit 2 (PIK3R2), which are both negative regulators of VEGF signaling. SPRED-1 inhibits the activation of the mitogen-activated protein (MAP) kinase pathway, which blocks ERK activity. PIK3R2 represses the activity of PI3K, leading to the inhibition of AKT phosphorylation. When miRNA-126 was knocked down in cells, the phosphorylation of AKT and ERK were significantly decreased, thus there was increased VEGF signalling (Fish et al., 2008). Interestingly, another arm of the VEGF signaling pathway involving the phosphorylation of src, was not affected by miRNA-126 knockdown. This indicated that miRNA-126 does not regulate all VEGF signalling effects (Fish et al., 2008).

The functions of miRNA-126 *in vivo* were explored through a miRNA-126 homogenous deficient mouse model. Researchers obtained lower amounts of miRNA-126 -/- mice than expected from heterozygous crosses, due to some embryonic death in result of systemic edema, hemorrhages, and ruptured blood vessels (S. Wang et al.,

2008). Isolated aortic rings from miRNA-126 -/- mice had impaired outgrowth in response to VEGF, suggesting that these knockout mice had defective angiogenesis (S. Wang et al., 2008). The involvement of angiogenesis required for cardiac repair following myocardial infarction was observed in viable miRNA-126 -/- mice. About 70% of wild-type mice survived at three-weeks post-infarction however, 50% of miRNA-126 -/- mice died within one week and 100% died by three weeks (S. Wang et al., 2008).

The delivery of miRNA-126 may be beneficial in various diseases. Human endothelial progenitor cell (EPC) exosomes have demonstrated the ability to transfer miRNA-126 into endothelial cells (Zhou et al., 2018). In an LPS-lung injury mouse model, the delivery of EPC exosomes decreased the amount of neutrophils and cytokines in the BALF, lung edema and lung injury compared to the delivery of murine fibroblast exosomes which do not contain much miRNA-126 (Zhou et al., 2019). This complemented the groups' previous findings that demonstrated EPC exosomes protected mice from sepsis-induced ALI (Zhou et al., 2018).

Proangiogenic therapy through increased VEGF signalling produces enhanced blood vessel formation. However, the formed blood vessels in response to the VEGF pathway are commonly immature and leaky. Blood vessel maturation occurs in response to Ang-1 signalling through the Tie2 receptor. Interestingly, the overexpression of miRNA-126 *in vitro* resulted in increased Tie2 phosphorylation in response to Ang-1 stimulation (Sessa et al., 2012). This was in result of miRNA-126 repressing PIK3R2, which negatively regulates Tie2 signalling (Sessa et al., 2012). Therefore, the delivery of miRNA-126 will induce blood vessel formation and maturation through VEGFR2 and Tie2 signalling (Cheng & Fish, 2015) **(Figure 1.4).** It is possible that enhanced delivery or expression of miRNA-126 would improve ARDS by decreased endothelial leakage.

In conclusion, ARDS is a complex disease and its pathophysiology involves a multitude of factors and pathways. It involves alterations of gas exchange due to changes in alveolar perfusion or ventilation and involves increased pulmonary microvascular permeability resulting in alveolar fluid accumulation and lung tissue damage. An abundance of molecules and pathways are involved in the manifestation and progression of ARDS including neutrophils, PRRs, VEGF, Tie2, miRNA-126 and

many others. Understanding the pathophysiology of ARDS will assist in the development of therapeutics and/or management techniques in ARDS patients.

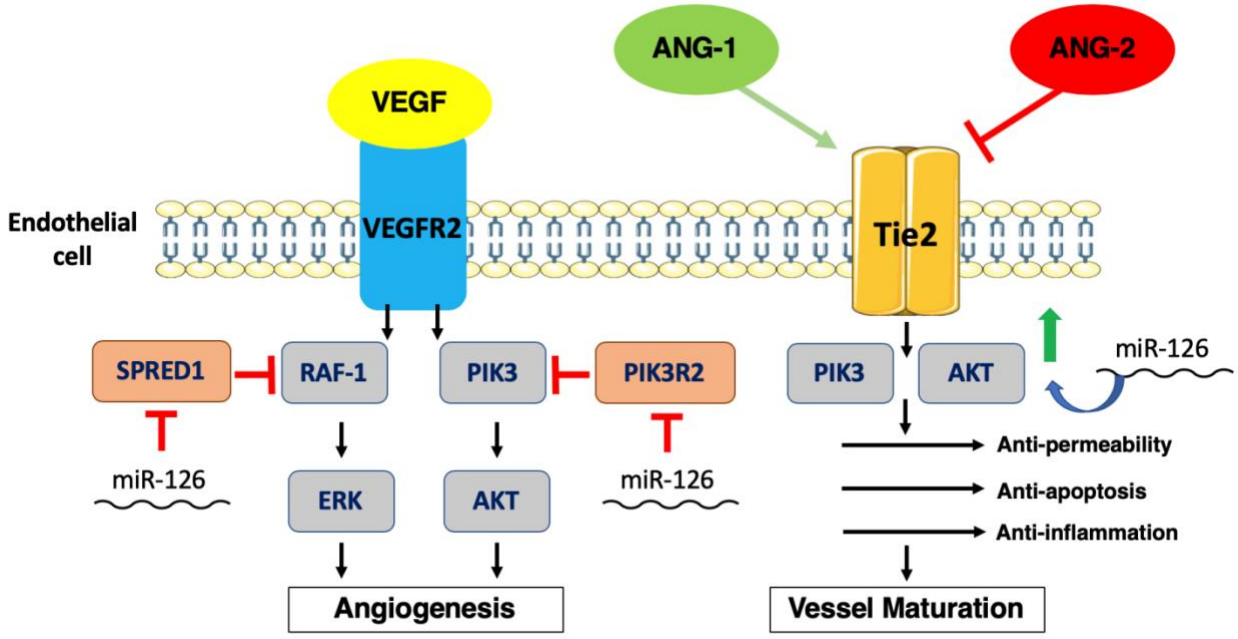

Figure 1.4. miRNA-126 control VEGFR2 and Tie2 signalling pathways, important regulators of endothelial permeability. VEGF binds to its receptor, VEGFR2 on endothelial cells to signalling through a number of downstream pathways including RAF-1 and PIK3, to induce angiogenesis. miRNA-126 inhibits negatively regulators of the VEGFR2 pathway, SPRED1 and PIK3R2, which increases angiogenesis. The Tie2 receptor is abundant on endothelial cells. It has two main ligands, Ang-1 which is an agonist and Ang-2 which is an antagonist. Binding of Ang-1 to Tie2 activates PIK3 and AKT downstream signalling, inducing anti-permeability, anti-apoptosis, and anti-inflammatory responses, which overall enhance vessel maturation. Ang-2 binding to Tie2 will inhibit these outcomes. It has been shown that the overexpression of miR-126 increases Ang-1 signalling through Tie2. It is also hypothesized that PIK3R2 negatively regulates PIK3 signalling in the Tie2 downstream pathway, which is alleviated by the presence of miRNA-126. Overall, miRNA-126 increases angiogenesis and vessel maturation.

1.2. Targeting the Pulmonary Endothelium in lung injury

Targeting drug delivery to the endothelium has been suggested to increase drug efficacy and specificity while reducing off-target effects in certain diseases. The general idea behind targeting the vasculature is combining the delivery of drugs with ligands of certain surface endothelial markers (Kiseleva et al., 2018). The choice of endothelial target may be dependent on the disease of interest, for example if one was trying to treat an inflammatory disease the ligand may target cell adhesion molecules, which typically increase in expression during inflammation. For example, a group delivered an anti-ICAM-1 antibody conjugated to dexamethasone, which was then loaded onto nanostructured lipid carriers, and administered to an LPS-induced ALI mouse model. The administration of this endothelial targeted drug significantly attenuated TNF-α, IL-6, and neutrophil infiltration in the BALF and improved pulmonary tissue structure compared to dexamethasone alone and other controls (Li et al., 2018). Another group targeted a drug to PECAM, another endothelial cell adhesion marker. They conjugated a PECAM antibody with catalase, which is an enzyme that converts H_2O_2 into water and oxygen, into a pulmonary vascular oxidative stress mouse model. First, in healthy mice, an intravenous injection of PECAM-catalase resulted in significantly more catalase in the lungs compared to mice given the IgG-catalase control (Christofidou-Solomidou et al., 2003). This increase was due to the deposition of PECAM-catalase on the luminal side of alveolar capillaries (Christofidou-Solomidou et al., 2003). Further, in mice that were subjected to H_2O_2-induced oxidative stress, PECAM-catalase reduced lethality by 80% compared to IgG-catalase that reduced it by only 20% (Christofidou-Solomidou et al., 2003).

In addition to drug delivery, endothelial targeting can also be beneficial for gene transduction, a potential therapeutic mechanism in cardiovascular and pulmonary diseases. A group conjugated adeno-associated virus-2, a common vector used for gene therapy, with a SIGYPLP peptide that targets endothelial cells (Nicklin et al., 2001). They demonstrated that this construct significantly increased transfection of endothelial cells and decreased transfection of smooth muscle cells and hepatocytes *in vitro* compared to adeno-associated virus-2 conjugated to a control peptide (Nicklin et al., 2001). Another group used endothelial targeting to silence a gene specifically in

endothelial cells. This group engineered lentiviral vectors with a heme oxygenase-1 (HO-1) miRNA that was controlled by a VE-cadherin promoter, making it specific to lung endothelial HO-1 (Zhang et al., 2013). Two weeks after intranasal instillation of lenti-VE HO-1 miRNA there was a significant reduction in HO-1 levels in the lung compared to mice that received a lenti-VE control miRNA, which was in result of decreased endothelial HO-1 and not HO-1 levels in lung epithelial cells or macrophages (Zhang et al., 2013). After the two weeks, some mice were exposed to room air and some to hyperoxia conditions. Mice that received the lenti-VE HO-1 miRNA had significantly increased lung cell apoptosis, protein in their BALF, ROS production, and pro-inflammatory cytokines production compared to mice that received the lenti-VE control miRNA in both room air and hyperoxia conditions (Zhang et al., 2013). This indicates a protective role for lung endothelial HO-1 in healthy and hyperoxia conditions and further, a system for endothelial cell-specific gene silencing.

Targeting genes or drugs specifically to endothelial cells is considered quite effective in a number of *in vitro* and *in vivo* models. However, simply administering endothelial-targeted drugs to patients with ARDS will unlikely lead to significant improvements in outcome. This is because most compounds experience great difficulty in accumulating in injured lung regions. This is especially challenging in ARDS because the lung is a heterogenous mix of injured and uninjured regions, thus drugs that do penetrate the lungs are preferentially directed to healthy areas. Therefore, instead of generally targeting the endothelium, the injured endothelium, specifically, should be targeted in ARDS. In order to achieve this, we propose the use of ultrasound and microbubble-mediated (USMB) drug delivery. This method will be described in detail in the next section.

1.3 Ultrasound and Microbubble (USMB)-mediated drug delivery

A particular drug delivery method that has shown potential to increase therapeutic uptake and action in a number of specific tissues and organs is ultrasound-microbubble (USMB)-mediated drug delivery. The therapeutic of interest is either encapsulated in the microbubble, attached to the outer shell of the microbubble, or is simply co-administered with the microbubbles. The ultrasound probe is then positioned at the target area.

Microbubbles that flow through the vasculature of the target tissue or organ will experience ultrasound energy, which will cause the microbubbles to oscillate and/or cavitate. Microbubble cavitation will lead to increased drug uptake into the target area through sonoporation, which is the formation of tiny transient pores in nearby plasma membranes, and increased endocytosis. Overall, this system shows the potential to increase drug uptake in the area of interest and reduce off-target effects. USMB has increased drug delivery to the heart (Liu et al., 2015), muscle (Wang et al., 2019), brain (Ye et al., 2018; Zhao et al., 2018), kidneys (Gao et al., 2014), tumors (Chen et al., 2018; Jing et al., 2019) and other tissues however, we were the first group to demonstrate its use in a lung injury model (Sugiyama et al., 2018).

USMB has demonstrated the ability to increase drug deposition in the brain as it can increase the opening of the blood-brain barrier (BBB). In rats with cerebral ischemia reperfusion injury, microbubbles attached to phosphatidylserine were administered and ultrasound treatment was provided in order to open the BBB. USMB treatment demonstrated increased Evan's blue dye leakage through the BBB and resulted in a two-fold increase in the number of microglia and macrophages that took up phosphatidylserine (Zhao et al., 2018). Another technique known as focused ultrasound combined with microbubble-mediated intranasal delivery (FUSIN) is an approach that delivers nanoparticles to the brain with very minimal systemic exposure. In this paper, scientists demonstrated enhanced deposition of inhaled gold nanoclusters in the brainstem of mice when ultrasound was applied compared to inhalation treatment alone (Ye et al., 2018).

The use of USMB has also shown promise in enhancing drug delivery to tumors in various cancerous *in vivo* models. For example, endostatin, an antiangiogenic drug, has shown to be effective in cancer treatment when combined with chemotherapy. However, its systemic administration does not lead to efficient accumulation of the drug in tumors. One group decided to use USMB to enhance the deposition of Endostar, an endostatin drug, in tumors in a breast carcinoma mouse model. Mice that received Endostar with USMB exhibited a three-fold-increase in its deposition and a significantly greater tumor growth inhibition rate compared to mice that received Endostar alone or Endostar conjugated to microbubbles (Jing et al., 2019). Moreover, a group

demonstrated that USMB could reduce the nephrotoxicity of cisplatin. They injected cisplatin-conjugated microbubbles to mice bearing a head and neck tumor 2 times a week until day 33. Mice that received cisplatin with USMB treatment to the tumor site showed significantly decreased levels of cisplatin in the kidney and liver and reduced tumor size compared to mice that received the cisplatin alone, suggesting this system decreases systemic toxicity (Chen et al., 2018).

In addition, USMB can be used to transfect genes in target areas. This was demonstrated by a group that used USMB to transfect the TNF-α receptor in the ankle joint of rats with collagen-induced arthritis. The plasmid was either locally injected into the ankle joint synovial fluid or nearby skeletal muscle. When plasmid was administered to either injection site and combined with USMB there was enhanced deposition of the TNF-α receptor in the joint, reduction in TNF-α plasma levels, and improved joint scores compared to rats that received the plasmid without USMB treatment (Wang et al., 2019).

As described, USMB can be used to enhance the deposition of drugs or transfection of plasmids into specific areas of the body. There are a number of factors that may influence the effectiveness of USMB including but not limited to the choice of microbubbles, the method of microbubble-drug loading, ultrasound settings, the target organ, and the delivered therapeutic. These components will be further discussed below and their bioeffects will be considered.

1.3.1 Ultrasound

Ultrasound waves are longitudinal waves that propagate at frequencies higher than 20kHz. An ultrasound transducer or probe will emit these waves, which are often referred to as pulses. Ultrasound does not emit ionizing radiation like other imaging modalities such as CT scans and X-rays, is easy to use at the bedside, and is considerably cheaper and faster than magnetic resonance imaging (MRI). In clinical practice, ultrasound is a common modality for diagnostic imaging. The literature demonstrates the valuable use of ultrasound in mediating destruction of microbubbles as a drug delivery system. Although this has yet to be executed in clinic, this drug delivery system has shown great potential in improving the efficacy and safety of

different therapies in a number of animal models. Further research is required to optimize this drug delivery system prior to applying it in practice.

1.3.1.1 Ultrasound for Imaging

Ultrasound, also known as sonography, is used to visualize internal regions of the body such as blood vessels, organs, tendons, and other tissues, and is commonly used during pregnancy to examine the development of the fetus. An ultrasound transducer is placed at the region of the structure of interest with a conductive medium such as a gel that will lie between the transducer and the skin to ensure direct contact. Ultrasound pulses will be emitted from the transducer and these will interact with the tissues in the body. Some of this energy is absorbed by the tissues and some is reflected back to the ultrasound probe. The ultrasound machine processes the speed and intensity of this reflected wave and creates an image on the screen. To determine how much energy is reflected, one must consider the acoustic impedance of the structure being imaged. Each material has an acoustic impedance value, a measure of sound wave resistance, which is calculated by the product of its density and the speed in which sound waves travel through it (“Ultrasound in Medicine and Biology,” 2013). A material with a large acoustic impedance value will absorb most of the energy and will reflect only a small amount off its surface. This will produce a bright image, such as when imaging bone with ultrasound (Venables, 2011). Contrast that to materials like air that have a 4000 to 5000-fold lower acoustic impedance than most structures in the body (“Ultrasound in Medicine and Biology,” 2013), which leads to the reflection of most ultrasound waves and prevents the establishment of a clear image (Venables, 2011). A large reflection results at the interface of two mediums that have a substantial difference in acoustic impedance values, such as soft tissue versus air in the lungs (Venables, 2011). For example, when imaging an aerated healthy lung with ultrasound, the image will only comprise of a horizontal line representing the pleural wall.

Due to the limitation of imaging healthy lung with ultrasound, textbooks traditionally deemed its use for lung assessment to be unsuitable. However, the low acoustic impedance of air may be advantageous in the diagnosis of certain lung diseases such as pulmonary fibrosis, tumors, and ARDS. In these lung diseases, air

content in the lung is decreased and the density of the lung is increased due to the presence of fluids, blood, collagen, or masses. When this occurs, the acoustic impedance of the area increases, and certain image signals are observed. For example, B-lines are vertical lines extending from the pleural line that indicate lung interstitial syndrome. The number of B-lines present increases as air content decreases. As air content decreases even further, one will be able to view the entire parenchyma, which is usually referred to as consolidation of the lung (Baston & West, 2016). This manifestation is commonly seen in patients with ARDS. Using sonography as a diagnosis method is available for a number of lung diseases, each with distinctive elements. In regard to our focus on ARDS, lung ultrasound can identify the presence of edema (e.g. B-lines, consolidation) and can detect the absence of a pneumothorax with the presence of lung sliding (Baston & West, 2016).

Typically, those with a suspected pneumonia or another lung disease require chest X-ray imaging for proper diagnosis. This form of imaging can lead to false negatives if the disease is in an early stage, if consolidation is in an area that is difficult to image, or if the degree of consolidation is less than 1 cm thick (Wang et al., 2016). CT scans, which provide superior images are another option however, they emit considerably more radiation and require patient transportation (Wang et al., 2016). Considering these limitations, lung ultrasound is potentially useful and has been the subject of extensive study. The use of lung ultrasound versus chest X-ray in the observation of postoperative pulmonary complications, like pneumonia or pulmonary edema, following cardiothoracic surgery was compared. This study found that lung ultrasound identified significantly more patients with pulmonary complications than a chest X-ray did (Touw et al., 2018). Further, ICU patients received lung ultrasound assessment significantly quicker than patients who received a chest X-ray (Touw et al., 2018). In addition, a group compared the sensitivity, specificity and diagnostic accuracy of detecting various indications of ARDS such as pleural effusion, alveolar consolidation and alveolar-interstitial syndrome. In all categories, ultrasonography was deemed significantly more accurate than both chest radiography and auscultation in confirming these factors and determining overall lung injury (Lichtenstein et al., 2004). Further, ultrasound can be used for daily monitoring of lung injury in patients with ARDS as the

machine is easy to bring to the bedside and patients (with severe ARDS) are typically placed in the prone position allowing access to the dorsum of the chest, where disease often dominates. Ultrasound may also differentiate between cardiogenic and non-cardiogenic interstitial syndrome, which is important to determine considering differences in treatment and management between these two diseases. Cardiogenic-induced edema is present when the following are observed; bright, laser-like B-lines at the septal ending points, a regular pleural line that slides, and no consolidation (Sureka et al., 2015). Furthermore, there is typically ultrasound-evidence of impaired cardiac function. Contrast that to a non-cardiogenic case; blurred B-lines not at septal end points, a pleural line that is irregular and does not slide much, consolidation that is usually heterogenous (Sureka et al., 2015) and (most importantly) normal cardiac function. Overall, lung ultrasound for diagnosis of various lung diseases is quick, effective, and is able to differentiate between cardiogenic and non-cardiogenic cases.

1.3.1.2 Ultrasound for drug delivery

Imaging settings for most tissues and organs have been accepted however, guidelines for using ultrasound for optimal USMB drug delivery are still under investigation. In order to optimize the delivery of therapeutics to certain tissues various ultrasound parameters should be considered such as the frequency, intensity, acoustic pressure, focus, and mechanical index. The frequency of the ultrasound should be varied depending on the type of microbubbles used, the tissue of interest, and the purpose of practice whether it be imaging or drug delivery. In most cases, frequency can be divided into three groups, low frequency (20-200kHz), medium frequency (0.7-3MHz) and high frequency (> 3MHz) (Boissenot et al., 2016), which can influence both ultrasound wave penetration depth and spatial resolution. In regard to imaging quality, one would obtain a higher resolution, or a clearer image, when using a higher frequency compared to a low frequency. This choice must be balanced to obtain an appropriate penetration depth, as the depth is inversely proportionate to the frequency. For example, at a frequency of 1MHz an ultrasound wave can penetrate 10 cm however, at 10MHz the penetration depth is only 1 cm (Boissenot et al., 2016). Altogether, using a higher frequency will result in high resolution images of structures close to the surface.

Another important parameter to consider is the intensity of the ultrasound machine, which is the amount of power applied by the ultrasound wave divided by the area of the targeted surface. Intensity can either be low at 0.125 to 3 W/cm^2 or high at 3 to several thousand W/cm^2 (Boissenot et al., 2016). The use of high intensity ultrasound is primarily used for ablation of tumors however, it should not be used during imaging or drug delivery because it can cause unwanted tissue fragmentation (Hoogenboom et al., 2015). Typically, low intensity ultrasound is used for drug delivery applications (Peruzzi et al., 2018). Intensity can influence the acoustic pressure, which is the amount of energy received by the target tissue. This is measured by obtaining the peak-positive acoustic pressure or the maximum pressure value and the peak-negative acoustic pressure or minimum pressure value that is measured by a hydrophone over the entire duration of the pulse (Boissenot et al., 2016). In terms of pulse administration, it can be continuous, indicating constant ultrasound energy directed to the tissue, or discontinuous, allowing a pulse to be administered every several seconds. The latter is preferred *in vivo* as it prevents thermal-induced effects since there is time in-between pulses for heat to dissipate.

In order to measure the bioeffects of the ultrasound, the mechanical index (MI) must be quantified. MI is a theoretical value that provides information about the degree of energy that is being administered and indicates the potential of non-thermal bioeffects. MI is calculated by dividing the peak-negative acoustic pressure by the square root of the frequency (Peruzzi et al., 2018). In clinic, the US Food and Drug Administration (FDA) approved a maximum MI of 1.9 for diagnostic imaging. Microbubbles will cavitate at an MI greater than 0.5, therefore an MI lower than the maximum 1.9 can be used for drug delivery which should be both safe and effective.

1.3.2 Microbubbles

The development of microbubbles for use as contrast agents and for drug delivery has expanded in the last several years. Currently, certain microbubble formulations have been approved for imaging in clinic however, their use as theranostics is still being investigated. Microbubbles are composed of a gas core of either air, perfluoropentane, perfluorocarbon or nitrogen (Liang et al., 2010), which is

surrounded by a shell comprised of either proteins, lipids, or polymers. Most microbubbles used for biomedical purposes are about 1-3 μm in diameter, with a 10 μm diameter limit to ensure that they can pass through pulmonary capillaries (Lindner et al., 2018).

The earliest microbubbles contained albumin shells and an air core. Protein shells are typically about 15-20 nm thick and are maintained through cross-linkages of covalent disulfide bonds, which results in a stiff structure (Borden, 2010). Albunex was the first protein coated microbubble to be FDA approved for contrast imaging of the left ventricle of the heart (Borden, 2010). Currently, Optison is one type of albumin coated microbubble that is used in clinic for contrast imaging. Optison microbubbles contain a perfluorocarbon gas core, which has a longer half-life in circulation than Albunex due to the low solubility of the core gas (Podell et al., 1999). A study compared the use of Albunex versus Optison in USMB delivery of a green fluorescent protein (GFP)-plasmid to the quadricep muscles in mice. Mice that received Optison microbubbles demonstrated significantly higher levels of GFP expression in the muscle tissue following ultrasound compared to mice that received Albunex, suggesting that Optison is superior for USMB plasmid delivery (Li et al., 2003).

The thickest microbubbles are those with polymer shells. These are generally 100 to 200 nm thick and are held together by covalent cross-linkages (Borden, 2010). Shells this thick cause microbubbles to be much more resistant to compression and expansion compared to other types of bubbles. Also, these microbubbles are often too large to inject intravenously. However, a number of recent techniques demonstrated the ability to reduce the size of polymer-coated microbubbles to only about 4-5 μm in diameter (Chlon et al., 2009). There are currently no clinically approved polymer-coated microbubbles, although they have been suggested to be effective in drug delivery.

Lipid shelled microbubbles are the most commonly used microbubbles for both contrast imaging and drug delivery. Lipid shells are advantageous compared to other compositions because the lipid monolayer forms spontaneously, with hydrophobic ends facing the core gas and hydrophilic tails positioned on the outside. This thin shell (1-3 nm thick) is held together by hydrophobic and van der Waal forces which are weak, allowing these bubbles to easily expand and compress during ultrasound application,

maintain a low surface tension, and exhibit high cohesiveness (Borden, 2010). There are a number of lipid-coated microbubbles on the market that are FDA approved for contrast imaging; one of the most commonly used is Definity from Lantheus Medical Imaging.

1.3.2.1 Microbubble and Drug Loading

A number of therapeutics can be delivered through USMB drug delivery such as small molecules, deoxyribonucleic acid (DNA), ribonucleic acid (RNA), and viral vectors (Mayer, Geis, Katus, & Bekeredjian, 2008). An important decision involves determining which method of drug and microbubble co-delivery is most suitable. One method involves producing the microbubbles with the bioactive substance present in hopes of incorporating this therapeutic into the microbubble shell (Frenkel, 2002). Another method involves attaching the drug of choice to the microbubble shell which is typically performed by simply incubating these compounds together (Cao et al., 2015). This assumed binding is often accomplished by weak non-covalent interactions or electrostatic forces. For example, it is common to use microbubbles with a cationic charge to deliver plasmids, as the positively charged shell is attracted to the negatively charged DNA. Further, microbubbles and the therapeutic can be simply co-administered to the patient (Sugiyama et al., 2018). For most therapeutics, co-administration of the drug and microbubbles has demonstrated to be as effective as the delivery of the drug encapsulated in or bound to microbubbles. However, therapeutics that are easily degraded in circulation should be incorporated into microbubbles to avoid destruction and increase available therapy at the site of interest.

Deciding which transport method will lead to the greatest drug delivery is based on a number of factors. One is the compatibility of the microbubble shell with the drug. The use of an albumin shell is deemed an acceptable binder of various drug compounds (Bekeredjian et al., 2005) however, as the example above, cationic lipids are better suited to deliver negatively charged compounds like DNA and RNA. Another component is determining the stability of the therapeutic after injection *in vivo*. For example, DNA is known to degrade quite rapidly after injection into the bloodstream. In cases like these, compounds should be combined or attached to microbubbles to avoid

degradation. Although co-administration may be more feasible for some compounds, drug encapsulation or attachment may increase tissue specificity and decrease adverse effects as the drug is typically inactive when bound to the microbubble and is only then released into its active form at the target site by ultrasound-mediated microbubble destruction (Liang et al., 2010).

When combining or attaching a compound to microbubbles, the amount of therapeutic delivered is limited by the carrying capacity of the microbubble shell. This may be of concern if the shell is thin, such as those composed of phospholipid shells which are typically 2-3 nm thick (Borden, 2010). However, there are ways around this limitation. The simplest aspect is to implement the use of microbubbles that have thicker shells, such as microbubbles made up of polymers or proteins. Another technique used to increase drug load is to incorporate additional shell layers. One group developed an oil shell layer surrounded by a typical lipid coating, which was demonstrated to have higher drug loading capacity than microbubbles with solely the lipid shell (May et al., 2002). Further, a microbubble made up of 5 lipid layers showed a 10-fold increase in DNA loading capacity, without any loss of oscillation or ultrasound-destruction ability (Borden et al., 2007). These solutions alter the microbubble composition to increase drug load however, another technique involves loading drugs into a separate drug carrier such as nanoparticles, which can then be attached or associated with regular microbubbles (Lum et al., 2005). One group used fluorescent nanobeads that were coated in avidin as their separate drug carrier. These were combined with lipid shelled microbubbles coated in polyethylene glycol (PEG)-biotin. The avidin on the nanoparticle and the biotin on the microbubble shell formed an attachment. This combination demonstrated increased drug loading for each microbubble and importantly did not interfere with microbubble movement or oscillation (Lum et al., 2005).

1.3.2.2 Comparing types of microbubbles for USMB drug delivery

A study compared the effectiveness of cationic versus neutral microbubbles in the delivery of a click beetle luciferase (CBLuc) reporter plasmid *in vitro* and *in vivo* in mouse tumors. Cells treated with cationic microbubbles in USMB had a significantly higher CBLuc expression compared to cells administered the plasmid with neutral

microbubbles in USMB (Wang et al., 2012). Similarly, mouse hind-limb tumors expressed significantly higher levels of the plasmid when treated with cationic bubbles compared to neutral bubbles in USMB plasmid delivery (Wang et al., 2012). Another group compared the use of biotinylated cationic microbubbles, cationic microbubbles, and neutral microbubbles in terms of their ability to enhance USMB gene transfer *in vitro*. Findings demonstrated that the biotinylated cationic microbubbles resulted in the highest gene transfer to cells, with cationic bubbles having the second highest uptake (Nomikou et al., 2011). In addition, pre-mixing cationic microbubbles or biotinylated microbubbles with the plasmid solution prior to administration to cells resulted in significantly more gene transfer compared to when microbubbles and plasmid were not pre-mixed (Nomikou et al., 2011).

Increased USMB-induced gene transfer with the use of cationic microbubbles compared to neutral microbubbles may be in result of cationic microbubbles being able to bind plasmid DNA and partially protect the DNA from degradation, whereas neutral microbubbles do not have this capacity (Panje et al., 2012). It is also interesting to note that plasmid uptake in hindlimb skeletal muscle following USMB exposure was the highest when the lowest amount of plasmid (10 µg) and cationic microbubbles (1×10^7) were used and the least efficient when the highest amount of plasmid (50µg) and cationic microbubbles (5×10^8) were administered (Panje et al., 2012).

Although cationic microbubbles are deemed more effective at gene transfection compared to neutral microbubbles, regardless of microbubble type, USMB significantly enhances gene uptake *in vitro* and *in vivo* compared to plasmid administration alone (Panje et al., 2012). Most literature compares the efficacy of cationic versus neutral microbubbles in targeted gene transfection however, it would be interesting to contrast them in terms of targeted delivering of other drugs or therapeutics.

1.3.3 The effects of USMB

Together, ultrasound and microbubbles can display a number of behaviours depending on various properties such as ultrasound parameters, the type of microbubbles used, and the area of the body being targeted. When moderate ultrasonic pressure is applied, the oscillation of the gas core of the microbubbles will portray a

backscatter which can be detected by the ultrasound machine. This backscatter is strongest when the microbubble is oscillating at its resonant frequency. Along with their high echogenicity, microbubbles scatter ultrasound energy non-linearly (Borden, 2010), overall producing a clear image. The use of microbubbles is advantageous as they are more compressible than solids or fluids, and their use is cheap and easily integrated into clinical practice (Borden, 2010). When ultrasound causes microbubbles to oscillate this may provoke shear stress on nearby cells. These forces can increase the permeability of the endothelial vasculature, allowing drugs to be taken up from the bloodstream into the target area through mechanisms such as sonoporation, also known as transient pore formation, and increased endocytosis (Peruzzi et al., 2018). These USMB-induced drug uptake mechanisms will be described in detail below.

1.3.3.1 Cavitation

An ultrasonic field can cause microbubbles to undergo cavitation. Cavitation is when microbubbles undergo expansion during peak-negative pressure or the rarefaction phase and contract during the peak-positive pressure or compression phase. When the peak-negative pressure is high and frequency is low, cavitation is most likely to occur. However, the degree of cavitation is also dependent on a number of other factors such as the viscosity of the fluid surrounding the tissues, the temperature, the exposure duration of ultrasound, and the physical properties of the microbubbles like gas, shell, and size (Liang et al., 2010). There are two different types of cavitation, inertial cavitation and stable (or non-inertial) cavitation. These two types of cavitation have distinct mechanisms that lead to enhanced drug uptake in cells **(Figure 1.5).**

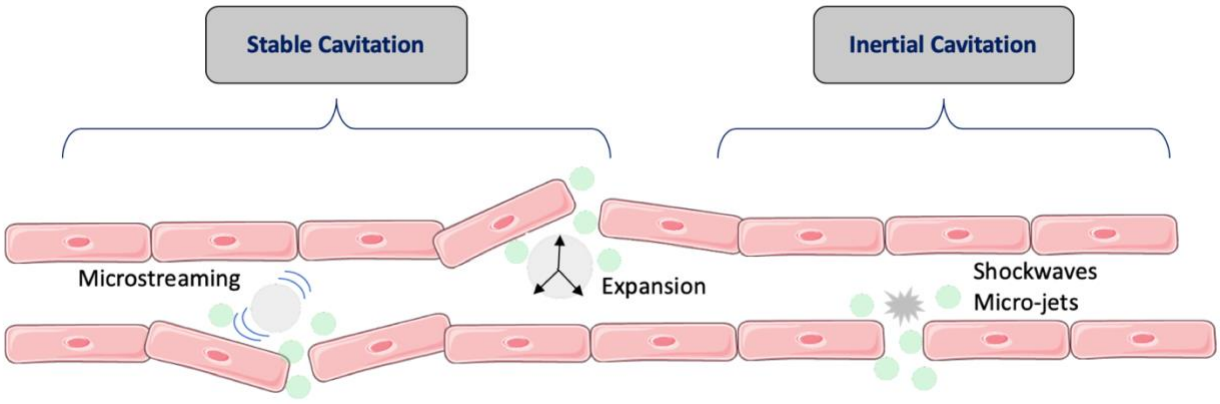

Figure 1.5. Ultrasound-mediated microbubble cavitation. Ultrasound can cause microbubbles to cavitate, which describes the process of microbubbles expanding during the rarefaction phase and contracting during the compression phase. Two types of microbubble cavitation can occur; stable cavitation and inertial cavitation. Inertial cavitation characterized an expansion that is followed by a forceful collapse. This induces shockwaves and microjets to occur, which can lead to increased drug uptake. In contrast, stable cavitation describes when microbubbles oscillate in size however, never collapse. Oscillations between expansion and contraction can induce shear stress on nearby cell membranes and can result in fluid microstreaming. The effects of both stable and inertial microbubble cavitation can enhance drug uptake through sonoporation and increased endocytosis.

Inertial cavitation describes when microbubbles increase in size and then forcefully collapse, typically observed when higher acoustic pressures are applied. Under high acoustic pressure, microbubbles will collapse if they are not able to resist the pressure of the surrounding fluid. When the microbubble bursts, the gas and liquid interface takes on an extremely fast speed which can induce a shock wave from within the microbubble and propagate outward into the surrounding fluid. This shock wave will cause damage to nearby tissues by inducing transient pore formations in cell membranes, in which drugs can accumulate through. However, if a microbubble is particularly close to cells, their explosion will be asymmetrical. This results in a jet stream of liquid moving from the microbubble to nearby cells, which can also induce the formation of pores.

At lower acoustic pressures microbubbles usually undergo stable cavitation, where they increase and decrease in size but do not rupture. The expansion and shrinkage of microbubbles that occurs during stable cavitation is commonly known as oscillation (Ahmadi et al., 2012). When the resonant frequency of a bubble matches the frequency of the acoustic wave, this bubble will undergo maximum oscillation (Ahmadi et al., 2012), which in turn maximizes its interactions with cells, streaming potential, shear stress, and the release of drugs if incorporated into the bubbles (Kooiman et al., 2014). When microbubbles undergo stable cavitation, they cause circulating fluid movement known as microstreaming. The shear potential and velocity of this fluid flow is dependent on the amplitude of microbubble oscillation (Sheffield et al., 2008). The velocity of the fluid is highest at the surface of the microbubble and decreases with distance. When microbubbles are relatively close to cells the force from the high velocity fluid induces a shearing force which often causes distortions and pore formations in cell membranes, leading to increased cell permeability. This can lead to increased drug uptake by cells.

1.3.3.2 Bioeffects

USMB can facilitate enhanced drug uptake through inertial and stable cavitation-induced effects on nearby cells. The main mechanisms include sonoporation, which involves the formation of tiny transient pores in cell membranes (Liang et al., 2010), and increased endocytosis (Fekri et al., 2016), both of which will be described in further detail. Other proposed mechanisms of USMB drug delivery include a rise in temperature that increases the fluidity of bilayers (Nozaki et al., 2003), mechanical energy absorbed by proteins that could alter the structure of cells and the disruption of the microbubble shell which can release attached drugs (Marmottant & Hilgenfeldt, 2003).

Sonoporation

Sonoporation involves the generation of pores within adjacent cell membranes in response to USMB. This method increases the permeability of the cells to the therapeutic that is co-administered however, the size of the pores and the duration they remain open will influence the quantity of drug that will be taken up. Pores of

approximately 100 nm in diameter were observed in MAT B III cells after ultrasound and microbubble exposure (Mehier-Humbert et al., 2005) however, another study using SK-BR-3 cells identified larger pores that ranged from 2-3 μm in size (Zhao et al., 2008). Interestingly, Karshafian *et al* demonstrated that drug uptake through sonoporation was in fact not limited by the size of the therapeutic *in vitro*, as a murine fibrosarcoma cell line was able to take up dextran molecules that ranged from 10 kDa to 2 MDa following USMB (Karshafian et al., 2010).

Although sonoporation may seem detrimental to cells, most pores close in less than 5 seconds (Mehier-Humbert et al., 2005) and the cell viability and shape is typically maintained (Zhao et al., 2008). High speed microscopes allow researchers to visualize pore formation and resolution in cells following USMB. One study demonstrated that pore formation occurred approximately 5 seconds following USMB exposure (van Wamel et al., 2006), whereas another study demonstrated pore formation by 3 μs (Kudo et al., 2009). Generally, pore formation is suggested to occur sometime between a couple of seconds to 10 seconds following USMB exposure however, these differences are typically due to variations in ultrasound parameters and the type of microbubbles used (Qin ett al., 2018). The degree of inertial versus stable cavitation may also influence the size and opening duration of the pore. Microbubbles that experienced inertial cavitation generated pores that were about 5.3 μm in diameter, which began to close 5 seconds after induction and were completely sealed by 1 minute (Hu et al., 2013). Sonoporation induced by stable cavitation led to a 10 μm diameter pore that began to seal after 6 seconds and was completely sealed by 30 seconds (Hu et al., 2013). Further this study determined that pores with an area of 100 μm^2 or larger would not reseal.

Pore resealing is thought to be in result of increased Ca^{2+} levels following sonoporation, which can independently seal the bilayer or induce intracellular vesicles to assist in this process. A study demonstrated that intracellular calcium levels increased from 100 nM to 500 nM following sonoporation (Fan et al., 2010). This increase occurred simultaneously with sonoporation, measured by propidium iodide (PI) uptake, thus it was thought that Ca^{2+} increased via transient pore formation. However, cells that lacked uptake of PI still experienced an increase in intracellular calcium that

occurred 6-42 seconds after USMB exposure, suggested to be a result of calcium waves (Fan et al., 2010). When a chelating agent was added, cells were less likely to repair USMB-induced pores compared to when Ca^{2+} was present (Hu et al., 2013).

Further, it is important to determine the ideal ultrasound parameters for drug uptake through sonoporation. It was observed that sonoporation led to maximum cell permeability and the least loss of viability *in vitro* when the following ultrasound parameters were used; a peak negative pressure of 570 kPa, a 32 μs pulse duration, and a 3 kHz pulse repetition frequency when in a 3.3% Definity solution (Karshafian et al., 2009). The optimal USMB parameters for drug delivery *in vivo* must be further investigated in a number of tissues and in various disease models.

Endocytosis

At first, USMB-induced drug uptake was thought to only occur through transient pore formation however, increased drug uptake in cells was observed past pore closure. Following USMB exposure, researchers discovered an increase of vesicles on vascular walls and in endothelial cells. Through further investigation, endocytosis was found as the other dominant method of USMB-induced drug uptake.

The effect of USMB on different types of membrane trafficking such as clathrin-mediated endocytosis and fluid-phase uptake that was either receptor or non-receptor mediated, was observed in epithelial cells and breast cancer cells. Clathrin-mediated endocytosis was significantly increased 5-minutes after USMB exposure compared to ultrasound exposure alone or other controls in both cell lines. This was explained by enhanced amounts of clathrin-coated pits and an increase in their size (Fekri et al., 2016). Further, USMB increased fluid-phase endocytosis 20-minutes following exposure suggesting that the mechanisms by which USMB influences clathrin-mediated and fluid phase endocytosis are separate (Fekri et al., 2016). Another group looked at the route of plasmid DNA uptake in HeLa cells following USMB. Plasmid DNA was delivered to late endosomes about 3-hours post-USMB (Delalande et al, 2015). Gene transfer was significantly reduced when cells were treated with chlorpromazine, an inhibitor of clathrin-dependent endocytosis however, inhibitors of the caveolin-dependent endocytosis pathway, filipin III and genistein, did not alter gene transfer (Delalande et

al., 2015). This finding confirmed clathrin-dependent endocytosis to be the main mechanism of plasmid DNA uptake.

Interestingly, the degree of uptake through sonoporation versus endocytosis following ultrasound and microbubble delivery is dependent on the acoustic pressure (De Cock et al., 2014). A study compared these two processes in cells exposed to FITC-dextran. It was demonstrated that when a higher acoustic pressure was applied there was more uptake through sonoporation compared to endocytosis (De Cock et al., 2014). Thus, one may alter the acoustic pressure to favour a specific drug uptake mechanism.

The mechanism by which USMB-induced cavitation results in increased drug uptake through endocytosis is not completely understood however, there are potential processes that may be involved. One possibility is the physical force or membrane deformation that USMB induces on endothelial cells, since shear stress is known to increase endocytosis in endothelial cells (VanBavel, 2007). This physical force may also cause cytoskeleton remodelling which may activate endocytosis. In addition, sonoporation may induce endocytosis since there is increased budding and vesicle formation to close the transient pores, which may be a prelude to endocytosis activation (Holopainen et al., 2000). Further investigation on how USMB increases drug uptake through increased endocytosis or vesicle trafficking is required.

1.3.3.3 Potential USMB Adverse Effects

The use of contrast agents in ultrasound imaging are considered safe. Unwanted adverse events following contrast agent administration in patients are rare, and if present are typically mild. The use of contrast agents for drug delivery requires a mechanical index that is normally higher than the ones used for imaging. Thus, it is important to observe the potential adverse effects of USMB drug delivery.

The long-term safety and neurological effects of repeated USMB-induced opening of the BBB in non-human primates was observed for 4 to 20 months. Results indicated that USMB opening of the BBB did not induce hemorrhages or edema and did not alter decision making or motor function (Downs et al., 2015). Thus, USMB was considered safe in non-human primates. Another study that performed a similar study in

rats also deemed frequent application of USMB-induced BBB opening to be safe (Tsai et al., 2018).

In an *in vivo* rabbit auricular blood vessel model, the effects of USMB on macroscopic extravasation and endothelial damage at various peak negative acoustic pressures were observed. One-hour after treatment, damage to the endothelium was proportional to the peak negative pressure amplitude and the damage was observed to be greater on the vessel distal to the transducer compared to the proximal side of the vessel (Hwang et al., 2005). Microscopic extravasation and endothelial damage were present at peak negative acoustic pressures above 3.35 MPa, which corresponds to a MI of about 3.2 at a 1.1 MHz frequency (Hwang et al., 2005). This MI is much greater than the FDA approved maximum MI of 1.9 and greater than MIs used in most USMB drug delivery studies. Therefore, as long at the MI and other ultrasound settings are in correspondence to FDA settings, any endothelial tissue damage should be minimal or rare. However, further investigation on the safety of USMB for drug delivery is required before it is translated into clinical practice.

One retrospective study compared mortality in ICU patients that had an echocardiogram performed with or without the ultrasound contrast agent, Optison. This study found that 1.3% of patients from the contrast group died compared to 1.1% from the control group (Exuzides et al., 2010). After propensity score matching, no difference in mortality was found between the two groups, confirming that using Optison for echocardiography does not increase the risk of mortality. Another retrospective study compared 24-hour mortality in hospitalized patients who received an echocardiogram with or without contrast agents. After analyzing a total of 4,300,966 patients, it was demonstrated that patients who received the contrast agent had a 24% decreased risk of mortality 24-hours after administration (Main et al., 2008) potentially due to improved diagnosis. Furthermore, a study observed the use of ultrasound contrast agents in patients with pulmonary hypertension. All 1513 patients received Definity and were monitored for 24 hours following injection. No adverse events occurred thus indicating that Definity is safe to use in pulmonary hypertension patients as an ultrasound contrast agent (Wever-Pinzon et al., 2012). Overall, ultrasound contrast agents appear safe to

use in all patients. In addition, choosing ultrasound as the imaging modality results in exposure to much less ionizing radiation than any other imaging tool.

CHAPTER 2: OBJECTIVES AND AIMS

2.1 USMB is a safe drug delivery system that increases the deposition of therapeutics in edematous lung tissue in mouse and pig lung injury models.

The use of ultrasound and microbubbles as a drug delivery system has expanded in the last several years. The application of USMB has been studied in a number of organs and tissues however, our group was the first to propose and demonstrate the use of USMB drug delivery in the lung. Ultrasound on the lung is typically neglected because it is known that ultrasound waves are scattered and reflected by air. We recognized that in lung diseases such ARDS, there are regions of the lung that are edematous and consolidated thus, ideal for ultrasound treatment. We hypothesize that ultrasound will specifically cavitate microbubbles and enhance drug uptake in edematous lung regions while sparing healthy, aerated ones. This provides a means of specifically targeting therapeutics to the injured lung, permitting a means of 'personalized medicine'. Further, we propose that this form of care is translational because portable ultrasound can easily be applied at the beside and most ICU physicians are trained in sonography. Therefore, this approach can easily be integrated into practice.

Aim 1: Determine if USMB is safe to use in hypoxemic conditions.

The use of microbubbles as ultrasound contrast agents is commonly used in ICU patients for diagnostic imaging. Safety data on USMB drug delivery is minimal and its effect on injured lung specifically, has yet been investigated. We propose evaluating the safety of USMB drug delivery in hypoxemic conditions in *E. coli*- and influenza-lung injury mouse models. To assess the effect of USMB in the setting of hypoxemia, we will measure oxygen saturation, lung edema, and lung injury.

To determine the effect of USMB on oxygen saturation we chose to use the MouseOx Plus device from Starr Life Sciences. This system provides mouse oxygen saturation values for both anesthetized and non-anesthetized mice. Prior to infection

and treatment, baseline oxygen saturation measurements will be taken. Mice will then be administered 5 X 10^7 CFUs of *E. coli* intratracheally to induce a lung infection that models ARDS. Oxygen saturation measurements 3-hours post-infection will confirm if mice are hypoxemic and thus, infected properly. At 6-hours post-infection, USMB treatment or a mock treatment is provided. The mice in the USMB group will be intravenously administered 1 X 10^9 Definity microbubbles and provided chest ultrasound for 5 minutes. In contrast, the control group is intravenously administered PBS and anesthetized for 5 minutes to mimic ultrasound-treatment conditions. Once mice are recovered from anesthesia, oxygen saturation is again measured. Further, oxygen saturation will be measured at 8, 16, 24, 32, and 48-hours post-infection. These oxygen saturation values generated from infected USMB mice will be compared to the infected control mice.

To further evaluate the safety of USMB in a longer-term hypoxemic setting, lung edema and lung injury will be evaluated. Because the *E. coli* infection results in only short-term injury, an influenza-lung injury model will be used in this case. Mice will be intranasally infected with influenza and on day-5 receive USMB or control treatment similar to above (day 5 was chosen because infected mice begin dying on or after day 6). At 1-hour post-treatment, lungs will be collected for edema or injury analysis. Lung edema can be measured by lung wet-to-dry ratio, with a higher ratio indicating increased edema. Values generated by infected mice that received USMB versus control treatment will be compared. Further, separate mice will be used to evaluate the effect of USMB on lung injury. Blinded histologic analysis of the lungs will be performed by a lung pathologist (Dr. David Hwang). Lung injury scores of infected mice that received USMB treatment will be compared to infected mice that received control treatment, and to healthy, untreated mice. If USMB does not worsen oxygen saturation, lung edema, or lung injury in hypoxemic condition we can conclude that this method of drug delivery is safe to use in lung injury.

Aim 2: Demonstrate that USMB can enhance the deposition and efficacy of gentamicin in the lungs of an E. coli-lung injury mouse model.

Clinical infectious disease guidelines suggest avoiding the use of aminoglycosides, like gentamicin, in the treatment of gram-negative induced pneumonia or ARDS because these antibiotics have poor lung penetration and can cause nephrotoxicity and ototoxicity at therapeutic doses (Kalil, Metersky, Klompas, Muscedere, Sweeney, Palmer, Napolitano, O'Grady, Bartlett, Carratalà, Solh, et al., 2016). We propose using USMB to enhance the delivery of gentamicin to injured lungs. This drug delivery system would allow the use of gentamicin at a low dose and would decrease off-target deposition thus, ideally averting toxicities.

In order to effectively test the potential of delivering low dose gentamicin in ARDS, we would need to design a replicable and appropriate animal model. Mice will be intratracheally infected with the gram-negative bacteria, *E. coli*. To ensure this animal model is representative of ARDS, the following will be investigated; lung edema, lung injury, and oxygen saturation. Lung edema will be measured by lung wet-to-dry ratio. Mice infected with *E. coli* should present with higher wet-to-dry lung ratios than mice intratracheally administered an equal volume of PBS, to confirm that the bacterial infection is heightening lung edema and microvascular permeability, which are hallmarks of ARDS. Lung injury will be scored in a blinded fashion and should portray a patchy injury to mimic the heterogeneity of the ARDS lung (Maunder et al., 1986). Finally, ARDS patients are often hypoxic thus, oxygen saturation values of infected mice should represent this.

If the *E. coli*-lung injury mouse model is representative of ARDS, the use of USMB to enhance gentamicin efficacy will be investigated. Mice will be given a 1.5 mg/kg dose of gentamicin, which is considerably lower than the clinically effective dose of 5 mg/kg. The effect of USMB and gentamicin administration will be compared to the following controls; PBS, gentamicin alone, gentamicin with microbubbles, and USMB without gentamicin. Efficacy of gentamicin will be determined by bacterial CFUs in the homogenized lungs 2-hours post-treatment. The deposition of gentamicin will be quantified in both the lung tissue and BALF 30-minutes following treatment. If USMB

significantly enhances gentamicin deposition and efficacy in the lungs of the ARDS moues model, this drug delivery system can be investigated in a larger animal model.

Aim 3: Evaluate the efficacy of USMB drug delivery to the injured lung in a porcine pneumonia model.

Although USMB enhances the delivery of gentamicin to injured lungs in mice, it does not suggest its feasibility in humans due to the large difference in size. In order to investigate the capability of USMB to enhance therapeutic uptake in edematous human lungs, a porcine model will be used. Pigs are similar in size and anatomy to humans and have been proposed as a model that is beneficial for translational medicine especially in the field of respiratory medicine (Judge et al., 2014).

To investigate the feasibility of USMB drug delivery to the injured lung in a large animal model, an *E. coli*-induced pneumonia will be generated in pigs. We designed a model where one lung lobe, the right middle lobe (RML), would be infected with *E. coli* and would act as the ultrasound treatment area. This single-lobe pneumonia model would allow assignment of other lobes as internal healthy controls. In all experiments, the left upper lobe (LUL) will serve as the internal healthy lung control.

To evaluate the feasibility of USMB in edematous pig lung, we first used Evans blue dye (EBD), a compound that binds to albumin in the blood, as our chosen ‘drug’ because it is cheap and easily quantified in tissue. Ultrasound imaging would be used to identify a region of the RML that is consolidated. It will be secured there by a metal arm for the duration of treatment. EBD and Definity microbubbles will be intravenously injected simultaneously through different venous ports at a constant rate. EBD will be extracted from RML and LUL lung tissues using formamide and quantified using a spectrophotometer at an absorbance of 620 nm. EBD in the RML versus the LUL will be compared in pigs that received EBD with or without USMB. Further, the ability of USMB to enhance drug uptake in *un*infected lung tissue will be evaluated.

CHAPTER 3: LUNG ULTRASOUND AND MICROBUBBLES ENHANCE AMINOGLYCOSIDE EFFICACY AND DEPOSITION TO THE LUNG IN *ESERCHERICHIA COLI*-INDUCED PNEUMONIA AND ACUTE LUNG INJURY

Adapted with permission from Sugiyama MG*, **Mintsopoulos V***, Raheel H, Goldenberg NM, Batt JE, Brochard L, Kuebler WM, Leong-Poi H, Karshafian R, & Lee WL. (2018). Lung ultrasound and microbubbles enhance aminoglycoside efficacy and delivery to the lung in *Escherichia coli-induced* pneumonia and acute respiratory distress syndrome. *Am J Respir Crit Care Med, 198*(3):404-408. (*contributed equally)

CHAPTER 3: LUNG ULTRASOUND AND MICROBUBBLES ENHANCE AMINOGLYCOSIDE EFFICACY AND DEPOSITION TO THE LUNG IN *ESCHERICHIA COLI*-INDUCED PNEUMONIA AND ACUTE LUNG INJURY

Acute respiratory distress syndrome (ARDS) is a devastating disorder characterized by lung microvascular leakage leading to pulmonary edema and hypoxemia (Murray & Nadel's Textbook of Respiratory Medicine, 2-Volume Set, 6th Edition, US Elsevier Health Bookshop, 2006). Its hallmark is heterogeneous involvement of the lung parenchyma, with thoracic computed tomographic scans revealing densely consolidated areas interspersed with relatively normal-appearing lung. Such heterogeneity greatly complicates management. Mechanical ventilation, although lifesaving, preferentially inflates the normal regions of the lung, causing overdistention and lung damage (Murray & Nadel's Textbook of Respiratory Medicine, 2-Volume Set, 6th Edition, US Elsevier Health Bookshop, 2006). Pharmaceutical agents such as antibiotics administered by inhalation distribute to the healthy rather than the injured regions of the lung, potentially causing off-target effects. By contrast, drugs administered systemically cannot target the injured lungs and are delivered to organs throughout the body, thereby predisposing to adverse effects (Smith et al., 2012). The inability to deliver therapy solely to the injured areas of the ARDS lung remains an intractable problem in critical care.

We hypothesized that thoracic ultrasound and microbubbles could be used to specifically enhance drug delivery to and uptake by the injured lung. Microbubbles (1–3 μm) are made up of a gas-filled core and an outer lipid shell and are used routinely as a contrast agent for echocardiographic studies, including in critically ill patients (Exuzides et al., 2010). When exposed to an ultrasound pulse, microbubbles undergo cavitation that induces shear stress on biological membranes within their vicinity, leading to the formation of transient pores and enhanced endocytosis (Fekri et al., 2016) at the

plasma membranes of cells. This induces enhanced uptake of local therapeutics such as drugs or genes (Cao et al., 2015); importantly, the process is effective at increasing uptake whether the drug is encapsulated by the microbubble, bound to its surface, or even only in its vicinity. This phenomenon has been harnessed to deliver genes to ischemic limbs (Cao et al., 2015). Ultrasound of the lung has traditionally been considered of limited utility (Sagar et al., 1978) because air causes reflection and scattering of ultrasound energy. We hypothesized that this very limitation can be harnessed in ARDS because ultrasound waves will preferentially penetrate damaged areas of lung (because they are filled with fluid or are atelectatic), leaving normal (air-filled) areas of lung mostly unaffected **(Figure 3.1.A).** In addition, by targeting the ultrasound transducer to the chest, the ultrasound energy is focused on the thorax, limiting the effect on other organs. Furthermore, circulating microbubbles may accumulate in injured regions owing to increased endothelial permeability.

To test this hypothesis, we focused our initial efforts on aminoglycoside antibiotics using a murine model of severe gram-negative bacterial pneumonia, one of the commonest causes of ARDS. Antibiotic resistance is growing worldwide (Cilloniz et al., 2016); many strains of enteric gram-negative bacilli are now resistant to cephalosporins and β-lactam/β-lactamase inhibitor combinations. Although almost 100% of gram-negative isolates remain sensitive to aminoglycosides, this class of antibiotics has traditionally been avoided for treating pneumonia because of poor lung penetration and the association of systemic therapeutic aminoglycoside concentrations with significant nephrotoxicity and ototoxicity (Kalil et al., 2016). Thus, developing an easy and safe method to increase the therapeutic index of aminoglycosides specifically in the lungs would be of great practical value.

C57BL/6 mice (male; aged 9–12 wk) were infected intratracheally with Escherichia coli (American Type Culture Collection 25922) and developed significant hypoxemia and lung edema within 3 hours; histological examination confirmed extensive neutrophilic lung injury that was bilateral **(Figure 3.1.B).** All work was performed with the approval of the local animal care committee (ACC 742).

To confirm the safety of microbubbles and ultrasound-mediated cavitation in this setting, we measured oxygen saturation by pulse oximetry before, during, and up to 48

hours after intravenous injection of 1×10^9 DEFINITY microbubbles (Lantheus Medical Imaging; dose based on previous work (Cao et al., 2015)) and thoracic ultrasound administration; no antibiotics were administered at this point. DEFINITY microbubbles are U.S. Food and Drug Administration–approved lipid-coated microbubbles that are widely used in diagnostic cardiovascular ultrasound. We used a SONOS 5500 (Philips Healthcare) ultrasound device and an S3 phased array transducer to induce microbubble cavitation, positioning the probe over the murine thorax (transmitter frequency, 1.3 MHz; 67 V; 0.2 W; mechanical index, 0.9; peak negative acoustic pressure, −900 to −1,200 kPa) with a pulsing interval of every 5 seconds for 5 minutes. Microbubbles and ultrasound were well tolerated, with the treatment resulting in no adverse effect on arterial oxygenation **(Figure 3.1.C).**

To establish whether ultrasound-induced microbubble cavitation (USMB) could enhance antibiotic delivery to the injured lung, in separate experiments we administered gentamicin (1.5 mg/kg) by intraperitoneal injection 6 hours after infection with *E. coli*. Microbubbles (1×10^9) were injected intravenously immediately afterward, and thoracic ultrasound was then applied as described earlier. Two hours later, animals were killed by cervical dislocation, and lung homogenates were plated on agar. Each experiment was repeated three times with similar results; statistical analysis was performed using Kruskal-Wallis one-way ANOVA and Dunn's multiple comparisons test using Prism software (GraphPad Software).

Compared with gentamicin alone (which was ineffective at this low dose), USMB caused an almost 1-log reduction in bacterial growth **(Figure 3.2.A).** In contrast, administration of either microbubbles and antibiotics (but without ultrasound) or ultrasound and microbubbles (but without antibiotics) was ineffective; this rules out a direct antibacterial effect of microbubbles and/or ultrasound alone. BAL fluid and lung homogenates from infected mice were analyzed for gentamicin concentrations by ELISA (EuroProxima). Thirty minutes after USMB, gentamicin concentrations in both BAL and lung tissue were significantly higher (at least twofold) in USMB-treated animals than in gentamicin-alone control animals **(Figures 3.2.B and 3.2.C).** Thus, USMB enhanced antibiotic delivery and bacterial killing. Interestingly, USMB was able to enhance gentamicin delivery despite the theoretical limitation of hypoxic

vasoconstriction in injured lung regions, perhaps owing to the extent of infected and injured lung in our model. With that caveat, although our model mimics pneumonia-induced ARDS (lung edema, bilateral injury, hypoxemia), it is possible that USMB-mediated antibiotic delivery would be beneficial in cases of localized (e.g., lobar) pneumonia as well.

Microbubble contrast agents are safe and have been used extensively in critically ill patients (Exuzides et al., 2010) and patients with ARDS (Mekontso Dessap et al., 2010). Similarly, thoracic ultrasound is now widely used for diagnosis of barotrauma, pulmonary edema, and lung consolidation (Lichtenstein et al., 1997; Nguyen et al., 2016; Pesenti et al., 2016). There is growing literature in other fields showing that USMB can dramatically enhance gene transfection and drug delivery (Cao et al., 2015; Christiansen et al., 2003); however, its use for the treatment of ARDS has remained unexplored owing to preconceived negative notions of lung ultrasound feasibility.

Given the limited mobility of patients with ARDS, the potential utility of bedside USMB therapy is high. In principle, USMB-induced drug delivery is targeted specifically to the injured areas of the lung, in essence providing precision medicine to the most critically ill patients. In this letter, we have focused on a very pragmatic goal: the enhanced delivery of aminoglycoside antibiotics in pneumonia to improve their therapeutic index. Further research will determine if USMB can enhance the delivery of other therapeutic cargoes to the injured lung.

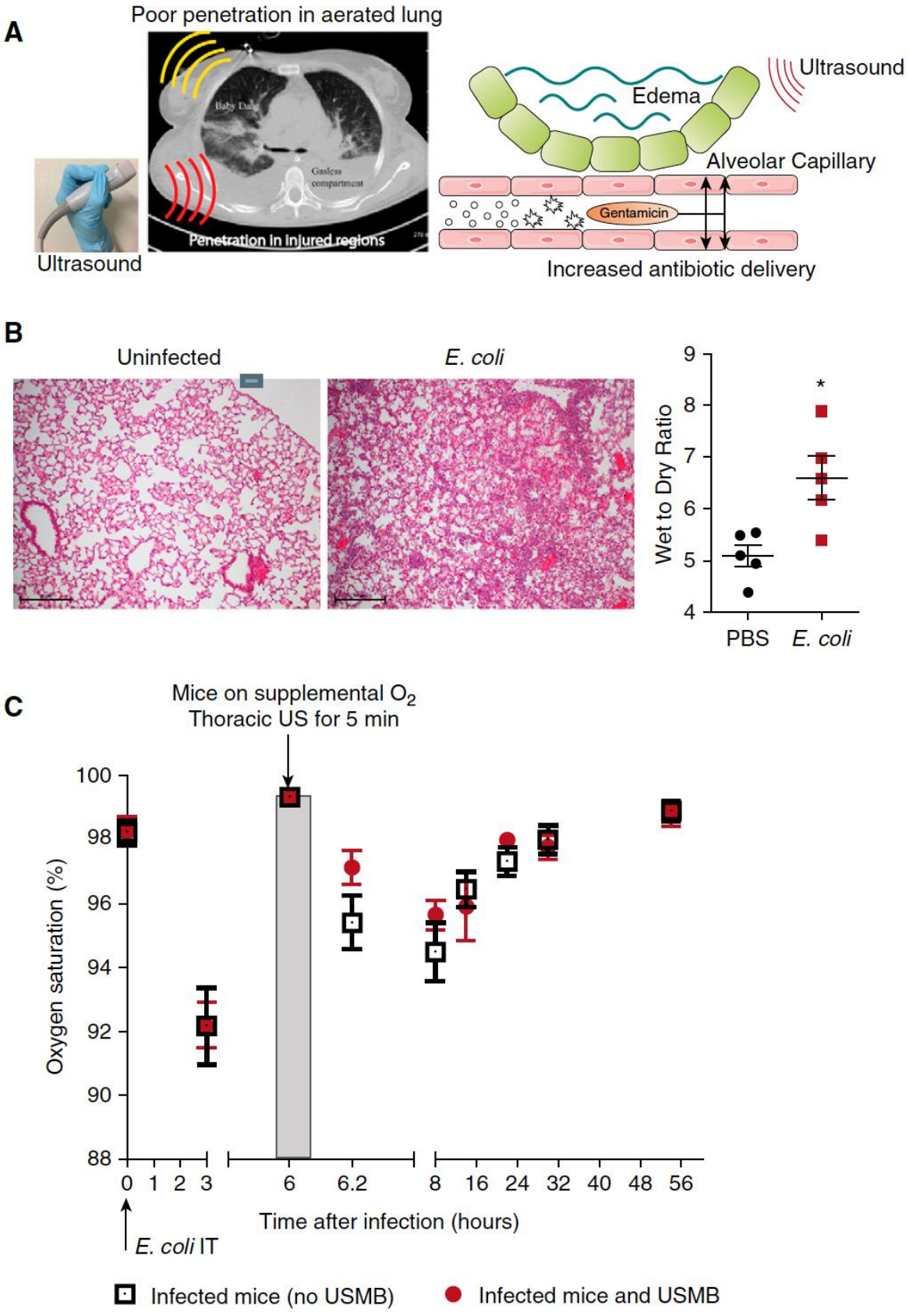
A
Poor penetration in aerated lung
Ultrasound
Penetration in injured regions
Gasless compartment
Edema
Ultrasound
Alveolar Capillary
Gentamicin
Increased antibiotic delivery
B
Uninfected
E. coli
Wet to Dry Ratio
PBS
E. coli
C
Mice on supplemental O2
Thoracic US for 5 min
Oxygen saturation (%)
Time after infection (hours)
E. coli IT
Infected mice (no USMB)
Infected mice and USMB

Figure 3.1. Concept and safety of ultrasound-induced microbubble cavitation (USMB) therapy to increase drug delivery to the injured lung. (A) Left panel shows an ultrasound (US) probe applied to the surface of the chest. In the normal regions, air-filled regions of lung cause scattering of the US waves (yellow waves). In contrast, damaged areas of the lung with acute respiratory distress syndrome are atelectatic or filled with fluid and allow penetration of the US beam (red waves). Note the marked heterogeneity of the lung in acute respiratory distress syndrome, with black (air-filled) areas of the lung interspersed with white (fluid-filled or atelectatic) regions. Right panel shows that cavitation of circulating microbubbles caused by the US pulse leads to enhanced cellular uptake of drugs in the vicinity of the microbubbles. The effect is similar whether the drugs are bound to or encapsulated by the microbubble or merely in close proximity. (B) Mice were infected with Escherichia coli intratracheally (IT). Representative hematoxylin and eosin–stained images from lung sections of uninfected and E. coli–infected mice are shown. Scale bars, 50 μm. Note the alveolar infiltrate and neutrophil recruitment. Far right panel shows that mice develop significant lung edema as measured by lung wet-to-dry ratio 6 hours after infection (*$P < 0.05$). (C) Safety study of arterial oxygen saturation as measured by pulse oximetry during and after the experiment. Mice were infected IT with E. coli as in B and developed hypoxemia within 3 hours. Mice were anesthetized with inhaled isoflurane and received supplemental O2 during USMB (gray rectangle). This accounts for the rise in arterial oxygen saturation. Afterward, animals were placed on room air and monitored for 48 hours. Control mice were infected but did not receive USMB. Note the comparable profile of O2 saturation in USMB-treated (red circles) and control mice (open squares). Data are mean and SEM ($n = 13$ [control] or 14 [USMB] mice per group from 0–8 h and $n = 8$ per group from 14–54 h). No antibiotics were administered in this safety experiment, and all mice survived. PBS = phosphate-buffered saline.

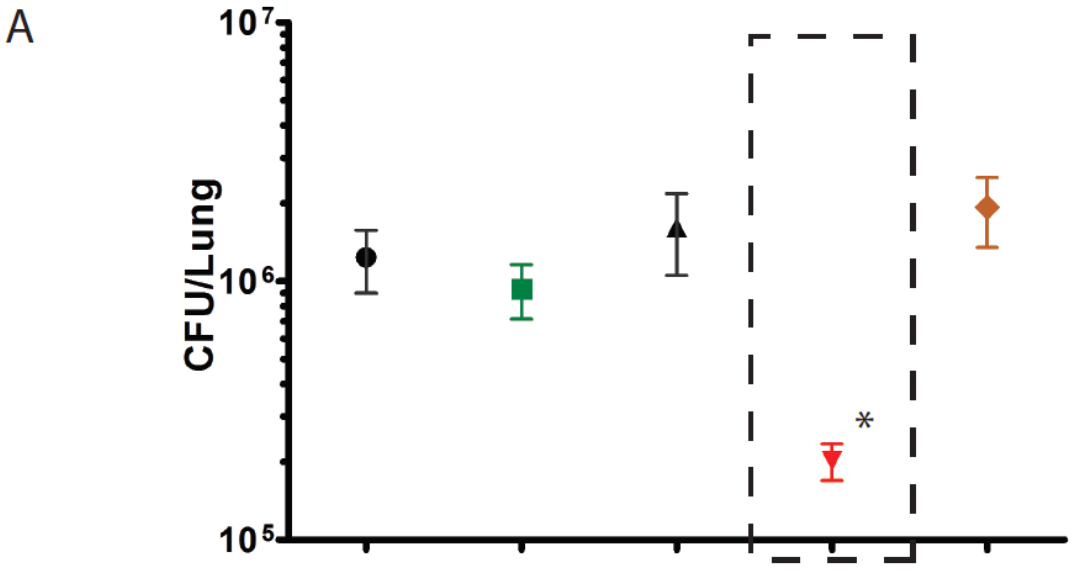

Intraperitoneal Abx	None	Gent	Gent	Gent	None
Intravenous MB	None	None	MB	MB	MB
Ultrasound	None	None	None	5 min	5 min

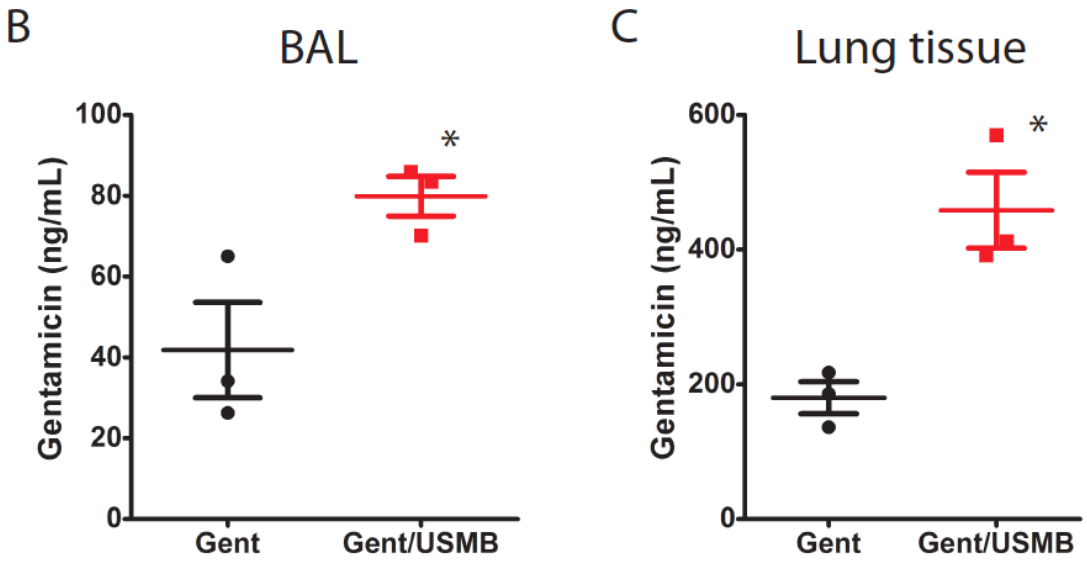

Figure 3.2. Effect of ultrasound-induced microbubble cavitation (USMB) treatment on the delivery and efficacy of gentamicin for Escherichia coli pneumonia. (A) Male C57BL/6 mice were infected intratracheally with 5×10^7 cfu of E. coli. Six hours later, mice received 1.5 mg/kg gentamicin (Gent) or no antibiotics (Abx) by intraperitoneal injection. Thirty minutes later, mice received an injection with 1 × 109 DEFINITY microbubbles (MB) into the tail vein, followed by thoracic ultrasound administration. Two hours later, mice were killed, and their lungs were homogenized to measure colony-forming units (CFUs). Control groups are as indicated. Data are mean ± SEM with n = 7 mice per group. Note the almost 1-log reduction in CFUs in mice receiving USMB with Gent (red triangle in dashed box) compared with control animals, including animals that received ultrasound and MB but no Abx. *P = 0.0013 by one-way ANOVA. By Dunn's multiple comparisons test, P < 0.05 for Gent/USMB vs. Gent alone and P < 0.01 for Gent/USMB vs. all other groups. (B) BAL concentrations of Gent by ELISA in infected mice treated with 1.5 mg/kg Gent alone or in combination with USMB. Concentrations were measured 30 minutes after USMB treatment. *P = 0.04 by two-tailed t test; n = 3 mice per group. (C) Corresponding lung homogenates probed for Gent, per gram of lung. *P = 0.03 by two-tailed t test. Data in B and C are mean and SEM.

CHAPTER 4: ULTRASOUND AND MICROBUBBLES FOR PRECISION DRUG DELIVERY IN A LARGE ANIMAL MODEL OF LUNG INJURY

4.1 Background

Acute respiratory distress syndrome (ARDS) is one of the most common disorders seen in critically ill patients. Despite optimal supportive care, the mortality rate in the most severe cases remains approximately 40% (Villar et al., 2014). ARDS is a progressive disorder that is characterized by a build-up of fluid in the lungs which results in pulmonary edema, hypoxemia and a loss of lung compliance (ARDS Definition Task Force et al., 2012). It occurs due to increased permeability of the alveolar-capillary membrane leading to protein-rich fluid accumulation in the alveoli. This syndrome can be caused by a myriad of direct and indirect lung insults however the most common precipitant of ARDS is bacterial- and viral-induced pneumonia (Bellani et al., 2016). Other than therapy directed at the underlying cause (e.g. antibiotics for bacterial pneumonia), there are currently no specific treatments for ARDS. Intensive care unit (ICU) patients with this disorder are typically managed with mechanical ventilation and other forms of supportive care aimed at preventing complications.

Computed tomographic scans of an ARDS lung typically demonstrate heterogeneity: consolidated, injured regions interspersed with regions that appear aerated and more healthy (Maunder et al., 1986). This lung mosaic constitutes a challenge for potential therapies. For example, mechanical ventilation – while life-saving - preferentially inflates normal regions of the lungs, predisposing to overdistension and aggravating lung damage (Beitler et al., 2016). Likewise, inhaled pharmacotherapies are preferentially directed to the non-edematous lung regions where they can cause adverse effects. In addition, oral and parenteral compound administration results in non-pulmonary drug delivery and may induce off-target and toxic effects. These issues indicate the necessity of delivering therapeutics specifically to the regions of the lung that are injured in ARDS.

Ultrasound and microbubble-mediated (USMB) drug delivery is a technique that is able to increase the deposition and efficacy of a number of compounds in various target organs and tissues such as the heart (Liu et al., 2015), brain (Zhao et al., 2018), kidneys (Gao et al., 2014), muscle (Cao et al., 2015) and tumors (Jing et al., 2019). Microbubbles are spheres of about 1-3 μm in diameter that have a gas-filled core and a shell composed of polymers, protein, or lipids. Certain microbubble formulations, such as Definity and Optison, are Food and Drug Administration (FDA)- approved as ultrasound contrast agents and are commonly used during echocardiograms. During USMB, the ultrasound transducer is directed to the tissue or organ of interest. Intravenously- administered microbubbles can be combined with a selected drug or therapeutic in various ways; the therapeutic can be encapsulated into the microbubble, attached to the microbubble shell, or can simply be co-administered. Microbubbles circulating through the target tissue will oscillate and cavitate in response to the applied ultrasound energy; this oscillation and cavitation results in enhancement of drug uptake by the surrounding tissues through two main mechanisms: sonoporation, which is the formation of tiny transient pores in nearby cell membranes, and increased endocytosis (Peruzzi et al., 2018).

Despite its apparent simplicity, the use of ultrasound on the lungs has traditionally been limited since air scatters and reflects ultrasound energy. However, in lung diseases such as pneumonia and ARDS, the air content in the lung is decreased and the density of the lung is increased due to the presence of fluid. In ARDS, the air content may decrease to the point where the whole parenchyma can be viewed, referred to as consolidation of the lung (Baston & West, 2016). In principle, ultrasound should only cavitate microbubbles circulating through edematous and injured regions since penetration of ultrasound energy is limited to these areas. In contrast, ultrasound cannot cavitate microbubbles circulating in healthy lung regions due to the scattering induced by air. There is also the possibility that microbubbles may accumulate in the injured lung regions due to their extravasation from the circulation. USMB drug delivery may therefore specifically enhance compound deposition in the regions of the lung that are injured or edematous. Our group was the first to demonstrate the feasibility of this concept: we established that USMB enhanced the delivery and efficacy of parenterally-

administered gentamicin in the lungs of an *Escherichia coli* (*E. coli*)-induced ARDS mouse model (Sugiyama et al., 2018), resulting in a ten-fold increase in lung bacterial killing. Importantly, this occurred at a low dose of gentamicin that by itself (i.e. in the absence of USMB) had no effect on bacterial colonies.

In follow-up to this work, we wished to evaluate the possibility that USMB might allow for increased compound deposition in the injured lung of a large animal model, which would suggest its feasibility in humans. In order to investigate this possibility, we used Evan's blue dye (EBD) as our USMB-delivered compound to the injured lung lobe of a porcine pneumonia model. We demonstrated that USMB enhances delivery of EBD to the injured lung lobe in pigs, supporting its potential utility in the delivery of therapeutic agents to injured lung regions in large animal models.

4.2 Methods

USMB Safety Experiments

C57BL/6J male mice aged 12-14 weeks old were purchased from Jackson Laboratories in Bar Harbor Maine. Mice were housed in the vivarium at St. Michael's Hospital and were provided access to food and water. Mice were provided one week of acclimation prior to the start of the study. All mice were infected in the designated Biosafety Level 2 facility in the vivarium where they were kept until the end of study. Experimental procedures were approved by the St. Michael's Hospital Animal Care Committee (ACC 772).

Mice were anesthetized with 5% isoflurane. The depth of anesthesia was monitored by breathing rate and toe pinch response. Once sedated, mice were intranasally infected with 5.8 X 10^5 plaque-forming units (PFUs) of influenza A virus (HKx31;H3N2) diluted with PBS to a total volume of 80 µl; virus was originally obtained from Dr. Tania Watts and propagated in accordance with published protocols (Balish et al., 2013). This infection results in an 70-100% mortality rate over the subsequent 12 days preceded by hypoxemia, lung edema and weight loss (Sugiyama et al., 2015). Mice were randomly allocated into either the treatment or control group.

Five days post-infection, mice were administered USMB treatment or control treatment. Mice in the USMB group were sedated with 3% isoflurane, administered 1 X

10^9 Definity (Lantheus Medical Imaging) (dose based on previous work (Sugiyama et al., 2018)) microbubbles diluted in PBS to a total volume of 100 µl intravenously through the tail vein, and were provided chest ultrasound for 5 minutes. Mice in the control group were anesthetized in an identical manner but received 100 µl of PBS instead of microbubbles and no thoracic ultrasound.

For ultrasound, we used a SONOS 5500 (Phillips Healthcare) ultrasound machine and an S3 phased array transducer which was positioned over the shaved chest of mice to induce microbubble cavitation in the lungs. The following ultrasound settings were used on mice; transmitter frequency, 1.3 MHz; 67 V; 0.2 W; mechanical index, 1.5; depth, 7 cm; pulse interval, 5 seconds. These settings were identical to our prior publication and were well tolerated by mice with no effect on arterial oxygen saturation (Sugiyama et al., 2018). One-hour post-treatment, mice were sacrificed via cardiac puncture and lungs were collected for analysis of lung edema or lung injury by histology. Lungs from healthy mice were also collected and analyzed as a control.

Measurement of edema

Following cardiac puncture, mice were injected with 5 ml of PBS through the left ventricle of the heart. Lungs were then collected and weighed immediately on pre-weighed plastic boats to obtain the wet lung weight. Lungs were then placed in a 64°C incubator and weighed every 24 hours until the weight remained consistent over two consecutive measurements. The final weight obtained was the dry lung weight.

Measurement of lung injury

Following sacrifice by cardiac puncture, mouse lungs were inflated with 600 µl of 10% buffered formalin and then immersed in this fixative for 48-hours prior to processing. Lungs were embedded in paraffin and sectioned at 5 µm serial sections, which were mounted on slides. Lung sections were dried overnight at 37°C then stained with hematoxylin and eosin. Sections were scored by a lung pathologist (D. Hwang, Sunnybrook Hospital) blinded to the allocation of animals using American Thoracic Society consensus criteria (Matute-Bello et al., 2011) and 20 random fields of view.

Escherichia coli

Escherichia coli (E. coli) from the American Type Culture Collection 25922 was grown in lysogeny broth (LB) overnight at 37°C at 250 rotations per minute (rpm). Prior to experimentation, the optical density (OD) of the *E. coil* was measured with a spectrophotometer (DU™ 800 spectrophotometer, Beckman Coulter); cultures were used in late exponential phase. 1 X 10^{10} CFU was delivered to each pig in a final volume of 150 ml.

Pigs

Female pigs ranging from 30 - 70 kg in weight were used. Pigs from Lifetime Solutions were used in all experiments. Sedation and anesthetization of pigs were conducted and managed by vivarium staff at St. Michael's Hospital. All experimental procedures involving pigs were indicated in an animal protocol that was approved by the St. Michael's Hospital Animal Care Committee (ACC 799).

Evan's blue dye pig experiment

Prior to the procedure, pigs were sedated and anesthetized, placed on a table with the right side down, and tilted at a 30° angle to elevate the head. A bronchoscope was then inserted through the trachea and directed through the RB2 airway to lead to the right middle lobe (RML). 1 X 10^{10} CFU of *E. coli* diluted in saline to a volume of 150 ml was administered to the RML through the bronchoscope. Pigs were then allowed to recover from anesthesia and returned to their pen; animals typically displayed a transient fever and mild hypoxemia (SpO2 > 90%). Twenty-four hours post-infection, pigs were sedated and placed on a table with the left side down. The right side of the chest was shaved. The ultrasound transducer was secured by a metal arm in a position that directed it to a consolidated area of the RML. Evan's blue dye (EBD) (Sigma-Aldrich, Catalog # 206334) was given at a dose of 6.5 mg/kg intravenously to pigs in a 0.5% solution diluted in saline. 6 X 10^{9} Definity microbubbles diluted in saline to a total volume of 5 ml were administered intravenously through a separate venous port. Both intravenous injections were administered simultaneously at a continuous rate over 8 minutes. Ultrasound treatment was provided for the duration of the infusion and for an

additional 2 minutes. A 500 ml intravenous saline flush was administered 20 minutes post-ultrasound treatment. Immediately prior to sacrifice, a needle was inserted into the RML under ultrasound guidance to indicate the area of insonation; no pneumothoraces were induced. Pigs were then euthanized with euthanyl at a dose of 1ml/5kg. Lung tissues of the RML and left upper lobe (LUL) as well as muscle, liver, kidney, and heart tissues were collected and stored for analysis.

The following ultrasound settings were used on pigs; transmitter frequency, 1.3 MHz; 69.6 V; 0.2 W; mechanical index, 1.5; depth, 8 cm; pulse interval, 2 seconds.

EBD analysis

Ten pieces of the RML and ten pieces of the LUL (each approximately 0.5 cm X 0.5 cm X 0.5 cm) were collected for EBD analysis. In regard to the treated RML, we collected lung pieces at 3 increasing depths from the surface where the ultrasound probe was positioned (Figure 4.1). Tissues were placed in 1 ml of formamide (Sigma-Aldrich) for 48 hours at room temperature. Quantification of EBD was obtained by measuring the OD at 620 nm (SpectraMAX 340, Molecular Devices). Lungs were then taken out of the solution and placed in a 64°C incubator for 48 hours to obtain the dry lung weight. A standard curve was used to convert the OD of the solution into µg/mL of EBD, which was then normalized to the dry weight of the tissue. The top three highest RML and LUL EBD µg/mL per dry lung weight (g) values were averaged for each pig. This average was then presented as µg/mL of EBD per dry lung weight (g) on a graph.

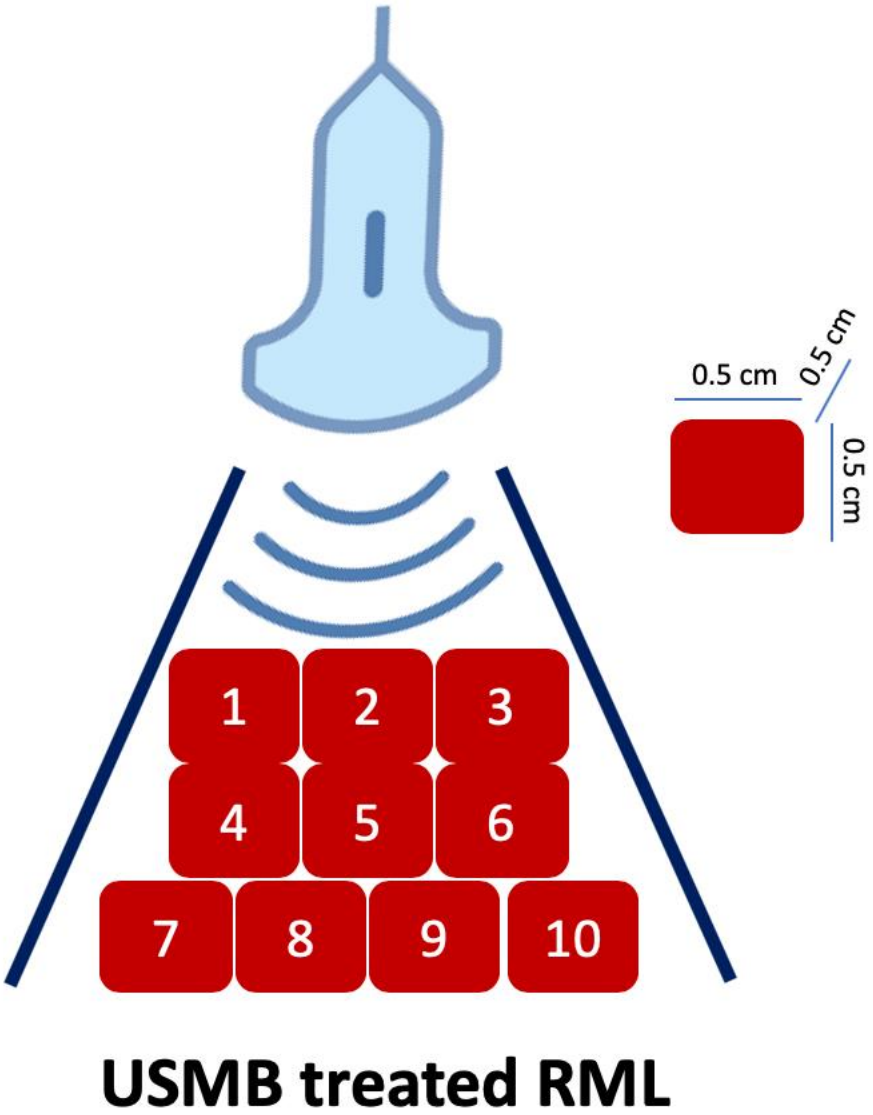

Figure 4.1 Lung tissue collection for EBD analysis. At sacrifice 10 pieces of the treated RML were collected for EBD analysis that were each 0.5 cm X 0.5 cm X 0.5 cm. These pieces were taken at 3 increased depths from the treated surface of the RML. Three pieces were taken from the surface (0 – 0.5 cm) another 3 pieces at the 2nd depth (0.5 – 1 cm), and 4 from the 3rd depth (1 – 1.5 cm). Four pieces were taken at the final depth because ultrasound waves spread outwards and therefore target a greater width at increased depth.

4.3 Results

USMB is safe to use on the injured lung

We previously reported that USMB does not affect oxygen saturation in an *E. coli*-induced ARDS mouse model (Sugiyama et al., 2018). To extend these findings, we analyzed the effect of USMB on lung edema and histologic lung injury. Mice were infected intranasally with human influenza virus; this results in progressive lung injury, hypoxemia and death approximately 6-9 days post-infection (Sugiyama et al., 2015). Five days post-influenza infection, mice were administered microbubbles and chest ultrasound (using identical settings as published previously (Sugiyama et al., 2018)) for 5 minutes while control mice were treated identically but received mock ultrasound treatment. Mice were sacrificed 1-hour after treatment and lungs were collected for blinded histological analysis that was scored according to consensus criteria (Matute-Bello et al., 2011). Infected mice that received USMB had a similar lung injury score compared to infected mice that received the control treatment **(Figure 4.2.A).** In addition, infected mice that received USMB had similar lung wet-to-dry ratios as infected mice that received the control treatment. Thus, USMB does not worsen lung injury or lung edema **(Figure 4.2.B).** We do not believe that our induced lung injury is saturated however, in order to confirm, we could infect mice with a reduced concentration of influenza and observe if USMB has an effect on lung injury.

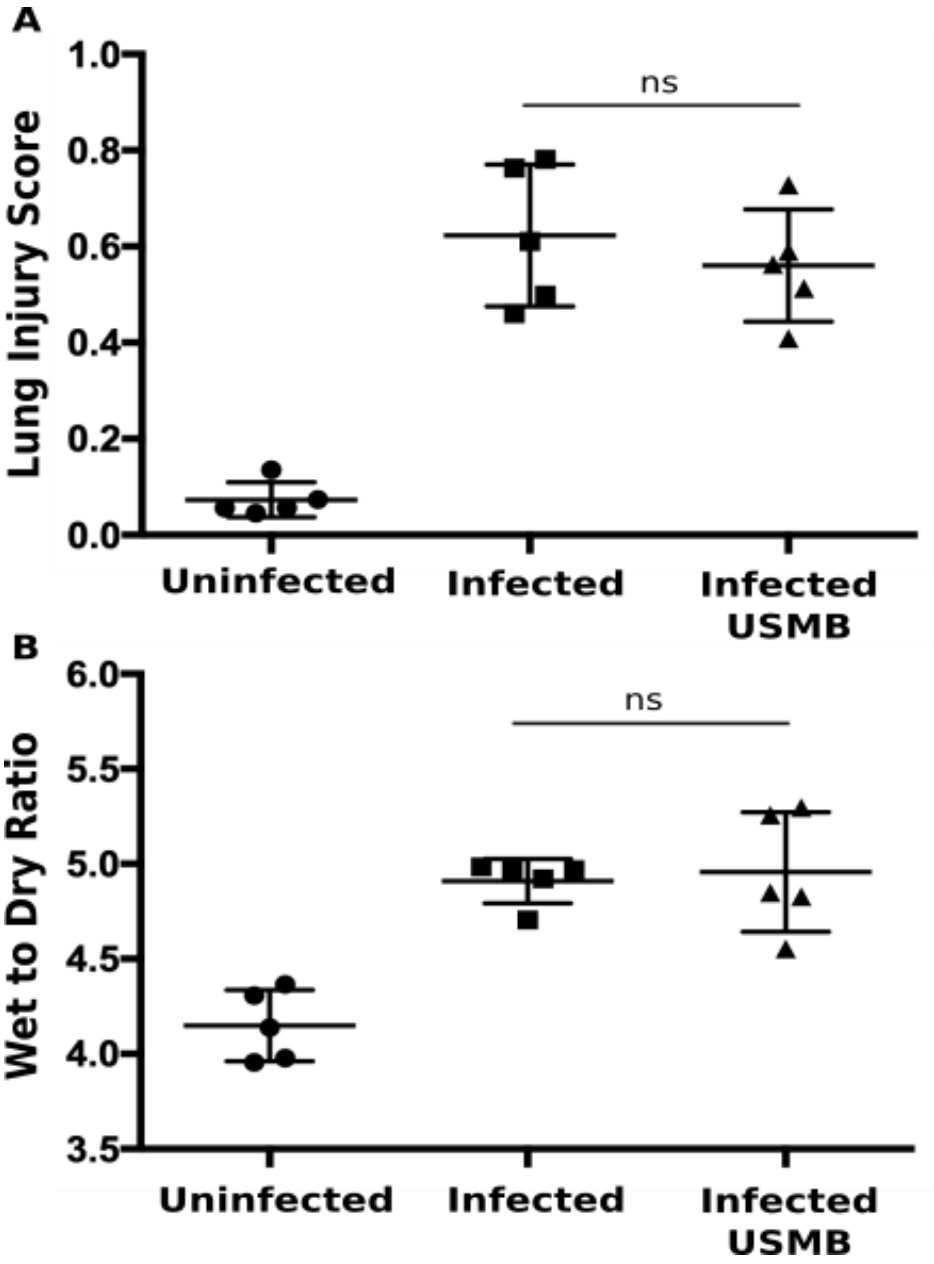

Figure 4.2. USMB is safe to use to increase drug delivery to the injured lung. Mice were intranasally infected with influenza. Day-5 post-infection a group of mice received USMB. Lungs were collected 1 hour after USMB or control anesthetic and were analyzed for lung injury or edema. **(A)** Lungs of mice were fixed in formalin for 48 hours, then processed and paraffin embedded. Lung slices of 5 um were cut onto slide and hematoxylin and eosin–stained. Images were blindly scored by pathologist, Dr. David Hwang. Lung slices were scored based the following criteria; neutrophils in the alveolar space, neutrophils in the interstitium, hyaline

membranes, proteinaceous debris, and alveolar thickening. These factors were combined to generate a final lung score of 0 to 1; 0 indicating a perfectly healthy lung and 1 indicating the worst damage. Lung scores between uninfected, infected, and infected + USMB mice were compared. **(B)** Lung edema was measured by wet to dry lung ratio. Wet lung weights were recorded following tissue collection from mice, then placed at 64 °C. Lungs were weighed every 24 hours until the weight was consistent between two consecutive measurements. The ratio of wet lung weight to dry lung weight was calculated and graphed. (Data is mean ± SEM; n=5 for all groups; ns = non-significant).

E. coli-induced pneumonia porcine model

We previously demonstrated that USMB can increase the deposition and efficacy of gentamicin at a low dose in the lungs of an *E. coli*-induced ARDS mouse model (Sugiyama et al., 2018). However, to determine whether USMB could exert a similar effect in humans, a larger animal model was needed. Female pigs (30 – 70 kg) were infected bronchoscopically with 1 X 10^{10} CFUs of *E. coli* (our institution does not permit porcine influenza infections). Twenty-four hours after infection, ultrasound imaging of the right middle lobe (RML) displayed lung edema and consolidation **(Figure 4.3.C)**; an advantage of this model is that the left upper lobe of each animal **(Figure 4.3.D)** serves as an internal control**.** At necropsy, injury of the RML was grossly apparent as evidenced by its dark red colour and increased edema **(Figure 4.3.A).** The healthy LUL remained a light pink colour and did not appear edematous **(Figure 4.3.B).** The degree of injury in the RML was sufficient to allow penetration of ultrasound energy and visualization of circulating microbubbles (**Figure 4.3.C**); in contrast, no circulating microbubbles could be seen when the ultrasound transducer was applied to the LUL (**Figure 4.3.D**).

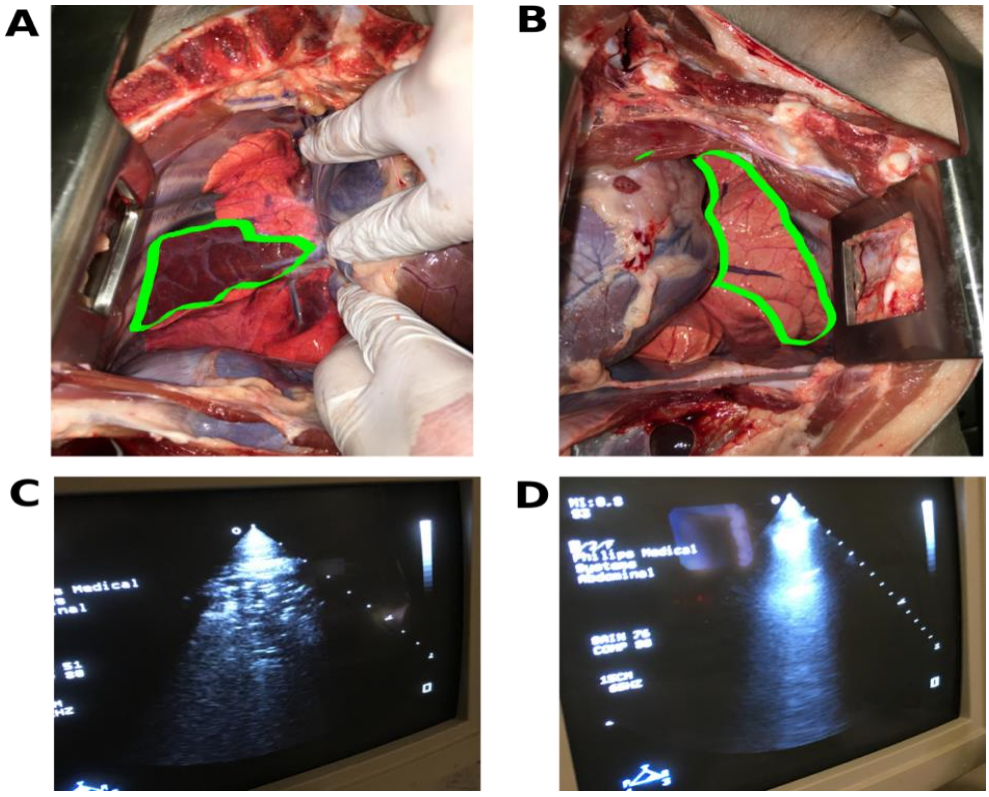

Figure 4.3. *E. coli*-pneumonia porcine model. A bronchoscope was directed to the right middle lobe (RML) where $1X10^{10}$ CFU of *E. coli* in a total volume of 150 ml was administered. Twenty-four hours post-infection **(A)** the RML, which is outlined in green, presented as a dark red colour and appeared injured at necropsy. In each pneumonia pig experiment, the left upper lobe (LUL) was collected and analyzed as an internal healthy control. **(B)** At necropsy the outlined LUL appeared healthy. Prior to necropsy, ultrasound was used to image the RML and LUL for the presence of edema. **(C)** The ultrasound transducer was directed to the RML. The opaque regions indicated areas of lung consolidation which denoted the presence of edema. **(D)** Ultrasonography of the LUL showed no consolidation. Note, the vertical opaque region here is a rib.

USMB enhances the deposition of EBD in the injured lung in pigs

Ultrasound-mediated microbubble cavitation leads to enhanced drug delivery whether the drug is bound to or encapsulated by the microbubbles or merely in its vicinity. As proof of principle in our pig pneumonia model, we assessed the ability of USMB to increase the deposition of circulating Evans Blue dye (EBD) in the injured RML. Evans Blue binds with nanomolar affinity to albumin and its accumulation in tissue can be quantified by spectrophotometry. This makes it a sensitive and inexpensive marker of USMB-induced internalization. Twenty-four hours following *E. coli*-infection of the RML, pigs were administered EBD intravenously simultaneously with microbubbles; the ultrasound transducer was applied to the RML. Pigs that received EBD with USMB treatment displayed significantly higher levels of EBD in the injured RML compared to the healthy LUL **(Figure 4.4.B).** The accumulation of EBD in the RML was not simply due to lung injury since pigs that received EBD without USMB did not exhibit any significant difference in EBD levels in the injured RML versus the uninjured LUL **(Figure 4.4.C).** Next, we aimed to identify if microbubbles alone or ultrasound alone could increase EBD deposition in the injured lung in pigs. Injection of Evans Blue dye with Definity microbubbles *without* ultrasound resulted in no difference in EBD levels in the infected RML versus the healthy LUL **(Figure 4.4.D).** Similarly, ultrasound administered to the RML without microbubbles did not enhance EBD deposition in the RML compared to the LUL **(Figure 4.4.D).** As additional controls, in separate animals the ultrasound transducer was directed to a region of the uninjured LUL while simultaneously administering intravenous EBD and microbubbles. Under these conditions there was no significant difference in EBD levels in the healthy lung region that received US compared to a healthy lung region that did not **(Figure 4.4.C).** Thus, the accumulation of Evans blue dye in the lung required three conditions: the presence of *injured* lung, the administration of thoracic ultrasound, and the administration of microbubbles. Thus, in a large animal model, USMB is effective at enhancing the uptake of circulating molecules specifically in the injured lung.

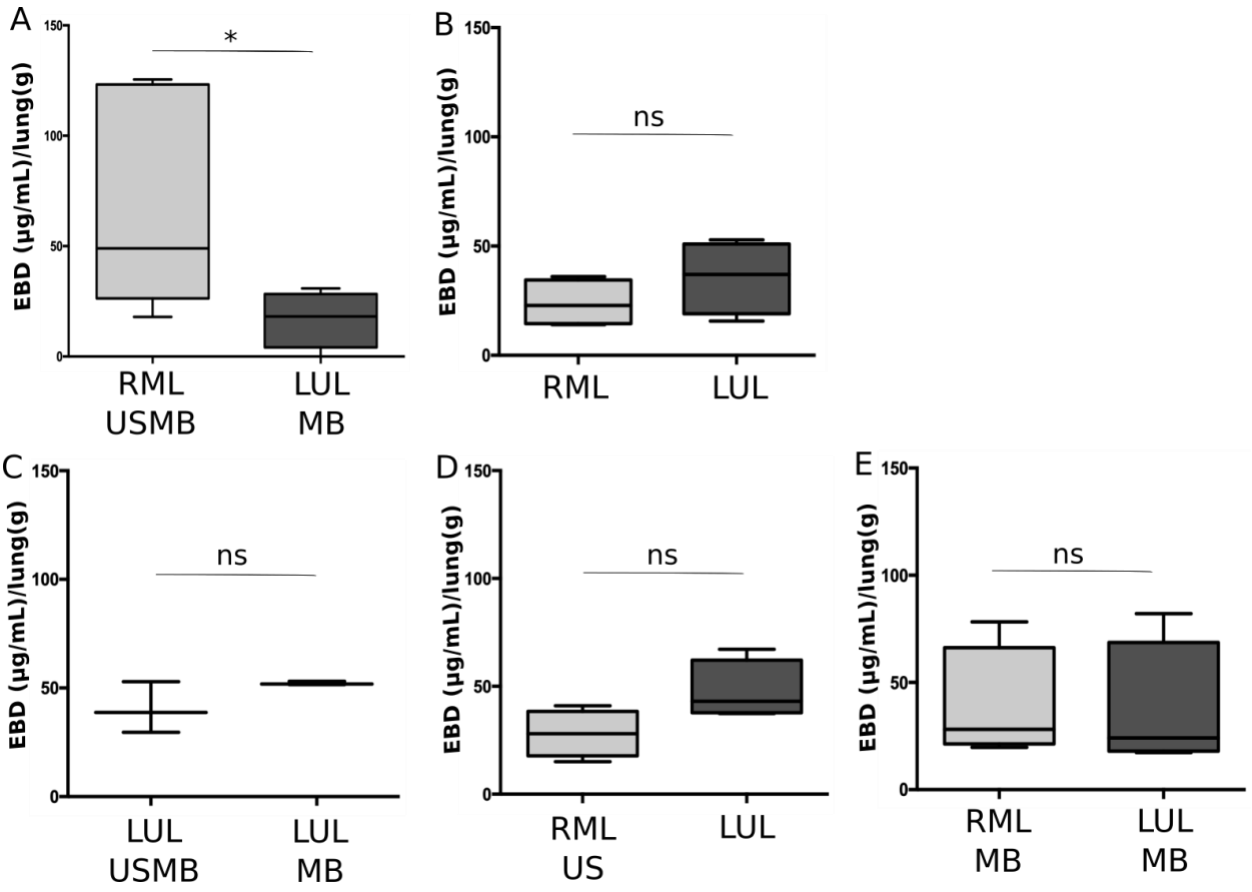

Figure 4.4. Ultrasound induced microbubble-cavitation (USMB) increases EBD deposition in the injured lung in an *E. coli*-pneumonia porcine model. A bronchoscope was used to delivery 1 X 10^{10} CFUs of *E. coli* to the RML. EBD and USMB treatment were administered 24-hours post-infection. Ten samples (0.5 cm X 0.5 cm X 0.5 cm) of the RML and the LUL were quantified for EBD deposition. The three highest values of each lobe were averaged and graphed to increase the sensitivity of the assay and to avoid sampling error (since we are unaware of the specific region that was insonated) **(A)** Pigs that received EBD with USMB, ultrasound directed to the injured RML (n=6). **(B)** Pigs that received EBD without USMB (n=4). **(C)** Pigs that received EBD with USMB, ultrasound directed to a healthy area on the LUL (n=3). **(D)** Pigs administered EBD with ultrasound directed at the injured RML (n=4). **(E)** Pigs that received EBD with microbubbles (n=4). (Data is mean ± SEM; *$p < 0.05$; ns = non-significant).

4.4 Discussion

We previously reported that USMB was able to enhance deposition of an aminoglycoside antibiotic in the murine lung, increasing bacterial killing almost 10-fold; this was achieved at a systemic dose that by itself was ineffective (Sugiyama et al., 2018). We now extend these findings to show that USMB facilitates delivery of circulating molecules in a porcine model of pneumonia. These much larger animals more closely approximate the size of a human patient. Importantly, we also show that USMB has no detrimental effect on the severity of lung injury or on the degree of lung edema.

Like any new therapeutic technique, safety is the primary concern. Definity microbubbles are routinely used in diagnostic ultrasound imaging, including in ICU patients. In a large cohort study of such patients, mortality did not differ between those who received an echocardiogram with or without ultrasound contrast (Exuzides et al., 2010). That said, the ultrasound parameters used in imaging may differ from those used in USMB drug delivery. Specifically, the mechanical index (MI), a theoretical value that measures the amount of energy administered and the resulting bioeffects, is higher in USMB drug delivery (Peruzzi et al., 2018) based on the assumption that sufficient energy to induce microbubble cavitation is required to induce enhanced drug uptake by the surrounding cells. The maximum mechanical index (MI) approved by the FDA for clinical use is 1.9 (Nelson et al., 2009); our study in mice and pigs used a MI of 1.5. In our previous study with aminoglycosides, USMB had no detrimental effect on arterial oxygenation as measured up to 48 hours after its administration (Sugiyama et al., 2018). Together with our current findings showing no effect on lung edema or on lung histology (e.g. Figure 4.2), the data suggest that USMB is not harmful to the lung. Our data leave open the possibility that an even lower MI would be sufficient for USMB-induced drug delivery. Accordingly, further research is ongoing to determine the optimal ultrasound settings for USMB-mediated drug delivery.

In addition to safety, our study addresses the important issue of clinical translatability to humans. The pigs in our study ranged from 30 to 70 kg, similar in size to a small human, and developed a clearly demarcated RML pneumonia that remained apparent almost 2 days after bronchoscopic infection. Despite the much larger size of

pigs compared to mice, ultrasound was able to induce RML-uptake of Evans Blue dye in a microbubble- and injury-dependent manner. Specifically, neither microbubbles alone nor ultrasound alone had any effect. It is noteworthy that the enhanced delivery of EBD was observed notwithstanding theoretical concerns of hypoxic vasoconstriction to the injured lung. It is also worth noting that we detected enhanced deposition of EBD several cm into the lung, at times limited by the thickness of the treated area (data not shown). While the average human thorax is about 15-25 cm in diameter (Bellemare et al., 2003), thoracic ultrasound is theoretically able to penetrate a maximum of 10 cm (Meineri, 2012). Thus, our data indicate that USMB is feasible in a larger animal. For it to be practical in humans, a much larger transducer would be required. In addition, a software algorithm to insonate an area only if microbubbles can be visualized (i.e. in the injured lung regions) would be useful at limiting unnecessary ultrasound exposure.

While our clinical interest is in ARDS, our pig model is one of lobar pneumonia. This was out of necessity as a pig ARDS model would essentially require an animal intensive care unit. Similarly, while our murine influenza model allows for over a week of follow-up before death (Sugiyama et al., 2015), our animal care facility does not permit influenza infections of pigs due to concern over swine flu. This limited us to short-term infections with *E. coli*. However, our lobar pneumonia model allows us to definitively establish the ability of USMB to induce drug uptake specifically in the injured lung. This ability would be of great utility in ARDS, given the heterogeneity of the disorder. Given that the disease is typically worse in the dorsal regions of the lung, ultrasound would have to be applied to the dorsum of the patient for maximum effect. Fortunately, it is now recommended that patients with severe ARDS be placed in a prone position for about 16 hours a day (Guérin et al., 2013).

Beyond its potential therapeutic applications, USMB-mediated drug delivery is likely to be useful for research into the pathogenesis of ARDS. For instance, the ability to deliver genetic material specifically to the injured lung would facilitate investigations into the molecular mechanisms of lung microvascular leakage. One could speculate that USMB-mediated gene and drug delivery could prove useful in a number of lung disorders in which alveoli become filled or replaced, such as during fibrosis or neoplasia.

In conclusion, the treatment of ARDS is greatly complicated by its heterogeneity in a given patient. Ultrasound and microbubbles enable the targeted delivery of circulating drugs specifically to the injured lung, without worsening oxygenation (Sugiyama et al., 2018), edema or lung injury. This technique is therefore likely to facilitate both research into and the therapy of acute lung injury.

CHAPTER 5: DISCUSSION AND FUTURE DIRECTIONS

The use of USMB drug delivery appears beneficial at enhancing the deposition and efficacy of a number of therapeutics in various target tissues. Our group is the first to demonstrate USMB drug delivery to the lung. Considering the properties of ultrasound, only the consolidated or edematous areas of the lung will allow ultrasound wave penetration. Therefore, we hypothesized that USMB drug delivery would solely increase drug uptake in edematous, injured lung areas while avoiding aerated, healthy lung regions.

We demonstrated that USMB enhances the delivery and efficacy of gentamicin in the lungs of *E. coli*-infected mice. In this case, we administered a low dose of gentamicin (1.5 mg/kg) which was therapeutically ineffective without USMB application. We further presented the effectiveness of USMB compound delivery to the injured lung in a large animal model, suggesting feasibility in humans. In our porcine pneumonia model, USMB significantly enhanced EBD levels in the treated, injured RML compared to the uninfected LUL. In contrast, EBD levels were similar in the RML and LUL in pigs that did not receive USMB treatment. Further, USMB was not effective at increasing EBD in healthy, non-edematous lung tissue thus, the effect of USMB drug delivery on the lung requires injury or edema.

5.1 USMB for delivery of genetic material to the injured lung

Given our success enhancing the delivery of circulating compounds, we hypothesized that USMB would be able to enhance the delivery of genetic material (e.g. plasmids) specifically to the injured lung in both small and large animals. A number of issues need to be discussed regarding this hypothesis, including selection of microbubbles, choice of plasmid, and identification of the specific cells transfected by USMB (e.g. endothelial vs epithelial).

Microbubble selection

The literature suggests that cationic microbubbles are superior in both *in vivo* and *in vitro* gene delivery compared to Definity microbubbles.

DNA plasmids have been delivered with neutral, slightly anionic and cationic microbubbles in the literature however, it has been demonstrated that use of cationic microbubbles results in the most significant enhancement of gene delivery compared to other types of microbubbles. In one study, the delivery of a reporter plasmid expressing firefly luciferase (Fluc) with cationic microbubbles was compared to its delivery with neutral microbubbles in ultrasound-mediated gene delivery. Overall, bioluminescence was increased when either cationic or neutral microbubbles were used with ultrasound treatment (Panje et al., 2012). However, cationic microbubble delivery of the plasmid resulted in significantly higher gene expression in the murine hindlimb skeletal muscle compared to when the plasmid was administered with neutral microbubbles (Panje et al., 2012). These findings are supported by the following reasons; First, cationic microbubbles displayed a high plasmid loading capacity, whereas neutral microbubbles essentially had no binding capacity; and secondly, plasmid DNA was degraded after DNase treatment when combined with neutral microbubbles and was partially protected when mixed with cationic microbubbles (Panje et al., 2012). A similar study also confirmed that cationic microbubbles attached to plasmid DNA via charge-coupling which partially protected the plasmid from DNA degradation (D. S. Wang et al., 2012). In vascular endothelial cells, cationic microbubbles led to a 20-fold increase in plasmid transfection compared to neutral microbubbles (D. S. Wang et al., 2012). Further, *in* vivo ultrasound-mediated transfection of a plasmid to a murine hind limb tumor with cationic microbubbles resulted in a significantly higher plasmid expression 12-48 hours post-treatment compared to neutral microbubble plasmid delivery (D. S. Wang et al., 2012). In another study, gene transfection efficacy was compared between neutral and cationic microbubbles in various cell lines *in vitro*. It was determined that cationic microbubbles significantly increased gene transfection compared to neutral microbubbles in HEK-293 and not in SV-LEC, SVEC4-10, and b.END.3 cell lines (Tlaxca et al., 2010).

In terms of microbubble concentration, Panje *et al* demonstrated that increasing microbubble concentration for both cationic and neutral microbubbles resulted in higher plasmid expression in murine hindlimb skeletal muscle (Panje et al., 2012). However, the lowest cationic microbubble concentration used (1×10^7) was the most efficient over neutral microbubbles. When the concentration of cationic microbubbles increased past 1×10^8, there was no significant difference in plasmid transfection efficacy between cationic and neutral microbubbles (Panje et al., 2012). *In vitro* studies that optimized ultrasound parameters suggested that 3.3% volume concentration of Definity microbubbles was ideal for the highest cell permeability and viability (Karshafian et al., 2009).

Panje *et al* also explored the effect of plasmid dose on *in vivo* transfection using cationic and neutral microbubbles in ultrasound-mediated gene delivery. Gene delivery increased as plasmid dose increased when delivered with either microbubble type (Panje et al., 2012). However, cationic microbubbles gene delivery enhancement compared to neutral microbubbles was highest when the lowest DNA dose (10 µg) and lowest when the highest dose of DNA (50 µg) was delivered (Panje et al., 2012).

Data suggests that ultrasound parameters can affect the permeability and viability of cells and can be optimized for therapeutic approaches. *In vitro* in KTH-C cells, the therapeutic ratio, which is the defined as the ratio of permeabilized cells to viable cells, was considered under a number of ultrasound conditions. It was determined that cell permeability increases and cell viability decreases with increasing peak negative pressure, pulse duration, pulse repetition, and with decreasing pulse center frequency while using Definity microbubbles (Karshafian et al., 2009). Lower pressure may be better suited for compound delivery in cells as it induces membrane permeabilization that is reversible. In HEK-293 cells, the transfection efficiency of a plasmid increased at an ultrasound power intensity of 1 W/cm^2 to 2 W/cm^2, which was thought to be due to a change from microbubble low-amplitude oscillation to high-amplitude oscillation (Tlaxca et al., 2010). Further, plasmid transfection did not increase when the power intensity was greater than 2 W/cm^2 (Tlaxca et al., 2010).

Preliminary data from our lab suggests that cationic microbubbles can enhance GFP-plasmid deposition into the injured lung in the presence of ultrasound; however,

Definity microbubbles (which are relatively neutral) cannot **(Supplemental Figure 5.1).** This data is similar to the findings in the literature. Additional replicates are required in order to confirm if cationic microbubbles are superior to Definity microbubbles in genetic delivery to the injured lung in mice.

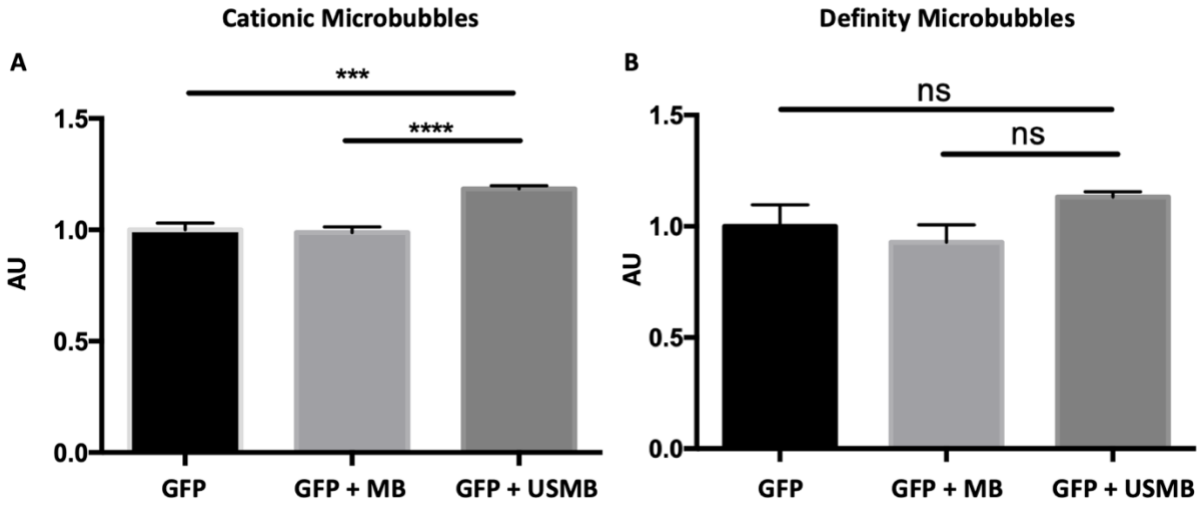

Supplemental Figure 5.1. Cationic microbubbles significantly enhance GFP plasmid deposition in the lung of influenza-infected mice in the presence of ultrasound however, Definity microbubbles do not. ***Methods:*** Mice were infected with influenza intratracheally (1.13 X 10^5 PFU; H3N2 – see influenza strain information in chapter 4.2). Day 3 post-infection mice were administered 10 µg of a GFP plasmid mixed with microbubbles (3 X 10^8 cationic / 1 X 10^9 Definity) intravenously and administered chest ultrasound for 5 minutes. Mice were sacrificed via cardiac puncture 24-hours after treatment and lungs were processed and imaged for GFP analysis. GFP intensity was quantified and normalized to the average value of mice that received GFP without microbubbles.

Overall, the data suggests that the use of cationic microbubbles in gene delivery is most efficient when using a low dose of both plasmid and microbubbles, at least in the context of the targeting of murine hindlimb skeletal muscle. It would be interesting to determine if this holds true in USMB gene delivery to the injured lung in our mouse and pig models.

Choice of genetic cargo to deliver

We aimed to use USMB to deliver genes to the injured lung endothelium in pigs in order to enhance the endothelial barrier and reduce lung edema. Tie2 expression was decreased in the injured RML in our porcine pneumonia model **(Supplemental Figure 5.2.A).** In pilot experiments, USMB with the use of cationic microbubbles enhanced Tie2 plasmid deposition in the treated, injured RML compared to the untreated, injured lingula **(Supplemental Figure 5.2.B).** In addition, USMB Tie2 delivery resulted in a decreased lung wet-to-dry ratio in the RML versus the lingula, suggesting it reduced edema **(Supplemental Figure 5.2.C).** While preliminary, this is the first demonstration *in vivo* that manipulation of Tie2 expression improves lung edema.

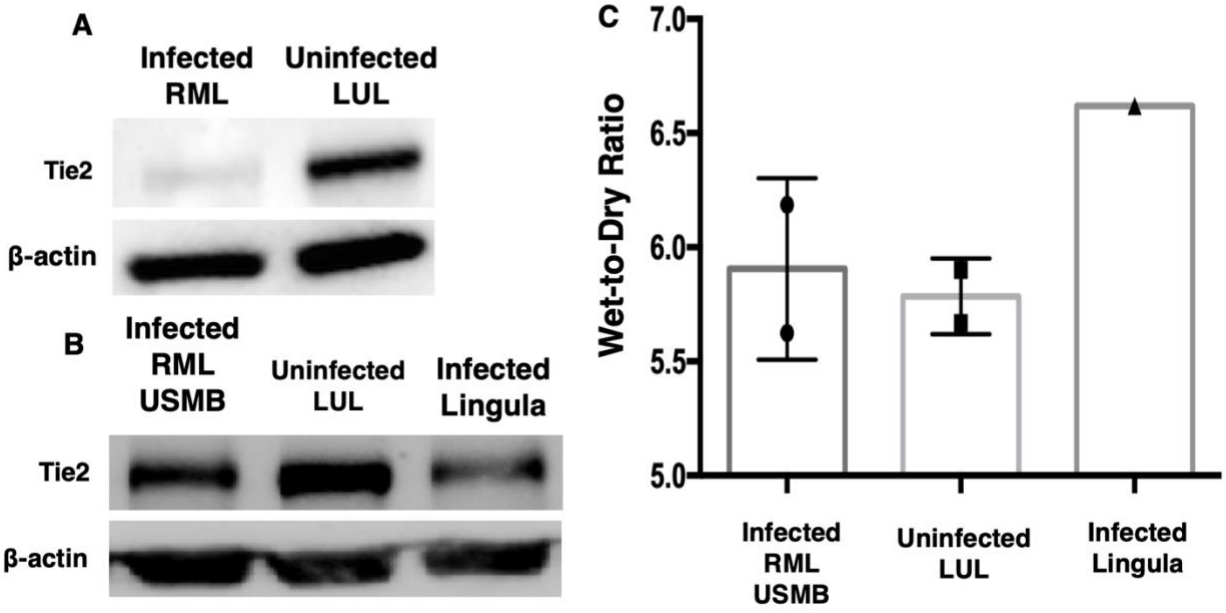

Supplemental Figure 5.2. USMB delivery of Tie2 to the injured right middle lobe in our pig pneumonia model. ***Methods:*** *E. coli* (1 X 10^{10} CFUs diluted with saline to 150 ml) was instilled into the right middle lobe (RML). Forty-four hours post-infection pigs were sacrificed and the infected RML and the uninfected left upper lobe (LUL) were collected for protein analysis. **(A)** Western blot images showing the expression of Tie2 (140 kD) in the infected RML and uninfected LUL. β-actin (42 kD) was used as a protein loading control. Tie2 levels were decreased in the infected RML compared to the internal uninfected LUL (n=2). **(B, C)** ***Methods:*** In this experiment, pigs were administered *E. coli* (1 X 10^{10} CFUs diluted with 150 ml of saline) to both the RML and the lingula (the anatomic equivalent of the RML on the left side). Twenty hours post-infection, 150 μg of Tie2 plasmid mixed with 3 X 10^{9} cationic microbubbles was intravenously administered to pigs while ultrasound was applied to the RML. Pigs were sacrificed 24-hours post-treatment and lung tissue (RML, lingula, and LUL) was collected and analyzed for Tie2 protein expression and lung edema. **(B)** Western blot quantifying Tie2 protein levels in the infected and treated RML compared to the uninfected and untreated LUL and infected and untreated lingula (n=2). **(C)** Lung wet-to-dry ratios of the infected and treated RML is lower than the infected and untreated lingula, suggesting that USMB delivery of Tie2 to the infected lung reduces lung edema.

Which cells take up genes following USMB treatment?

We demonstrated that USMB can increase the deposition of compounds to the injured lungs in mice and pig lung injury models. Although this is advantageous, it is important to determine which cells in the lung accumulate the majority of the administered compounds following USMB treatment. We hypothesized that compounds were taken up mostly by epithelial or endothelial cells, considering the lung is mainly comprised of these cell types. To investigate this question, a bicistronic plasmid, miRNA-126-GFP, which expresses miRNA-126 and GFP separately, was administered to influenza-infected mice with USMB treatment. Lungs were collected 24-hours after treatment, fixed, and stained. The co-localization of GFP with lung endothelial cells and lung epithelial type I cells was analyzed. GFP colocalized with endothelial cells suggesting that endothelial cells take up the GFP plasmid following USMB treatment in our influenza-induced ARDS mouse model **(Supplemental Figure 5.3).** Cao *et al* experienced a similar observation in ischemic hindlimb muscle of rats following USMB. The researchers demonstrated that miRNA-126-3p was delivered to both the vascular and peri-vascular area in the ischemic hindlimb muscle in rats (Cao et al., 2015). In order to colocalize delivery with a specific cell type, this group delivered a fluorescent miRNA to the ischemic hindlimb muscle with USMB. Day 1 post-USMB, fluorescent miRNA colocalized to endothelial cells (Cao et al., 2015). It would be interesting to observe if this finding holds true in delivery of other therapeutics or delivery to other organs.

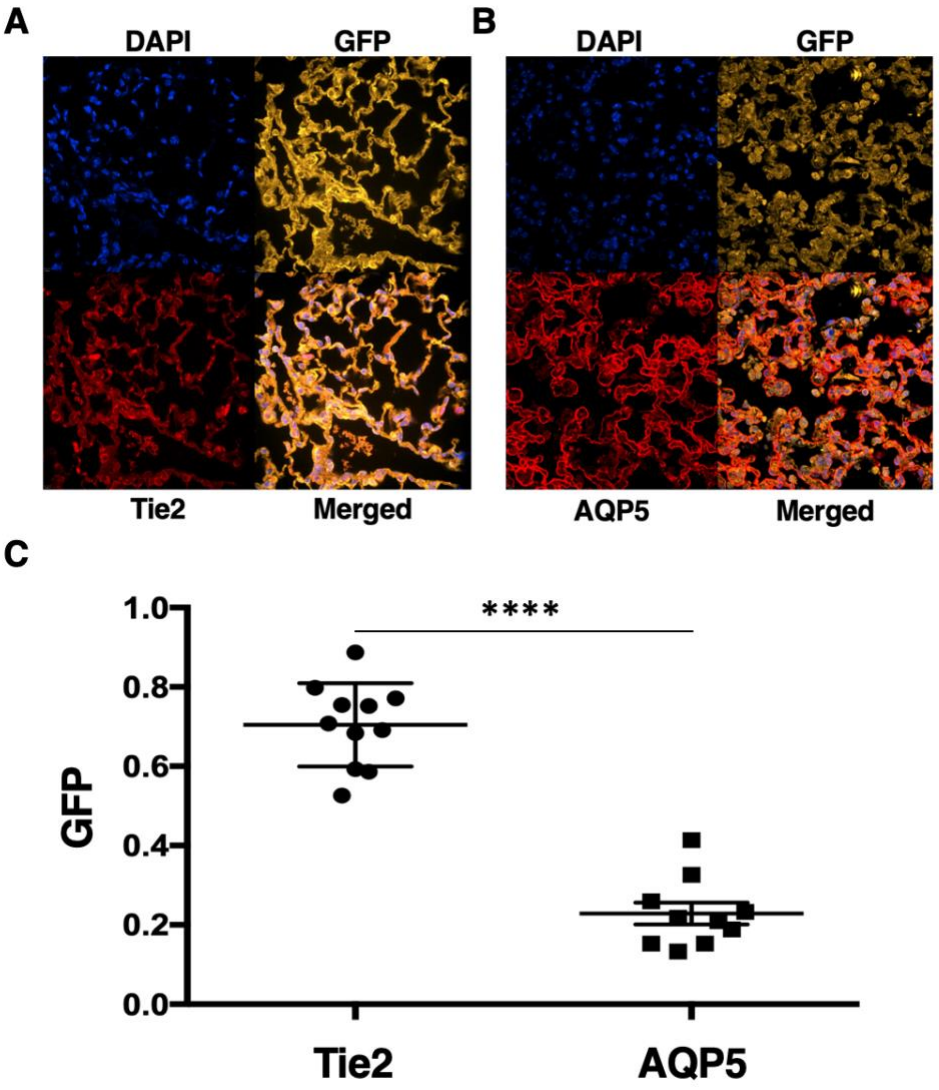

Supplemental Figure 5.3. USMB delivers GFP plasmid to endothelial cells in influenza-injured mouse lung. ***Methods:*** Mice were intratracheally infected with influenza (1.13×10^5 PFU; H3N2 – see influenza strain information in chapter 4.2). On Day 3 post-infection, mice were intravenously injected with 3×10^8 cationic microbubbles conjugated to 10 µg of a bicistronic miRNA-126-GFP plasmid and administered chest ultrasound for 5 minutes. Twenty-four hours after treatment, mice were sacrificed via cardiac puncture and lungs were collected for immunohistochemistry. Lung slices were stained with anti-GFP and either anti-Tie2 or anti-AQP5. (**A)** Nuclear DAPI staining (Top left) Anti-GFP staining (Cy3, top right); Anti-Tie2 (Cy5, bottom left); Merged DAPI, anti-GFP and anti-Tie2 (bottom right) **(B)** A) Nuclear DAPI staining (Top left) Anti-GFP staining (Cy3, top right); Anti-AQP5 (Cy5, bottom left); Merged DAPI, anti-GFP and anti-AQP5 (bottom right). **(C)** GFP was significantly co-localized to Tie2 (endothelial

cells) compared to APQ5 (epithelial cells) in the lung. Co-localization analysis was conducted based on the Manders split coefficients. (n=1; ****=p<0.0001).

5.2. Limitations

5.2.1 The effect of USMB drug/gene delivery to the injured lung on physiological outcomes

Although our study was the first to demonstrate the use of USMB drug delivery to the injured lung, it did have a number of limitations. The first limitation involves the lack of accounting for physiological outcomes in both our small and large animal models post-USMB treatment. In our *E. coli*-induced ARDS mouse model, we only demonstrated that USMB increased the deposition of gentamicin in the lungs and also that it reduced bacterial colonies in the lung. In this proof-of-principle study, we did not assess physiological outcomes in mice post-USMB delivery of gentamicin such as weight, temperature, activity, oxygen saturation, heart rate and mortality. This was not feasible because of the short-term nature of this model; at the dose of *E. coli* used, most mice actually recover spontaneously. Similarly, in our pig pneumonia model, we confirmed that USMB increased deposition of EBD in the injured lung. However, we are not certain if USMB delivery of either drugs or genes would result in improved physiological outcomes and reduced mortality in our pig pneumonia model. This is because both mice and pigs recover quickly from *E. coli* infection. We have observed that the administration of an *E. coli* dose that is too potent can induce mortality shortly after infection in mice. Therefore, this model would not allow us enough time for USMB treatment or for the assessment of physiological outcomes. If the dose is not as high and mice do not succumb to infection shortly afterwards, they typically fully recover in about 1-2 days post-infection without treatment. Thus, if we were to monitor physiological outcomes post USMB in this model, differences may only be based on solely short-term data. In order to assess the effect of USMB drug or gene delivery on physiological outcomes and mortality, our published 12-day long influenza-infected mouse survival model could be used (Sugiyama et al., 2015).

5.2.2 Does USMB drug delivery to the injured lung decrease off-target deposition?

Another limitation in this study is a lack of data suggesting that there is less deposition of drugs/genes in off-target organs when USMB is applied compared to in its absence. In our *E. coli*-induced ARDS mouse model, we administered a low dose of gentamicin to the lungs with USMB. We did confirm that there is increased gentamicin deposition in the lung therefore, there should theoretically be less gentamicin available to deposit in other organs and/or tissues. In addition, we used a low dose of gentamicin that is unlikely to cause any toxicities. However, considering that gentamicin use is often avoided due to the risk of ototoxicity and nephrotoxicity at even therapeutic doses, gentamicin levels in the ear, kidney, and other major organs should be quantified for safety reasons. If there is less gentamicin in the ear and kidney of USMB treated mice compared to control mice, this would suggest that USMB delivery of low dose gentamicin to the injured lung may avoid clinically common toxicities. Similarly, in our pig pneumonia model, EBD levels and gene (e.g. Tie2) expression in major organs such as the heart, liver, and kidney will have to be determined.

5.2.3 Which cells express USMB-delivered Tie2 plasmid?

Tie2 is a receptor that is enriched in endothelial cells however, 2-7% of monocytes also express Tie2 (Venneri et al., 2007). The expression of Tie2 is decreased in *E. coli*-infected pig lung. This decrease is mainly explained by a decrease in endothelial Tie2 expression because of the larger proportion of Tie2-expressing endothelial cells versus Tie2-expressing monocytes present in the lung. However, following USMB Tie2 gene delivery to the injured lung in pigs, we are unsure which cells in the lung are expressing it. Although we have demonstrated that USMB delivers a GFP plasmid to lung endothelial cells in mice, we are uncertain if this is consistent with USMB Tie2 delivery. In order to determine which cells are expressing the delivered Tie2 plasmid, a co-localization analysis could be conducted. Also, lung cells can be sorted based on their type and analyzed for Tie2 protein expression. These findings will confirm which cells are taking up and expressing the Tie2 plasmid in the injured lung

following USMB delivery. This may also provide insight into the mechanism in which Tie2 delivery reduces lung edema.

5.3. Future Directions

The literature on USMB drug delivery both *in vitro* and *in vivo* is inconsistent in terms of the various parameters used including but not limited to microbubble composition, microbubble concentration, therapeutic dose, and ultrasound settings. Each of these factors can have a significant impact on the degree of therapeutic deposition and efficacy in target tissues and can also affect potential safety concerns. These discrepancies between USMB parameters create difficulty in combining sets of data and confirming optimal parameters for therapy. A number of studies have compared various ultrasound parameters to suggest the most appropriate settings for USMB drug/gene delivery.

Ideally future experiments should be considered that test the effect of various USMB parameters on the delivery and therapeutic efficacy of compounds to the injured lung including the types of microbubbles used, the dose of microbubbles and drug/gene and varying ultrasound settings. However, the ideal settings used to deliver drugs to the injured lung in mice may not be consistent with the ideal parameters for pigs. First experiments that compare various USMB parameters in drug delivery to the injured lung should begin on mice. The optimal settings could then be tested on pigs for feasibility in humans. Optimization of ultrasound settings is the subject of ongoing research in our lab.

5.4. USMB gene delivery to the injured lung in mice (pilot experiments)

Methods:

For detailed information on mouse strains, pathogen strains, and ultrasound settings, please refer to section 4.2

USMB delivery of RNA to the injured lung in mice

Male mice (10-12 weeks old) were anesthetized with isoflurane and provided supplemental oxygen. A long, beveled catheter was fed through the trachea and into the right bronchus to deliver 5 X 10^7 CFU of *E. coli* (diluted in saline to a volume of 50 µl) to the right lung lobe. Six-hours post-infection, mice were again anesthetized, and their chest was shaved. Cationic microbubbles (1 X 10^8) incubated with 5 µg of RNA-tagged-Alexa-555 (Thermofisher) was intravenously administered via tail vein to the mice and chest ultrasound was applied for 5 minutes. Mice were sacrificed 10 minutes after treatment via cardiac puncture, their circulation was flushed with 5 ml of PBS and their lungs were collected and immediately frozen in optimal cutting temperature (OCT) compound. Frozen lungs were then sectioned at 5 µm, stained with DAPI, and imaged at 20X using the Zeiss slide scanner.

miRNA-126 overexpression in HPMECs in vitro

Human pulmonary microvascular endothelial cells (HPMECs) were seeded onto a 12-well plate at a 60% confluency. They were transfected with 1 µg of miRNA-126 or a control miRNA using HiPerfect (Qiagen, Valencia, CA). Twenty-four hours after transfection, cells were infected with influenza (H3N2) at a multiplicity of infection (MOI) of 1 for 24-hours. Cell lysates were analyzed via SDS-PAGE western blots using 15% polyacrylamide gels then transferred to nitrocellulose membranes. The membrane was blocked using 5% BSA and probed overnight at 4°C with the primary antibody. The next day, the membrane was washed, probed with horseradish peroxidase–conjugated secondary antibodies for 1 hour at room temperature, washed, and then visualized by enhanced chemiluminescence (Bio-Rad).

Lung tissue analysis of influenza-infected mice

Male mice (aged 10-12 weeks) were intranasally infected with influenza (H3N2) at 5.8 X 10^8 PFU (diluted in saline to a total volume of 80 µl). Mice were monitored daily for signs of distress (weight, temperature, oxygen saturation, and activity). On day 4 post-infection, mice were sacrificed via cardiac puncture, and lungs were flash frozen. Half the lung tissue was taken for qPCR analysis, where RNA was isolated (RNeasy Mini Kit, Qiagen), converted into cDNA via reverse transcriptase, and quantified for PIK3R2 mRNA (forward: 5'-CCCACAGCCCAGCTAATGAA-3'; reverse: 5'-ACTTCCAGAAGTCACAGGCG-3'). 18S was used as a reference gene. The other half of the lung tissue was homogenized in 1 ml of Radioimmunoprecipitation assay buffer (RIPA) per 100 mg of lung tissue. The supernatant was then analyzed for Tie2 protein expression via Western blot (see above for western blot protocol).

USMB gene delivery to the lung in influenza-infected mice

Male C57 mice (aged 10-12 weeks) were intratracheally infected with influenza (H3N2) at 1.13 X 10^5 PFU (diluted in saline to a total volume of 80 µl). Mice were monitored daily for signs of distress (weight, temperature, oxygen saturation, and activity). On day 3 post-infection, mice were anesthetized, intravenously administered cationic microbubbles (3 X 10^8) incubated with 10 µg of a miRNA-126-GFP plasmid (from Dr. Jason Fish) and provided chest ultrasound for 5 minutes. Twenty-four hours after treatment, mice were sacrificed via cardiac puncture and lungs were flash frozen. miRNA was extracted via the miRNeasy kit (Qiagen), converted to cDNA with the High capacity cDNA synthesis kit (Thermofisher), and analyzed for miRNA-126 (Thermofisher, Cat # 4427975 Assay ID 002228) levels via qPCR. SnoU6 (Thermofisher, Cat # 4427975 Assay ID 001973) was used as a miRNA reference gene.

Results

In Chapter 3 we demonstrated that USMB increases the deposition and efficacy of low dose gentamicin in the lung of an ARDS mouse model. However, we did not sample solely the regions that were injured but instead analyzed the whole lung tissue and BALF. In order to demonstrate that USMB favours therapeutic delivery to the injured lung over the uninjured lung, we performed a pilot study that involved a unilateral infected mouse model. *E. coli* was delivered intratracheally to the right lung. Six hours post-infection an RNA-tagged Alexa-555 molecule was delivered with cationic microbubbles intravenously and ultrasound was administered to the full chest for 5 minutes. Following cardiac puncture and a saline flush, lungs were collected and analyzed for fluorescence. Pilot studies demonstrated increased fluorescence in the injured lung versus uninjured lung when USMB was provided but not in its absence, **(Supplemental Figure 5.4.).** Additionally, USMB increased the overall fluorescence in the injured lung compared to both uninjured and injured lungs of mice that did not receive USMB. These pilot experiments indicate the potential of USMB to enhance the deposition of therapeutics specifically to edematous regions over aerated regions.

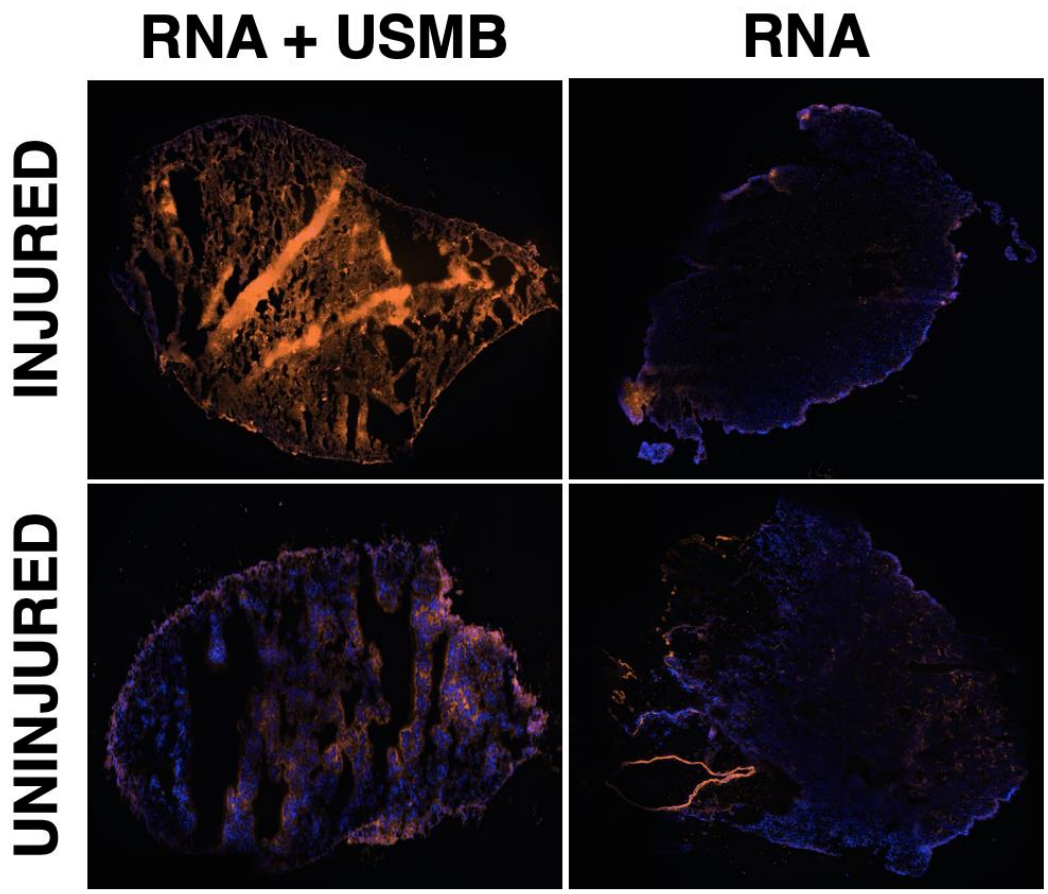

Supplemental Figure 5.4. USMB enhances the deposition of RNA-Alexa 555 specifically in the injured lung of *E. coli*-infected mice. *E. coli* was administered into the right lung lobe in mice. Six-hours post-infection, mice were administered RNA-tagged Alexa-555 conjugated to cationic microbubbles through the tail vein and chest ultrasound was applied for 5 minutes. Ten minutes following treatment, mice were sacrificed via cardiac puncture, and lungs were flushed and collected for RNA analysis. Frozen lung sections were cut at 5 μm, stained with DAPI, and imaged at 20X for Alexa-555 quantification. Pilot studies revealed that USMB increased RNA deposition in the injured lung but not the uninjured lung compared to delivery of RNA without USMB treatment.

USMB may be able to deliver therapeutic miRNA to the injured lung to improve outcomes in ARDS or pneumonia. Using miRNAs as therapeutic agents is advantageous for various reasons. First, miRNAs are well conserved across species thus, findings in animal models may lead to efficient translation to human applications.

Secondly, miRNAs can target a number of different mRNAs that are involved in various pathways, which may result in a greater effect than only targeting one gene or one protein. However, the delivery of miRNAs as therapy does come with limitations. Due to the presence of RNases, miRNAs must be either chemically modified or encapsulated within a drug delivery system. Also, the delivery of miRNAs is not specific to certain tissues or organs and may result in adverse and off-target effects. We propose the use of USMB to safely and effectively deliver miRNAs to target regions in the body. The endothelial specific miRNA-126 is found to be decreased in ARDS animal models. Its presence targets VEGFR2 and Tie2 signalling pathways, which promote angiogenesis and vessel maturation, respectively. We hypothesize that USMB delivery of miRNA-126 to the injured lung may improve outcomes in patients with ARDS.

We first observed the effect of miRNA-126 overexpression in human pulmonary microvascular endothelial cells *in vitro* 24-hours post-influenza infection. The overexpression of miRNA-126 significantly decreased influenza-induced cleaved-caspase-3 protein expression compared to scramble miRNA **(Supplemental Figure 5.5).** This finding suggests that miRNA-126 protects cells from influenza-induced apoptosis. Next, we aimed to identify if PIK3R2, a target of miRNA-126, was upregulated in our influenza-infected mice. Four-days following intranasal influenza infection, mouse lungs were collected and PIK3R2 mRNA levels we analyzed through qPCR and compared to healthy controls. Although not significant, there is a trend that demonstrates increased PIK3R2 mRNA levels in infected mouse lungs compared to uninfected mouse lungs **(Supplemental Figure 5.6.A).** These findings line up with the literature that demonstrates a decrease in miRNA-126 lung expression in a rat ARDS model (C. Huang et al., 2014). Therefore, the increase in PIK3R2 mRNA is suggested to be due to less miRNA-126-mediated inhibition following lung infection. Considering miRNA-126 is protective against flu-induced apoptosis *in vitro* and there is greater expression of PIK3R2 in flu-infected mice *in vivo*, we hypothesized that miRNA-126 administration to mice may enhance survival post-influenza infection. We further postulated that USMB would enhance the deposition of miRNA-126 into the injured lung and provide a greater survival benefit compared to miRNA-126 administration alone.

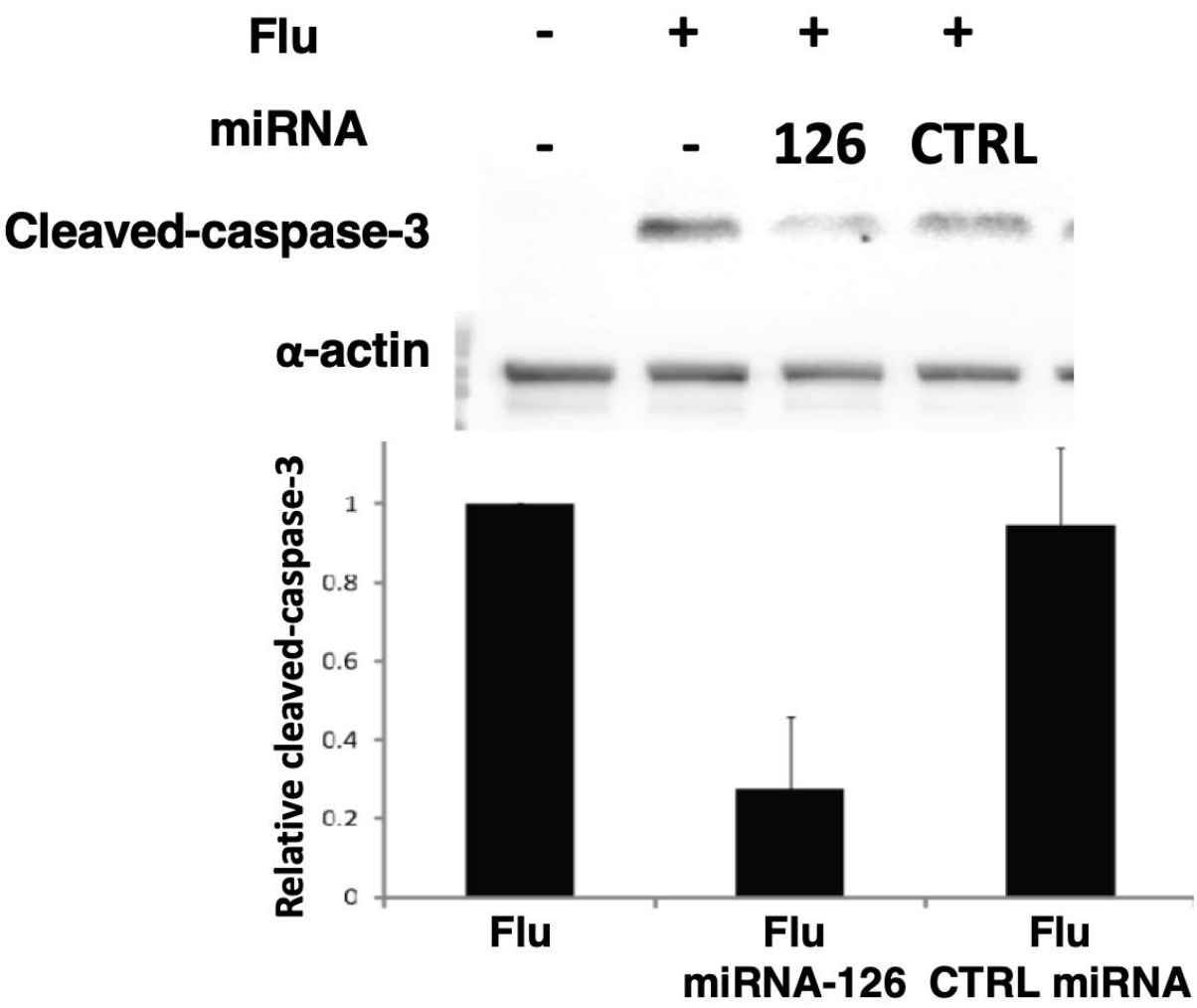

Supplemental Figure 5.5. miRNA-126 overexpression decreases flu-induced cleaved-caspase-3 protein levels in HPMECs. HPMECs were seeded in a 12-well plate at 60% confluency. They were transfected with miRNA-126 or control miRNA. 24-hours after transfection, cells were infected with flu at a multiplicity of infection (MOI) of 1. 24-hours after influenza infection, cells were lysed and processed for protein analysis via western blot. Infected HPMECs transfected with miRNA-126 displayed less relative cleaved-caspase-3 protein levels compared to infected HPMECs transfected with control miRNA. Cleaved-caspase-3 is an indicator of cell apoptosis thus, miRNA-126 decreased flu-induced cell apoptosis.

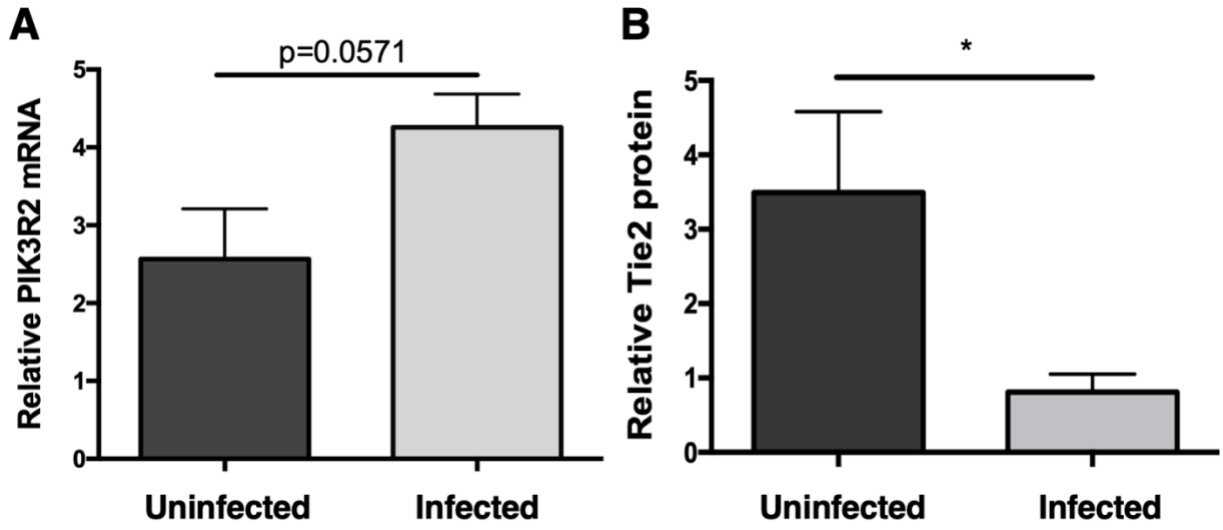

Supplemental Figure 5.6. PIK3R2 and Tie2 expression in mouse lungs on day 4 post-influenza infection. Mice were intranasally infected with influenza. Day 4 post-infection mice were sacrificed via cardiac puncture and lungs were collected for mRNA and protein analysis. (A) PIK3R2 mRNA levels were increased in the lungs of infected mice compared to healthy mice controls (n-4). (B) Tie2 protein levels were significantly decreased in the lungs of infected mice compared to healthy controls (n=6-8). (Data is mean ± SEM; * = $p < 0.05$)

First, we identified the potential of USMB to enhance a miRNA-126 -encoding plasmid that also encodes GFP. Mice were administered influenza intratracheally. On day 3 post-infection, mice were intravenously administered 10 μg of the miRNA-126-GFP plasmid with cationic bubbles and treated with chest ultrasound for 5 minutes. All control mice received mock ultrasound. Twenty-four hours after treatment mice were sacrificed and lungs were analyzed for plasmid deposition. Pilot experiments demonstrated that USMB enhanced miRNA-126 levels in the lungs compared to mice administered miRNA-126 alone, miRNA-126 with microbubbles, or PBS (**Supplemental Figure 5.7**).

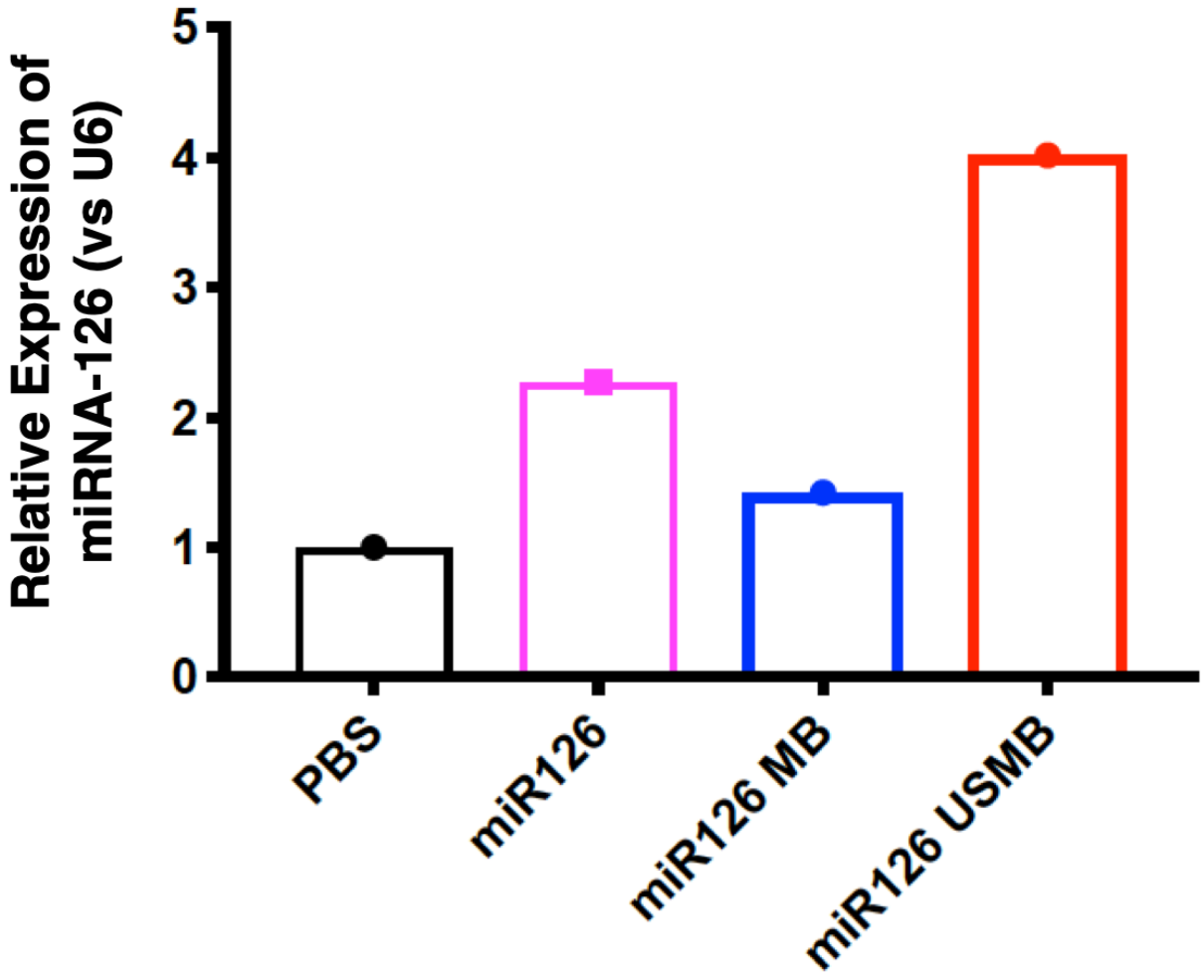

Supplemental Figure 5.7. USMB increases the deposition of miRNA-126 in the lungs of influenza-infected mice. Mice were intratracheally infected with influenza. Day 3 post-infection mice were intravenously injected with cationic bubbles conjugated to miRNA-126-GFP plasmid and administered chest ultrasound for 5 minutes. 24-hours post-treatment, mice were sacrificed via cardiac puncture and lungs were collected for miRNA analysis via qPCR. Mice that received miRNA-126 with USMB treatment had higher levels of miRNA-126 in the lungs compared to mice that received miRNA-126 alone and miRNA-126 with microbubbles but no ultrasound. Data is presented as relative miRNA-126 values versus U6. (n=1).

Our next steps would include investigating the potential of USMB targeted lung delivery of miRNA-126 to enhance survival post-influenza infection in mice.

Although a promising therapeutic, miRNAs are difficult to deliver to the correct cells, tissues, or area. The delivery of miRNA-126 to endothelial cells has been demonstrated by the use of human EPC exosomes, while another miRNA was delivery encapsulated in liposomes (Cheng & Fish, 2015). However, an issue with these delivery methods is that miRNA is not being directly targeted to the area of interest. USMB may avoid that issue and increase the delivery of miRNAs and other therapeutics to the region of interest while reducing off-target deposition. Further, it is typically difficult to deliver compounds to the injured lung in ARDS due to edema and hypoxic vasoconstriction. Our pilot data suggest that despite this obstacle, USMB was able to efficiently deliver miRNA-126 to the lung in an ARDS mouse model.

There is precedent for the proposed experiments. Cao *et al* demonstrated the use of USMB to deliver miRNA-126-3p and miRNA-126-5p to the ischemic limb in a rat model, another area that is difficult to deliver compounds to in result of poor tissue perfusion and vascularization (Cao et al., 2015). Rats received a miRNA-126-3p and USMB treatment on day 14, 16, and 18 after femoral artery ligation and stripping. USMB delivery of miRNA-126-3p demonstrated increased delivery in the ischemic hindlimb compared to miRNA-126-3p delivery alone, which remained elevated for 3 days and returned to basal levels on day 28 (Cao et al., 2015). This was inversely correlated with the expression of miRNA-126-3p targets, PIK3R2 and SPRED1.

5.5 Conclusion

USMB is effective in both small and large animals to specifically target therapeutics to the edematous lung in ARDS and pneumonia. Increased penetration of drugs to the target area will in theory reduce off-target deposition and effects and likely result in therapeutic efficacy at a lower dose. There are a number of publications that present the benefit of USMB drug and gene delivery to various tissues and organs in small animal models. However, we are the first group to demonstrate the use of USMB drug delivery to injured lung. Further, we demonstrate the use of USMB in a large animal model and confirm its safety, two deficient areas in USMB drug delivery literature. The use of USMB drug delivery to the injured lung may result in improved efficacy of potential ARDS treatments and lead to better outcomes and reduced mortality in patients. However, prior to clinical translation, further studies on large animal model efficacy and safety must be completed. In addition, optimal ultrasound parameters and microbubble composition must be determined for therapeutic delivery to the injured lung in critically ill patients.

REFERENCES

Abadie, Y., Bregeon, F., Papazian, L., Lange, F., Chailley-Heu, B., Thomas, P., … Delclaux, C. (2005). Decreased VEGF concentration in lung tissue and vascular injury during ARDS. *The European Respiratory Journal*, *25*(1), 139–146. https://doi.org/10.1183/09031936.04.00065504

Acute Respiratory Distress Syndrome Network, Brower, R. G., Matthay, M. A., Morris, A., Schoenfeld, D., Thompson, B. T., & Wheeler, A. (2000). Ventilation with Lower Tidal Volumes as Compared with Traditional Tidal Volumes for Acute Lung Injury and the Acute Respiratory Distress Syndrome. *New England Journal of Medicine*, *342*(18), 1301–1308. https://doi.org/10.1056/NEJM200005043421801

Ahmadi, F., McLoughlin, I. V., Chauhan, S., & ter-Haar, G. (2012). Bio-effects and safety of low-intensity, low-frequency ultrasonic exposure. *Progress in Biophysics and Molecular Biology*, *108*(3), 119–138. https://doi.org/10.1016/J.PBIOMOLBIO.2012.01.004

Amin, Z., & Amanda, A. P. (2017). *Comparison of New ARDS Criteria (Berlin) with Old Criteria (AECC) and its Application in Country with Limited Facilities*. *J Gen Emerg Med* (Vol. 2). Retrieved from www.scientonline.org

Ángel Monsalve-Naharro, J., Domingo-Chiva, E., Castillo, S. G., Cuesta-Montero, P., & María Jiménez-Vizuete, J. (2017). Inhaled nitric oxide in adult patients with acute respiratory distress syndrome Óxido nítrico inhalado en pacientes adultos con síndrome de distrés respiratorio agudo. *Farm Hosp*, *41*(2), 292–312. https://doi.org/10.7399/fh.2017.41.2.10533

Angelini, D. J., Hyun, S.-W., Grigoryev, D. N., Garg, P., Gong, P., Singh, I. S., … Goldblum, S. E. (2006). TNF-α increases tyrosine phosphorylation of vascular endothelial cadherin and opens the paracellular pathway through fyn activation in human lung endothelia. *American Journal of Physiology-Lung Cellular and Molecular Physiology*, *291*(6), L1232–L1245. https://doi.org/10.1152/ajplung.00109.2006

Angkasekwinai, P., Park, H., Wang, Y.-H., Wang, Y.-H., Chang, S. H., Corry, D. B., … Dong, C. (2007). Interleukin 25 promotes the initiation of proallergic type 2 responses. *The Journal*

of Experimental Medicine, *204*(7), 1509–1517. https://doi.org/10.1084/jem.20061675

ARDS Definition Task Force, Ranieri, V. M., Rubenfeld, G. D., Thompson, B. T., Ferguson, N. D., Caldwell, E., … Slutsky, A. S. (2012a). Acute Respiratory Distress Syndrome. *JAMA*, *307*(23), 2526–2533. https://doi.org/10.1001/jama.2012.5669

ARDS Definition Task Force, Ranieri, V. M., Rubenfeld, G. D., Thompson, B. T., Ferguson, N. D., Caldwell, E., … Slutsky, A. S. (2012b). Acute Respiratory Distress Syndrome. *JAMA*, *307*(23), 2526–2533. https://doi.org/10.1001/jama.2012.5669

Artigas, A., Camprubí-Rimblas, M., Tantinyà, N., Bringué, J., Guillamat-Prats, R., & Matthay, M. A. (2017). Inhalation therapies in acute respiratory distress syndrome. *Annals of Translational Medicine*, *5*(14), 293. https://doi.org/10.21037/atm.2017.07.21

Ashbaugh, D., Boyd Bigelow, D., Petty, T., & Levine, B. (1967). ACUTE RESPIRATORY DISTRESS IN ADULTS. *The Lancet*, *290*(7511), 319–323. https://doi.org/10.1016/S0140-6736(67)90168-7

Balish, A. L., Katz, J. M., & Klimov, A. I. (2013). Influenza: Propagation, Quantification, and Storage. *Current Protocols in Microbiology*, *29*(1), 15G.1.1-15G.1.24. https://doi.org/10.1002/9780471729259.mc15g01s29

Baston, C., & West, T. E. (2016). Lung ultrasound in acute respiratory distress syndrome and beyond. *Journal of Thoracic Disease*, *8*(12), E1763–E1766. https://doi.org/10.21037/jtd.2016.12.74

Bazzoni, G., & Dejana, E. (2004). Endothelial Cell-to-Cell Junctions: Molecular Organization and Role in Vascular Homeostasis. *Physiological Reviews*, *84*(3), 869–901. https://doi.org/10.1152/physrev.00035.2003

Beauchamp, N. M., Busick, R. Y., & Alexander-Miller, M. A. (2010). Functional Divergence among CD103 Dendritic Cell Subpopulations following Pulmonary Poxvirus Infection. *JOURNAL OF VIROLOGY*, *84*(19), 10191–10199. https://doi.org/10.1128/JVI.00892-10

Beitler, J. R., Malhotra, A., & Thompson, B. T. (2016). Ventilator-induced Lung Injury. *Clinics in Chest Medicine*, *37*(4), 633–646. https://doi.org/10.1016/j.ccm.2016.07.004

Bekeredjian, R., Grayburn, P. A., & Shohet, R. V. (2005). Use of ultrasound contrast agents for gene or drug delivery in cardiovascular medicine. *Journal of the American College of*

Cardiology, *45*(3), 329–335. https://doi.org/10.1016/j.jacc.2004.08.067

Belaaouaj, A., McCarthy, R., Baumann, M., Gao, Z., Ley, T. J., Abraham, S. N., & Shapiro, S. D. (1998). Mice lacking neutrophil elastase reveal impaired host defense against gram negative bacterial sepsis. *Nature Medicine*, *4*(5), 615–618. Retrieved from http://www.ncbi.nlm.nih.gov/pubmed/9585238

Bellani, G., Laffey, J. G., Pham, T., Fan, E., Brochard, L., Esteban, A., … ESICM Trials Group. (2016). Epidemiology, Patterns of Care, and Mortality for Patients With Acute Respiratory Distress Syndrome in Intensive Care Units in 50 Countries. *JAMA*, *315*(8), 788. https://doi.org/10.1001/jama.2016.0291

Bellani, G., Laffey, J. G., Pham, T., Fan, E., Brochard, L., Esteban, A., … Pesenti, A. (2016). Epidemiology, Patterns of Care, and Mortality for Patients With Acute Respiratory Distress Syndrome in Intensive Care Units in 50 Countries. *JAMA*, *315*(8), 788. https://doi.org/10.1001/jama.2016.0291

Bellemare, F., Jeanneret, A., & Couture, J. (2003). Sex Differences in Thoracic Dimensions and Configuration. *American Journal of Respiratory and Critical Care Medicine*, *168*(3), 305–312. https://doi.org/10.1164/rccm.200208-876OC

Bernard, G. R., Artigas, A., Brigham, K. L., Carlet, J., Falke, K., Hudson, L., … Spragg, R. (1994). The American-European Consensus Conference on ARDS. Definitions, mechanisms, relevant outcomes, and clinical trial coordination. *American Journal of Respiratory and Critical Care Medicine*, *149*(3), 818–824. https://doi.org/10.1164/ajrccm.149.3.7509706

Besnier, E., Brakenhielm, E., Richard, V., & Tamion, F. (2017). Does anti-VEGF bevacizumab improve survival in experimental sepsis? *Critical Care (London, England)*, *21*(1), 163. https://doi.org/10.1186/s13054-017-1734-x

Boissenot, T., Bordat, A., Fattal, E., & Tsapis, N. (2016). Ultrasound-triggered drug delivery for cancer treatment using drug delivery systems: From theoretical considerations to practical applications. *Journal of Controlled Release*, *241*, 144–163. https://doi.org/10.1016/j.jconrel.2016.09.026

Borden, M. (2010). Microbubble Compositions, Properties and Biomedical Applications (For types of microbubble shells). *Bubble Sci Eng Technol.*, *1*, 3–17.

https://doi.org/10.1179/175889709X446507.Microbubble

Calfee, C. S., Matthay, M. A., Eisner, M. D., Benowitz, N., Call, M., Pittet, J.-F., & Cohen, M. J. (2011). Active and Passive Cigarette Smoking and Acute Lung Injury after Severe Blunt Trauma. *American Journal of Respiratory and Critical Care Medicine*, *183*(12), 1660–1665. https://doi.org/10.1164/rccm.201011-1802OC

Cao, W. J., Rosenblat, J. D., Roth, N. C., Kuliszewski, M. A., Matkar, P. N., Rudenko, D., … Leong-Poi, H. (2015). Therapeutic Angiogenesis by Ultrasound-Mediated MicroRNA-126-3p Delivery. *Arteriosclerosis, Thrombosis, and Vascular Biology*, *35*(11), 2401–2411. https://doi.org/10.1161/ATVBAHA.115.306506

Carman, C. V., & Springer, T. A. (2004). A transmigratory cup in leukocyte diapedesis both through individual vascular endothelial cells and between them. *The Journal of Cell Biology*, *167*(2), 377–388. https://doi.org/10.1083/jcb.200404129

Carmeliet, P., Lampugnani, M.-G., Moons, L., Breviario, F., Compernolle, V., Bono, F., … Dejana, E. (1999). Targeted Deficiency or Cytosolic Truncation of the VE-cadherin Gene in Mice Impairs VEGF-Mediated Endothelial Survival and Angiogenesis. *Cell*, *98*(2), 147–157. https://doi.org/10.1016/S0092-8674(00)81010-7

Chen, H.-K., Zhang, S.-M., Chang, J.-L., Chen, H.-C., Lin, Y.-C., Shih, C.-P., … Wang, C.-H. (2018). Insonation of Systemically Delivered Cisplatin-Loaded Microbubbles Significantly Attenuates Nephrotoxicity of Chemotherapy in Experimental Models of Head and Neck Cancer. *Cancers*, *10*(9), 311. https://doi.org/10.3390/cancers10090311

Cheng, H. S., & Fish, J. E. (2015). Neovascularization Driven by MicroRNA Delivery to the Endothelium. *Arteriosclerosis, Thrombosis, and Vascular Biology*, *35*(11), 2263–2265. https://doi.org/10.1161/ATVBAHA.115.306558

Chignard, M., & Balloy, V. (2000). Neutrophil recruitment and increased permeability during acute lung injury induced by lipopolysaccharide. *American Journal of Physiology-Lung Cellular and Molecular Physiology*, *279*(6), L1083–L1090. https://doi.org/10.1152/ajplung.2000.279.6.L1083

Chlon, C., Guédon, C., Verhaagen, B., Shi, W. T., Hall, C. S., Lub, J., & Böhmer, M. R. (2009). Effect of Molecular Weight, Crystallinity, and Hydrophobicity on the Acoustic Activation of

Polymer-Shelled Ultrasound Contrast Agents. *Biomacromolecules*, *10*(5), 1025–1031. https://doi.org/10.1021/bm801243u

Cho, C.-H., Kammerer, R. A., Lee, H. J., Steinmetz, M. O., Ryu, Y. S., Lee, S. H., … Koh, G. Y. (2004). COMP-Ang1: a designed angiopoietin-1 variant with nonleaky angiogenic activity. *Proceedings of the National Academy of Sciences of the United States of America*, *101*(15), 5547–5552. https://doi.org/10.1073/pnas.0307574101

Choi, W. S., Baek, J. H., Seo, Y. Bin, Kee, S. Y., Jeong, H. W., Lee, H. Y., … Transgovernmental Enterprise for Pandemic Influenza in Korea, T. E. for P. I. in. (2014). Severe influenza treatment guideline. *The Korean Journal of Internal Medicine*, *29*(1), 132–147. https://doi.org/10.3904/kjim.2014.29.1.132

Christiansen, J. P., French, B. A., Klibanov, A. L., Kaul, S., & Lindner, J. R. (2003). Targeted tissue transfection with ultrasound destruction of plasmid-bearing cationic microbubbles. *Ultrasound in Medicine & Biology*, *29*(12), 1759–1767. Retrieved from http://www.ncbi.nlm.nih.gov/pubmed/14698343

Christofidou-Solomidou, M., Scherpereel, A., Wiewrodt, R., Ng, K., Sweitzer, T., Arguiri, E., … Muzykantov, V. R. (2003). PECAM-directed delivery of catalase to endothelium protects against pulmonary vascular oxidative stress. *American Journal of Physiology-Lung Cellular and Molecular Physiology*, *285*(2), L283–L292. https://doi.org/10.1152/ajplung.00021.2003

Cilloniz, C., Martin-Loeches, I., Garcia-Vidal, C., San Jose, A., & Torres, A. (2016). Microbial Etiology of Pneumonia: Epidemiology, Diagnosis and Resistance Patterns. *International Journal of Molecular Sciences*, *17*(12). https://doi.org/10.3390/ijms17122120

Clark, S. R., Ma, A. C., Tavener, S. A., McDonald, B., Goodarzi, Z., Kelly, M. M., … Kubes, P. (2007). Platelet TLR4 activates neutrophil extracellular traps to ensnare bacteria in septic blood. *Nature Medicine*, *13*(4), 463–469. https://doi.org/10.1038/nm1565

Costa, E. L. V., & Amato, M. B. P. (2013). The new definition for acute lung injury and acute respiratory distress syndrome. *Current Opinion in Critical Care*, *19*(1), 16–23. https://doi.org/10.1097/MCC.0b013e32835c50b1

Dantzker, D. R., Brook, C. J., Dehart, P., Lynch, J. P., & Weg, J. G. (1979). Ventilation-perfusion

distributions in the adult respiratory distress syndrome. *The American Review of Respiratory Disease*, *120*(5), 1039–1052. https://doi.org/10.1164/arrd.1979.120.5.1039

David, S., Ghosh, C. C., Kümpers, P., Shushakova, N., Van Slyke, P., Khankin, E. V, … Parikh, S. M. (2011). Effects of a synthetic PEG-ylated Tie-2 agonist peptide on endotoxemic lung injury and mortality. *American Journal of Physiology. Lung Cellular and Molecular Physiology*, *300*(6), L851-62. https://doi.org/10.1152/ajplung.00459.2010

De Cock, I., Zagato, E., Braeckmans, K., Luan, Y., De Jong, N., De Smedt, S. C., & Lentacker, I. (2014). Ultrasound and microbubble mediated drug delivery: Acoustic pressure as determinant for uptake via membrane pores or endocytosis. https://doi.org/10.1016/j.jconrel.2014.10.031

Delalande, A., Leduc, C. E., Midoux, P., Postema, M., & Pichon, C. (2015). EFFICIENT GENE DELIVERY BY SONOPORATION IS ASSOCIATED WITH MICROBUBBLE ENTRY INTO CELLS AND THE CLATHRIN-DEPENDENT ENDOCYTOSIS PATHWAY. https://doi.org/10.1016/j.ultrasmedbio.2015.03.010

Donnelly, S. C., MacGregor, I., Zamani, A., Gordon, M. W., Robertson, C. E., Steedman, D. J., … Haslett, C. (1995). Plasma elastase levels and the development of the adult respiratory distress syndrome. *American Journal of Respiratory and Critical Care Medicine*, *151*(5), 1428–1433. https://doi.org/10.1164/ajrccm.151.5.7735596

Downs, M. E., Buch, A., Sierra, C., Karakatsani, M. E., Teichert, T., Chen, S., … Ferrera, V. P. (2015). Long-Term Safety of Repeated Blood-Brain Barrier Opening via Focused Ultrasound with Microbubbles in Non-Human Primates Performing a Cognitive Task. *PloS One*, *10*(5), e0125911. https://doi.org/10.1371/journal.pone.0125911

Eliceiri, B. P., Paul, R., Schwartzberg, P. L., Hood, J. D., Leng, J., & Cheresh, D. A. (1999a). Selective requirement for Src kinases during VEGF-induced angiogenesis and vascular permeability. *Molecular Cell*, *4*(6), 915–924. https://doi.org/10.1016/S1097-2765(00)80221-X

Eliceiri, B. P., Paul, R., Schwartzberg, P. L., Hood, J. D., Leng, J., & Cheresh, D. A. (1999b). Selective requirement for Src kinases during VEGF-induced angiogenesis and vascular permeability. *Molecular Cell*, *4*(6), 915–924. Retrieved from

http://www.ncbi.nlm.nih.gov/pubmed/10635317

Estimated Influenza Illnesses, Medical visits, Hospitalizations, and Deaths in the United States — 2017–2018 influenza season | CDC. Retrieved from https://www.cdc.gov/flu/about/burden/2017-2018.htm

Exuzides, A., Main, M. L., Colby, C., Grayburn, P. A., Feinstein, S. B., & Goldman, J. H. (2010). A Retrospective Comparison of Mortality in Critically Ill Hospitalized Patients Undergoing Echocardiography With and Without an Ultrasound Contrast Agent. *JACC: Cardiovascular Imaging*, *3*(6), 578–585. https://doi.org/10.1016/J.JCMG.2010.04.006

Fan, Z., Kumon, R. E., Park, J., & Deng, C. X. (2010). Intracellular delivery and calcium transients generated in sonoporation facilitated by microbubbles. *Journal of Controlled Release : Official Journal of the Controlled Release Society*, *142*(1), 31–39. https://doi.org/10.1016/j.jconrel.2009.09.031

Fekri, F., Delos Santos, R. C., Karshafian, R., & Antonescu, C. N. (2016a). Ultrasound Microbubble Treatment Enhances Clathrin-Mediated Endocytosis and Fluid-Phase Uptake through Distinct Mechanisms. *PLOS ONE*, *11*(6), e0156754. https://doi.org/10.1371/journal.pone.0156754

Fekri, F., Delos Santos, R. C., Karshafian, R., & Antonescu, C. N. (2016b). Ultrasound Microbubble Treatment Enhances Clathrin-Mediated Endocytosis and Fluid-Phase Uptake through Distinct Mechanisms. *PLOS ONE*, *11*(6), e0156754. https://doi.org/10.1371/journal.pone.0156754

Ferguson, N. D., Fan, E., Camporota, L., Antonelli, M., Anzueto, A., Beale, R., … Ranieri, V. M. (2012). The Berlin definition of ARDS: an expanded rationale, justification, and supplementary material. *Intensive Care Medicine*, *38*(10), 1573–1582. https://doi.org/10.1007/s00134-012-2682-1

Fiedler, U., Scharpfenecker, M., Koidl, S., Hegen, A., Grunow, V., Schmidt, J. M., … Augustin, H. G. (2004). The Tie-2 ligand Angiopoietin-2 is stored in and rapidly released upon stimulation from endothelial cell Weibel-Palade bodies. *Blood*, *103*(11), 4150–4156. https://doi.org/10.1182/blood-2003-10-3685

Fish, J. E., Santoro, M. M., Morton, S. U., Yu, S., Yeh, R.-F., Wythe, J. D., … Srivastava, D. (2008).

miR-126 regulates angiogenic signaling and vascular integrity. *Developmental Cell*, *15*(2), 272. https://doi.org/10.1016/J.DEVCEL.2008.07.008

Frantzeskaki, F., & Orfanos, S. E. (2018). Treating nosocomial pneumonia: what's new. *ERJ Open Research*, *4*(2). https://doi.org/10.1183/23120541.00058-2018

Frenkel, P. A. (2002). Dna-loaded albumin microbubbles enhance ultrasound-mediated transfection in vitro, *28*(6). Retrieved from http://resolver.scholarsportal.info/resolve/03015629/v28i0006/817_dameutiv.xml

Fukuhara, S., Sako, K., Minami, T., Noda, K., Kim, H. Z., Kodama, T., … Mochizuki, N. (2008). Differential function of Tie2 at cell–cell contacts and cell–substratum contacts regulated by angiopoietin-1. *Nature Cell Biology*, *10*(5), 513–526. https://doi.org/10.1038/ncb1714

Fukumura, D., Gohongi, T., Kadambi, A., Izumi, Y., Ang, J., Yun, C. O., … Jain, R. K. (2001). Predominant role of endothelial nitric oxide synthase in vascular endothelial growth factor-induced angiogenesis and vascular permeability. *Proceedings of the National Academy of Sciences of the United States of America*, *98*(5), 2604–2609. https://doi.org/10.1073/pnas.041359198

Gajic, O., Dabbagh, O., Park, P. K., Adesanya, A., Chang, S. Y., Hou, P., … U.S. Critical Illness and Injury Trials Group: Lung Injury Prevention Study Investigators (USCIITG-LIPS). (2011). Early Identification of Patients at Risk of Acute Lung Injury. *American Journal of Respiratory and Critical Care Medicine*, *183*(4), 462–470. https://doi.org/10.1164/rccm.201004-0549OC

Gallagher, D. C., Parikh, S. M., Balonov, K., Miller, A., Gautam, S., Talmor, D., & Sukhatme, V. P. (2007). CIRCULATING ANGIOPOIETIN 2 CORRELATES WITH MORTALITY IN A SURGICAL POPULATION WITH ACUTE LUNG INJURY/ADULT RESPIRATORY DISTRESS SYNDROME. *Shock*, *29*(6), 1. https://doi.org/10.1097/shk.0b013e31815dd92f

Gao Smith, F., Perkins, G. D., Gates, S., Young, D., McAuley, D. F., Tunnicliffe, W., … BALTI-2 study investigators, for the B.-2 study. (2012). Effect of intravenous β-2 agonist treatment on clinical outcomes in acute respiratory distress syndrome (BALTI-2): a multicentre, randomised controlled trial. *Lancet (London, England)*, *379*(9812), 229–235. https://doi.org/10.1016/S0140-6736(11)61623-1

Gao, X.-P., Zhu, X., Fu, J., Liu, Q., Frey, R. S., & Malik, A. B. (2007). Blockade of class IA

phosphoinositide 3-kinase in neutrophils prevents NADPH oxidase activation- and adhesion-dependent inflammation. *The Journal of Biological Chemistry*, *282*(9), 6116–6125. https://doi.org/10.1074/jbc.M610248200

Gao, Y., Wu, S., Li, L., Wang, G., Shen, W., Xu, Y., … Tan, K. (2014). Ultrasound-targeted stromal cell-derived factor-1-loaded microbubble destruction promotes mesenchymal stem cell homing to kidneys in diabetic nephropathy rats. *International Journal of Nanomedicine*, *9*, 5639. https://doi.org/10.2147/IJN.S73950

Garin, N., Genné, D., Carballo, S., Chuard, C., Eich, G., Hugli, O., … Perrier, A. (2014). β-Lactam Monotherapy vs β-Lactam–Macrolide Combination Treatment in Moderately Severe Community-Acquired Pneumonia. *JAMA Internal Medicine*, *174*(12), 1894. https://doi.org/10.1001/jamainternmed.2014.4887

Gattinoni, L. (2016). Ultra-protective ventilation and hypoxemia. *Critical Care*, *20*(1), 130. https://doi.org/10.1186/s13054-016-1310-9

Gattinoni, L., Carlesso, E., & Cressoni, M. (2015). Selecting the 'right' positive end-expiratory pressure level. *Current Opinion in Critical Care*, *21*(1), 50–57. https://doi.org/10.1097/MCC.0000000000000166

Gattinoni, L., Taccone, P., Carlesso, E., & Marini, J. J. (2013). Prone Position in Acute Respiratory Distress Syndrome. Rationale, Indications, and Limits. *American Journal of Respiratory and Critical Care Medicine*, *188*(11), 1286–1293. https://doi.org/10.1164/rccm.201308-1532CI

Gattinoni, L., Tognoni, G., Pesenti, A., Taccone, P., Mascheroni, D., Labarta, V., … Latini, R. (2001). Effect of Prone Positioning on the Survival of Patients with Acute Respiratory Failure. *New England Journal of Medicine*, *345*(8), 568–573. https://doi.org/10.1056/NEJMoa010043

Geng, P., Ma, T., Xing, J., Jiang, L., Sun, H., Zhu, B., … Zhang, J. (2018). Dexamethasone ameliorates H 2 S-induced acute lung injury by increasing claudin-5 expression via the PI3K pathway. https://doi.org/10.1177/0960327117721961

Grégoire, M., Uhel, F., Lesouhaitier, M., Gacouin, A., Guirriec, M., Mourcin, F., … Tadié, J.-M. (2018). Impaired efferocytosis and neutrophil extracellular trap clearance by macrophages in ARDS. *European Respiratory Journal*, *52*(2), 1702590.

https://doi.org/10.1183/13993003.02590-2017

Griffiths, M. J. D., & Evans, T. W. (2005). Inhaled Nitric Oxide Therapy in Adults. *New England Journal of Medicine*, *353*(25), 2683–2695. https://doi.org/10.1056/NEJMra051884

Grommes, J., & Soehnlein, O. (2011). Contribution of neutrophils to acute lung injury. *Molecular Medicine (Cambridge, Mass.)*, *17*(3–4), 293–307. https://doi.org/10.2119/molmed.2010.00138

Guerin, C., Gaillard, S., Lemasson, S., Ayzac, L., Girard, R., Beuret, P., … Kaidomar, M. (2004). Effects of Systematic Prone Positioning in Hypoxemic Acute Respiratory Failure. *JAMA*, *292*(19), 2379. https://doi.org/10.1001/jama.292.19.2379

Guérin, C., Reignier, J., Richard, J.-C., Beuret, P., Gacouin, A., Boulain, T., … Ayzac, L. (2013). Prone Positioning in Severe Acute Respiratory Distress Syndrome. *New England Journal of Medicine*, *368*(23), 2159–2168. https://doi.org/10.1056/NEJMoa1214103

Guillot, L., Nathan, N., Tabary, O., Thouvenin, G., Le Rouzic, P., Corvol, H., … Clement, A. (2013). Alveolar epithelial cells: Master regulators of lung homeostasis. *The International Journal of Biochemistry & Cell Biology*, *45*, 2568–2573. https://doi.org/10.1016/j.biocel.2013.08.009

Hallstrand, T. S., Hackett, T. L., Altemeier, W. A., Matute-Bello, G., Hansbro, P. M., & Knight, D. A. (2014). Airway epithelial regulation of pulmonary immune homeostasis and inflammation. *Clinical Immunology*, *151*, 1–15. https://doi.org/10.1016/j.clim.2013.12.003

Han, S., Lee, S.-J., Kim, K. E., Lee, H. S., Oh, N., Park, I., … Koh, G. Y. (2016). Amelioration of sepsis by TIE2 activation-induced vascular protection. *Science Translational Medicine*, *8*(335), 335ra55. https://doi.org/10.1126/scitranslmed.aad9260

Hashemian, S. M., Mortaz, E., Tabarsi, P., Jamaati, H., Maghsoomi, Z., Khosravi, A., … Adcock, I. M. (2014). Elevated CXCL-8 expression in bronchoalveolar lavage correlates with disease severity in patients with acute respiratory distress syndrome resulting from tuberculosis. *Journal of Inflammation*, *11*(1), 21. https://doi.org/10.1186/1476-9255-11-21

Hashimoto, T., & Pittet, J.-F. (2006). Angiopoietin-2: modulator of vascular permeability in acute lung injury? *PLoS Medicine*, *3*(3), e113. https://doi.org/10.1371/journal.pmed.0030113

Heemskerk, N., Schimmel, L., Oort, C., van Rijssel, J., Yin, T., Ma, B., … van Buul, J. D. (2016). F-

actin-rich contractile endothelial pores prevent vascular leakage during leukocyte diapedesis through local RhoA signalling. *Nature Communications*, *7*(1), 10493. https://doi.org/10.1038/ncomms10493

Heffernan, D. S., Dossett, L. A., Lightfoot, M. A., Fremont, R. D., Ware, L. B., Sawyer, R. G., & May, A. K. (2011). Gender and acute respiratory distress syndrome in critically injured adults: a prospective study. *The Journal of Trauma*, *71*(4), 878-83; discussion 883-5. https://doi.org/10.1097/TA.0b013e31822c0d31

Henderson, W. R., Chen, L., Amato, M. B. P., & Brochard, L. J. (2017). F ifty Y ears of R esearch in ARDS.Respiratory Mechanics in Acute Respiratory Distress Syndrome. *American Journal of Respiratory and Critical Care Medicine*, *196*(7), 822–833. https://doi.org/10.1164/rccm.201612-2495CI

Hess, D. R., & Faarc, R. (2015). Recruitment Maneuvers and PEEP Titration. https://doi.org/10.4187/respcare.04409

Hidalgo, A., Peired, A. J., Wild, M., & Frenette, P. S. (2007). Complete identification of E-selectin ligand activity on neutrophils reveals a dynamic interplay and distinct functions of PSGL-1, ESL-1 and CD44. https://doi.org/10.1016/j.immuni.2007.03.011

Hind, L. E., Vincent, W. J. B., & Huttenlocher, A. (2016). Leading from the back: the role of the uropod in neutrophil polarization and migration. *Developmental Cell*, *38*(2), 161. https://doi.org/10.1016/J.DEVCEL.2016.06.031

Holopainen, J. M., Angelova, M. I., & Kinnunen, P. K. J. (2000). Vectorial Budding of Vesicles by Asymmetrical Enzymatic Formation of Ceramide in Giant Liposomes. *Biophysical Journal*, *78*(2), 830–838. https://doi.org/10.1016/S0006-3495(00)76640-9

Hoogenboom, M., Eikelenboom, D., den Brok, M. H., Heerschap, A., Fütterer, J. J., & Adema, G. J. (2015). Mechanical High-Intensity Focused Ultrasound Destruction of Soft Tissue: Working Mechanisms and Physiologic Effects. *Ultrasound in Medicine & Biology*, *41*(6), 1500–1517. https://doi.org/10.1016/j.ultrasmedbio.2015.02.006

Hu, Y., Wan, J. M. F., & Yu, A. C. H. (2013). MEMBRANE PERFORATION AND RECOVERY DYNAMICS IN MICROBUBBLE-MEDIATED SONOPORATION. *Ultrasound in Medicine & Biology*, *39*, 2393–2405. https://doi.org/10.1016/j.ultrasmedbio.2013.08.003

Huang, C., Xiao, X., Chintagari, N. R., Breshears, M., Wang, Y., & Liu, L. (2014). MicroRNA and mRNA expression profiling in rat acute respiratory distress syndrome. *BMC Medical Genomics*, *7*(1), 46. https://doi.org/10.1186/1755-8794-7-46

Huang, L.-Y., Stuart, C., Takeda, K., D'Agnillo, F., & Golding, B. (2016). Poly(I:C) Induces Human Lung Endothelial Barrier Dysfunction by Disrupting Tight Junction Expression of Claudin-5. *PLOS ONE*, *11*(8), e0160875. https://doi.org/10.1371/journal.pone.0160875

Hudry-Clergeon, H., Stengel, D., Ninio, E., & Vilgrain, I. (2005). Platelet-activating factor increases VE-cadherin tyrosine phosphorylation in mouse endothelial cells and its association with the PtdIns3'-kinase. *The FASEB Journal*, *19*(6), 512–520. https://doi.org/10.1096/fj.04-2202com

Hurley, J. V. (1978). Current views on the mechanisms of pulmonary oedema. *The Journal of Pathology*, *125*(2), 59–79. https://doi.org/10.1002/path.1711250202

Hwang, J.-A., Lee, E. H., Lee, S. Do, Park, J. B., Jeon, H., & Cho, C.-H. (2009). COMP-Ang1 ameliorates leukocyte adhesion and reinforces endothelial tight junctions during endotoxemia. *Biochemical and Biophysical Research Communications*, *381*, 592–596. https://doi.org/10.1016/j.bbrc.2009.02.096

Hwang, J. H., Brayman, A. A., Reidy, M. A., Matula, T. J., Kimmey, M. B., & Crum, L. A. (2005). Vascular effects induced by combined 1-MHz ultrasound and microbubble contrast agent treatments in vivo. *Ultrasound in Medicine & Biology*, *31*(4), 553–564. https://doi.org/10.1016/j.ultrasmedbio.2004.12.014

Hwang, J. H., Brayman, A. A., Reidy, M. A., Matula, T. J., Kimmey, M. B., & Crum, L. A. (2005). VASCULAR EFFECTS INDUCED BY COMBINED 1-MHZ ULTRASOUND AND MICROBUBBLE CONTRAST AGENT TREATMENTS IN VIVO. https://doi.org/10.1016/j.ultrasmedbio.2004.12.014

Investigators, W. G. for the A. R. for A. R. D. S. T. (ART), Cavalcanti, A. B., Suzumura, É. A., Laranjeira, L. N., Paisani, D. de M., Damiani, L. P., … Carvalho, C. R. R. de. (2017). Effect of Lung Recruitment and Titrated Positive End-Expiratory Pressure (PEEP) vs Low PEEP on Mortality in Patients With Acute Respiratory Distress Syndrome: A Randomized Clinical Trial. *JAMA*, *318*(14), 1335. https://doi.org/10.1001/JAMA.2017.14171

Jang, A. S., Concel, V. J., Bein, K., Brant, K. A., Liu, S., Pope-Varsalona, H., … Leikauf, G. D. (2011). Endothelial dysfunction and claudin 5 regulation during acrolein-induced lung injury. *American Journal of Respiratory Cell and Molecular Biology*, *44*(4), 483–490. https://doi.org/10.1165/rcmb.2009-0391OC

Jeong, S. J., Han, S. H., Kim, C. O., Choi, J. Y., & Kim, J. M. (2013). Anti-vascular endothelial growth factor antibody attenuates inflammation and decreases mortality in an experimental model of severe sepsis. *Critical Care (London, England)*, *17*(3), R97. https://doi.org/10.1186/cc12742

Jho, D., Mehta, D., Ahmmed, G., Gao, X.-P., Tiruppathi, C., Broman, M., & Malik, A. B. (2005). Angiopoietin-1 Opposes VEGF-Induced Increase in Endothelial Permeability by Inhibiting TRPC1-Dependent Ca ^{2} Influx. *Circulation Research*, *96*(12), 1282–1290. https://doi.org/10.1161/01.RES.0000171894.03801.03

Jing, Y., Xiu-Juan, Z., Hong-Jiao, C., Zhi-Kui, C., Qing-Fu, Q., En-Sheng, X., & Li-Wu, L. (2019). Ultrasound-targeted microbubble destruction improved the antiangiogenic effect of Endostar in triple-negative breast carcinoma xenografts. *Journal of Cancer Research and Clinical Oncology*. https://doi.org/10.1007/s00432-019-02866-7

Jones, M. L., Takei, F., Ward, P. A., & Beaudet, A. L. (2019). *The role of P-selectin and ICAM-1 in acute*. Retrieved from http://www.jimmunol.org/content/157/10/4609

Judge, E. P., Hughes, J. M. L., Egan, J. J., Maguire, M., Molloy, E. L., & O'Dea, S. (2014). Anatomy and Bronchoscopy of the Porcine Lung. A Model for Translational Respiratory Medicine. *Http://Dx.Doi.Org/10.1165/Rcmb.2013-0453TR*. https://doi.org/10.1165/RCMB.2013-0453TR

Kalil, A. C., Metersky, M. L., Klompas, M., Muscedere, J., Sweeney, D. A., Palmer, L. B., … Brozek, J. L. (2016). Management of Adults With Hospital-acquired and Ventilator-associated Pneumonia: 2016 Clinical Practice Guidelines by the Infectious Diseases Society of America and the American Thoracic Society. *Clinical Infectious Diseases*, *63*(5), e61–e111. https://doi.org/10.1093/cid/ciw353

Kalil, A. C., Metersky, M. L., Klompas, M., Muscedere, J., Sweeney, D. A., Palmer, L. B., … Brozek, J. L. (2016). Management of Adults With Hospital-acquired and Ventilator-associated

Pneumonia: 2016 Clinical Practice Guidelines by the Infectious Diseases Society of America and the American Thoracic Society. *Clinical Infectious Diseases: An Official Publication of the Infectious Diseases Society of America*, *63*(5), e61. https://doi.org/10.1093/CID/CIW353

Kangelaris, K. N., Sapru, A., Calfee, C. S., Liu, K. D., Pawlikowska, L., Witte, J. S., … Network, and B. I. A. (2012). The association between a Darc gene polymorphism and clinical outcomes in African American patients with acute lung injury. *Chest*, *141*(5), 1160–1169. https://doi.org/10.1378/chest.11-1766

Karshafian, R., Bevan, P. D., Williams, R., Samac, S., & Burns, P. N. (2009). • Original Contribution SONOPORATION BY ULTRASOUND-ACTIVATED MICROBUBBLE CONTRAST AGENTS: EFFECT OF ACOUSTIC EXPOSURE PARAMETERS ON CELL MEMBRANE PERMEABILITY AND CELL VIABILITY. *UMB*, *35*, 847–860. https://doi.org/10.1016/j.ultrasmedbio.2008.10.013

Karshafian, R., Samac, S., Bevan, P. D., & Burns, P. N. (2010). Microbubble mediated sonoporation of cells in suspension: Clonogenic viability and influence of molecular size on uptake. *Ultrasonics*, *50*, 691–697. https://doi.org/10.1016/j.ultras.2010.01.009

Keiper, T., Al-Fakhri, N., Chavakis, E., Athanasopoulos, A. N., Isermann, B., Herzog, S., … Chavakis, T. (2005). The role of junctional adhesion molecule-C (JAM-C) in oxidized LDL-mediated leukocyte recruitment. *The FASEB Journal*, *19*(14), 2078–2080. https://doi.org/10.1096/fj.05-4196fje

Kiseleva, R. Y., Glassman, P. M., Greineder, C. F., Hood, E. D., Shuvaev, V. V, & Muzykantov, V. R. (2018). Targeting therapeutics to endothelium: are we there yet? https://doi.org/10.1007/s13346-017-0464-6

Koch, S., Tugues, S., Li, X., Gualandi, L., & Claesson-Welsh, L. (2011). Signal transduction by vascular endothelial growth factor receptors. *Biochemical Journal*, *437*(2), 169–183. https://doi.org/10.1042/BJ20110301

Koh, H., Tasaka, S., Hasegawa, N., Yamada, W., Shimizu, M., Nakamura, M., … Ishizaka, A. (2007). Protective role of vascular endothelial growth factor in endotoxin-induced acute lung injury in mice. *Respiratory Research*, *8*(1), 60. https://doi.org/10.1186/1465-9921-8-

60

Kooiman, K., Vos, H. J., Versluis, M., & de Jong, N. (2014). Acoustic behavior of microbubbles and implications for drug delivery. *Advanced Drug Delivery Reviews*, *72*, 28–48. https://doi.org/10.1016/j.addr.2014.03.003

Koulouras, V., Papathanakos, G., Papathanasiou, A., & Nakos, G. (2016). Efficacy of prone position in acute respiratory distress syndrome patients: A pathophysiology-based review. *World Journal of Critical Care Medicine*, *5*(2), 121–136. https://doi.org/10.5492/wjccm.v5.i2.121

Kudo, N., Okada, K., & Yamamoto, K. (2009). Sonoporation by Single-Shot Pulsed Ultrasound with Microbubbles Adjacent to Cells. *Biophysical Journal*, *96*(12), 4866–4876. https://doi.org/10.1016/J.BPJ.2009.02.072

Kümpers, P., Gueler, F., David, S., Slyke, P. Van, Dumont, D. J., Park, J.-K., … Shushakova, N. (2011). *The synthetic Tie2 agonist peptide vasculotide protects against vascular leakage and reduces mortality in murine abdominal sepsis*. *Critical Care* (Vol. 15). https://doi.org/10.1186/cc10523

Kuwabara, H., Kokai, Y., Kojima, T., Takakuwa, R., Mori, M., & Sawada, N. (2001). *Occludin Regulates Actin Cytoskeleton in Endothelial Cells*. *CELL STRUCTURE AND FUNCTION* (Vol. 26). Retrieved from https://www.jstage.jst.go.jp/article/csf/26/2/26_2_109/_pdf/-char/en

Lakshmikanthan, S., Sobczak, M., Li Calzi, S., Shaw, L., Grant, M. B., & Chrzanowska-Wodnicka, M. (2018). Rap1B promotes VEGF-induced endothelial permeability and is required for dynamic regulation of the endothelial barrier. *Journal of Cell Science*, *131*(1). https://doi.org/10.1242/jcs.207605

Le Borgne, M., Etchart, N., Goubier, A., Lira, S. A., Sirard, J. C., van Rooijen, N., … Dubois, B. (2006). Dendritic cells rapidly recruited into epithelial tissues via CCR6/CCL20 are responsible for CD8+ T cell crosspriming in vivo. *Immunity*, *24*(2), 191–201. https://doi.org/10.1016/j.immuni.2006.01.005

Leckband, D., & Sivasankar, S. (2000). Mechanism of homophilic cadherin adhesion. *Current Opinion in Cell Biology*, *12*(5), 587–592. Retrieved from http://www.ncbi.nlm.nih.gov/pubmed/10978894

Lee, J., Park, D. Y., Park, D. Y., Park, I., Chang, W., Nakaoka, Y., … Koh, G. Y. (2014). Angiopoietin-1 suppresses choroidal neovascularization and vascular leakage. *Investigative Ophthalmology and Visual Science*, *55*(4), 2191–2199. https://doi.org/10.1167/iovs.14-13897

Lemos-Filho, L. B., Mikkelsen, M. E., Martin, G. S., Dabbagh, O., Adesanya, A., Gentile, N., … US Critical Illness and Injury Trials Group: Lung Injury Prevention Study Investigators (USCIITG-LIPS). (2013). Sex, Race, and the Development of Acute Lung Injury. *Chest*, *143*(4), 901–909. https://doi.org/10.1378/chest.12-1118

Li, G., Flodby, P., Luo, J., Kage, H., Sipos, A., Gao, D., … Borok, Z. (2014). Knockout mice reveal key roles for claudin 18 in alveolar barrier properties and fluid homeostasis. *American Journal of Respiratory Cell and Molecular Biology*, *51*(2), 140310133341003. https://doi.org/10.1165/rcmb.2013-0353OC

Li, S., Chen, L., Wang, G., Xu, L., Hou, S., Chen, Z., … Du, Y.-Z. (2018). Anti-ICAM-1 antibody-modified nanostructured lipid carriers: a pulmonary vascular endothelium-targeted device for acute lung injury therapy. *Journal of Nanobiotechnology*, *16*(1), 105. https://doi.org/10.1186/s12951-018-0431-5

Li, T., Tachibana, K., Kuroki, M., & Kuroki, M. (2003). Gene Transfer with Echo-enhanced Contrast Agents: Comparison between Albunex, Optison, and Levovist in Mice—Initial Results. *Radiology*, *229*(2), 423–428. https://doi.org/10.1148/radiol.2292020500

Liang, H. D., Tang, J., & Halliwell, M. (2010). Sonoporation, drug delivery, and gene therapy. *Proceedings of the Institution of Mechanical Engineers, Part H: Journal of Engineering in Medicine*, *224*(2), 343–361. https://doi.org/10.1243/09544119JEIM565

Lichtenstein, D., Goldstein, I., Mourgeon, E., Cluzel, P., Grenier, P., & Rouby, J.-J. (2004). *CLINICAL INVESTIGATIONS Comparative Diagnostic Performances of Auscultation, Chest Radiography, and Lung Ultrasonography in Acute Respiratory Distress Syndrome*. Retrieved from http://www.anesthesiology.org.

LICHTENSTEIN, D., MÉZIÈRE, G., BIDERMAN, P., GEPNER, A., & BARRÉ, O. (1997). The Comet-tail Artifact. *American Journal of Respiratory and Critical Care Medicine*, *156*(5), 1640–1646. https://doi.org/10.1164/ajrccm.156.5.96-07096

Lindner, J. R., Porter, T. R., & Park, M. M. (2018). *American Society of Echocardiography Guidelines and Recommendations for Contrast Echocardiography: A Summary for Applications Approved by the U.S. Food and Drug Administration*. Retrieved from https://www.asecho.org/wp-content/uploads/2018/07/Contrast-Echo-On-Label-Summary-FINAL-rev.pdf

Liu, M., Gu, C., & Wang, Y. (2014). Upregulation of the tight junction protein occludin: effects on ventilation-induced lung injury and mechanisms of action. *BMC Pulmonary Medicine*, *14*, 94. https://doi.org/10.1186/1471-2466-14-94

Liu, Y., Li, L., Su, Q., Liu, T., Ma, Z., & Yang, H. (2015). Ultrasound-Targeted Microbubble Destruction Enhances Gene Expression of microRNA-21 in Swine Heart via Intracoronary Delivery. *Echocardiography*, *32*(9), 1407–1416. https://doi.org/10.1111/echo.12876

London, N. R., Zhu, W., Bozza, F. A., Smith, M. C. P., Greif, D. M., Sorensen, L. K., … Li, D. Y. (2010). Targeting Robo4-Dependent Slit Signaling to Survive the Cytokine Storm in Sepsis and Influenza. *Science Translational Medicine*, *2*(23), 23ra19-23ra19. https://doi.org/10.1126/scitranslmed.3000678

Lorente, J. A., Cardinal-Fernández, P., Muñoz, D., Frutos-Vivar, F., Thille, A. W., Jaramillo, C., … Thompson, T. B. (2015). Acute respiratory distress syndrome in patients with and without diffuse alveolar damage: an autopsy study. *Intensive Care Medicine*, *41*(11), 1921–1930. https://doi.org/10.1007/s00134-015-4046-0

Lum, A. F. H., Borden, M. A., Dayton, P. A., Kruse, D. E., Simon, S. I., & Ferrara, K. W. (2005). Ultrasound radiation force enables targeted deposition of model drug carriers loaded on microbubbles. https://doi.org/10.1016/j.jconrel.2005.11.006

M. Heidemann, S., Nair, A., Bulut, Y., & Sapru, A. (2017). *Pathophysiology and Management of Acute Respiratory Distress Syndrome in Children*. *Pediatric Clinics of North America* (Vol. 64). https://doi.org/10.1016/j.pcl.2017.06.004

Ma, S.-C., Li, Q., Peng, J.-Y., Zhouwen, J.-L., Diao, J.-F., Niu, J.-X., … Jiang, W.-G. (2017). Claudin-5 regulates blood-brain barrier permeability by modifying brain microvascular endothelial cell proliferation, migration, and adhesion to prevent lung cancer metastasis. *CNS Neuroscience & Therapeutics*, *23*(12), 947–960. https://doi.org/10.1111/cns.12764

Main, M. L., Ryan, A. C., Davis, T. E., Albano, M. P., Kusnetzky, L. L., & Hibberd, M. (2008). Acute Mortality in Hospitalized Patients Undergoing Echocardiography With and Without an Ultrasound Contrast Agent (Multicenter Registry Results in 4,300,966 Consecutive Patients). *The American Journal of Cardiology*, *102*(12), 1742–1746. https://doi.org/10.1016/j.amjcard.2008.08.019

Mammoto, T., Parikh, S. M., Mammoto, A., Gallagher, D., Chan, B., Mostoslavsky, G., … Sukhatme, V. P. (2007). Angiopoietin-1 Requires p190 RhoGAP to Protect against Vascular Leakage *in Vivo*. *Journal of Biological Chemistry*, *282*(33), 23910–23918. https://doi.org/10.1074/jbc.M702169200

Marik, P. E., Meduri, G. U., Rocco, P. R. M., & Annane, D. (2011). Glucocorticoid Treatment in Acute Lung Injury and Acute Respiratory Distress Syndrome. *Critical Care Clinics*, *27*(3), 589–607. https://doi.org/10.1016/j.ccc.2011.05.007

Marik, P. E., Pastores, S. M., Annane, D., Meduri, G. U., Sprung, C. L., Arlt, W., … Vogeser, M. (2008). Recommendations for the diagnosis and management of corticosteroid insufficiency in critically ill adult patients: Consensus statements from an international task force by the American College of Critical Care Medicine. *Critical Care Medicine*, *36*(6), 1937–1949. https://doi.org/10.1097/CCM.0b013e31817603ba

Mark A. Borden, *,†,‡, Charles F. Caskey, †, Erika Little, †, Robert J. Gillies, ‡ and, & Ferrara†, K. W. (2007). DNA and Polylysine Adsorption and Multilayer Construction onto Cationic Lipid-Coated Microbubbles. https://doi.org/10.1021/LA7009034

Marmottant, P., & Hilgenfeldt, S. (2003). Controlled vesicle deformation and lysis by single oscillating bubbles. *Nature*, *423*(6936), 153–156. https://doi.org/10.1038/nature01613

Martin, T. R., Pistorese, B. P., Chi, E. Y., Goodman, R. B., & Matthay, M. A. (1989). Effects of leukotriene B4 in the human lung. Recruitment of neutrophils into the alveolar spaces without a change in protein permeability. *Journal of Clinical Investigation*, *84*(5), 1609–1619. https://doi.org/10.1172/JCI114338

Matthay, M. A., & Zemans, R. L. (2011). The Acute Respiratory Distress Syndrome: Pathogenesis and Treatment. *Annual Review of Pathology*, *6*, 147. https://doi.org/10.1146/ANNUREV-PATHOL-011110-130158

Matute-Bello, G., Downey, G., Moore, B. B., Groshong, S. D., Matthay, M. A., Slutsky, A. S., … Acute Lung Injury in Animals Study Group. (2011). An Official American Thoracic Society Workshop Report: Features and Measurements of Experimental Acute Lung Injury in Animals. *American Journal of Respiratory Cell and Molecular Biology*, *44*(5), 725–738. https://doi.org/10.1165/rcmb.2009-0210ST

Maunder, R. J., Shuman, W. P., McHugh, J. W., Marglin, S. I., & Butler, J. (1986). Preservation of normal lung regions in the adult respiratory distress syndrome. Analysis by computed tomography. *JAMA*, *255*(18), 2463–2465. Retrieved from http://www.ncbi.nlm.nih.gov/pubmed/3701964

May, D. J., Allen, J. S., & Ferrara, K. W. (2002). Dynamics and fragmentation of thick-shelled microbubbles. *IEEE Transactions on Ultrasonics, Ferroelectrics and Frequency Control*, *49*(10), 1400–1410. https://doi.org/10.1109/TUFFC.2002.1041081

Mayer, C. R., Geis, N. A., Katus, H. A., & Bekeredjian, R. (2008). Ultrasound targeted microbubble destruction for drug and gene delivery. *Expert Opinion on Drug Delivery*, *5*(10), 1121–1138. https://doi.org/10.1517/17425247.5.10.1121

McCarter, S. D., Mei, S. H. J., Lai, P. F. H., Zhang, Q. W., Parker, C. H., Suen, R. S., … Stewart, D. J. (2007). Cell-based Angiopoietin-1 Gene Therapy for Acute Lung Injury. *American Journal of Respiratory and Critical Care Medicine*, *175*(10), 1014–1026. https://doi.org/10.1164/rccm.200609-1370OC

Meade, M. O., Cook, R. J., Guyatt, G. H., Groll, R., Kachura, J. R., Bedard, M., … Stew-Art, T. E. (2000). *Interobserver Variation in Interpreting Chest Radiographs for the Diagnosis of Acute Respiratory Distress Syndrome*. *Am J Respir Crit Care Med* (Vol. 161). Retrieved from www.atsjournals.org

Medford, A. R. L., & Millar, A. B. (2006). Vascular endothelial growth factor (VEGF) in acute lung injury (ALI) and acute respiratory distress syndrome (ARDS): paradox or paradigm? *Thorax*, *61*(7), 621–626. https://doi.org/10.1136/thx.2005.040204

Meduri, G. U., Bridges, L., Siemieniuk, R. A. C., & Kocak, M. (2018). An Exploratory Reanalysis of the Randomized Trial on Efficacy of Corticosteroids as Rescue Therapy for the Late Phase of Acute Respiratory Distress Syndrome*. *Critical Care Medicine*, *46*(6), 884–891.

https://doi.org/10.1097/CCM.0000000000003021

Meduri, G. U., Siemieniuk, R. A. C., Ness, R. A., & Seyler, S. J. (2018). Prolonged low-dose methylprednisolone treatment is highly effective in reducing duration of mechanical ventilation and mortality in patients with ARDS. https://doi.org/10.1186/s40560-018-0321-9

Mehier-Humbert, S., Bettinger, T., Yan, F., & Guy, R. H. (2005). Plasma membrane poration induced by ultrasound exposure: Implication for drug delivery. *Journal of Controlled Release*, *104*(1), 213–222. https://doi.org/10.1016/j.jconrel.2005.01.007

Mehta, D., Konstantoulaki, M., Ahmmed, G. U., & Malik, A. B. (2005). Sphingosine 1-Phosphate-induced Mobilization of Intracellular Ca2+ Mediates Rac Activation and Adherens Junction Assembly in Endothelial Cells. *Journal of Biological Chemistry*, *280*(17), 17320–17328. https://doi.org/10.1074/JBC.M411674200

Meineri M, G. K. (2012). Lung ultrasound.

Mekontso Dessap, A., Boissier, F., Leon, R., Carreira, S., Roche Campo, F., Lemaire, F., & Brochard, L. (2010). Prevalence and prognosis of shunting across patent foramen ovale during acute respiratory distress syndrome*. *Critical Care Medicine*, *38*(9), 1786–1792. https://doi.org/10.1097/CCM.0b013e3181eaa9c8

Mercer, P. F., Williams, A. E., Scotton, C. J., José, R. J., Sulikowski, M., Moffatt, J. D., … Chambers, R. C. (2013). Proteinase-Activated Receptor-1, CCL2 and CCL7 Regulate Acute Neutrophilic Lung Inflammation. *American Journal of Respiratory Cell and Molecular Biology*, *50*(1), 130823120456000. https://doi.org/10.1165/rcmb.2013-0142OC

Millán, J., Cain, R. J., Reglero-Real, N., Bigarella, C., Marcos-Ramiro, B., Fernández-Martín, L., … Ridley, A. J. (2010). *Adherens junctions connect stress fibres between adjacent endothelial cells*. https://doi.org/10.1186/1741-7007-8-11

Millar, F. R., Summers, C., Griffiths, M. J., Toshner, M. R., Proudfoot, A. G., & Proudfoot, A. (2016). The pulmonary endothelium in acute respiratory distress syndrome: insights and therapeutic opportunities. https://doi.org/10.1136/thoraxjnl-2015-207461

Moss, M., & Mannino, D. M. (2002). Race and gender differences in acute respiratory distress syndrome deaths in the United States: an analysis of multiple-cause mortality data (1979-

1996). *Critical Care Medicine*, *30*(8), 1679–1685. Retrieved from http://www.ncbi.nlm.nih.gov/pubmed/12163776

Munita, J. M., & Arias, C. A. (2016). Mechanisms of Antibiotic Resistance. *Microbiology Spectrum*, *4*(2). https://doi.org/10.1128/microbiolspec.VMBF-0016-2015

Murray & Nadel's Textbook of Respiratory Medicine, 2-Volume Set, 6th Edition, US Elsevier Health Bookshop, 2006.

Murray, J. F., Matthay, M. A., Luce, J. M., & Flick, M. R. (1988). An Expanded Definition of the Adult Respiratory Distress Syndrome. *American Review of Respiratory Disease*, *138*(3), 720–723. https://doi.org/10.1164/ajrccm/138.3.720

Nakamura, T., Sato, E., Fujiwara, N., Kawagoe, Y., Maeda, S., & Yamagishi, S. (2011). Increased levels of soluble receptor for advanced glycation end products (sRAGE) and high mobility group box 1 (HMGB1) are associated with death in patients with acute respiratory distress syndrome. *Clinical Biochemistry*, *44*(8–9), 601–604. https://doi.org/10.1016/j.clinbiochem.2010.12.014

National Heart, Lung, and Blood Institute Acute Respiratory Distress Syndrome (ARDS) Clinical Trials Network, Matthay, M. A., Brower, R. G., Carson, S., Douglas, I. S., Eisner, M., … Thompson, B. T. (2011). Randomized, Placebo-controlled Clinical Trial of an Aerosolized β_2-Agonist for Treatment of Acute Lung Injury. *American Journal of Respiratory and Critical Care Medicine*, *184*(5), 561–568. https://doi.org/10.1164/rccm.201012-2090OC

National Heart and Lung Institutes: Respiratory diseases: task force on problems, research approaches, needs. (1972).

Nelson, T. R., Fowlkes, J. B., Abramowicz, J. S., & Church, C. C. (2009). *Ultrasound Biosafety Considerations for the Practicing Sonographer and Sonologist*. Retrieved from https://onlinelibrary.wiley.com/doi/pdf/10.7863/jum.2009.28.2.139

Nguyen, M., Benkhadra, S., Douguet, C., & Ela¨ıdela¨ıd Bouhemad, B. ´. (2016). IMAGES IN PULMONARY, CRITICAL CARE, SLEEP MEDICINE AND THE SCIENCES Real-Time Visualization of Left Lung Consolidation Relief Using Lung Ultrasound. *Am J Respir Crit Care Med*, *193*, 59–60. https://doi.org/10.1164/rccm.201601-0044IM

Nicklin, S. A., Buening, H., Dishart, K. L., de Alwis, M., Girod, A., Hacker, U., … Baker, A. H.

(2001). Efficient and Selective AAV2-Mediated Gene Transfer Directed to Human Vascular Endothelial Cells. *Molecular Therapy*, *4*(3), 174–181. https://doi.org/10.1006/mthe.2001.0424

Nomikou, N., Tiwari, P., Trehan, T., Gulati, K., & Mchale, A. P. (2011). Studies on neutral, cationic and biotinylated cationic microbubbles in enhancing ultrasound-mediated gene delivery in vitro and in vivo. *ACTA BIOMATERIALIA*. https://doi.org/10.1016/j.actbio.2011.09.010

Nozaki, T., Ogawa, R., Feril, L. B., Kagiya, G., Fuse, H., & Kondo, T. (2003). Enhancement of ultrasound-mediated gene transfection by membrane modification. *The Journal of Gene Medicine*, *5*(12), 1046–1055. https://doi.org/10.1002/jgm.445

Ognibene, F. P., Martin, S. E., Parker, M. M., Schlesinger, T., Roach, P., Burch, C., … Parrillo, J. E. (1986). Adult Respiratory Distress Syndrome in Patients with Severe Neutropenia. *New England Journal of Medicine*, *315*(9), 547–551. https://doi.org/10.1056/NEJM198608283150904

Orlova, V. V, Economopoulou, M., Lupu, F., Santoso, S., & Chavakis, T. (2006). Junctional adhesion molecule-C regulates vascular endothelial permeability by modulating VE-cadherin-mediated cell-cell contacts. *The Journal of Experimental Medicine*, *203*(12), 2703–2714. https://doi.org/10.1084/jem.20051730

Panje, C. M., Wang, D. S., Pysz, M. A., Paulmurugan, R., Ren, Y., Tranquart, F., … Willmann, J. K. (2012). Ultrasound-Mediated Gene Delivery with Cationic Versus Neutral Microbubbles: Effect of DNA and Microbubble Dose on *In Vivo* Transfection Efficiency. *Theranostics*, *2*(11), 1078–1091. https://doi.org/10.7150/thno.4240

Pelosi, P., Goldner, M., McKibben, A., Adams, A., Eccher, G., Caironi, O., … Marini, J. J. (2001). Recruitment and Derecruitment During Acute Respiratory Failure. *American Journal of Respiratory and Critical Care Medicine*, *164*(1), 122–130. https://doi.org/10.1164/ajrccm.164.1.2007010

Peruzzi, G., Sinibaldi, G., Silvani, G., Ruocco, G., & Casciola, C. M. (2018). Perspectives on cavitation enhanced endothelial layer permeability. *Colloids and Surfaces B: Biointerfaces*, *168*, 83–93. https://doi.org/10.1016/J.COLSURFB.2018.02.027

Pesenti, A., Musch, G., Lichtenstein, D., Mojoli, F., Amato, M. B. P., Cinnella, G., … Quintel, M. (2016). Imaging in acute respiratory distress syndrome. *Intensive Care Medicine*, *42*(5), 686–698. https://doi.org/10.1007/s00134-016-4328-1

Petrache, I., Birukova, A., Ramirez, S. I., Garcia, J. G. N., & Verin, A. D. (2003). The Role of the Microtubules in Tumor Necrosis Factor-α–Induced Endothelial Cell Permeability. *American Journal of Respiratory Cell and Molecular Biology*, *28*(5), 574–581. https://doi.org/10.1165/rcmb.2002-0075OC

Petrache, I., Verin, A. D., Crow, M. T., Birukova, A., Liu, F., & Garcia, J. G. N. (2001). Differential effect of MLC kinase in TNF-α-induced endothelial cell apoptosis and barrier dysfunction. *American Journal of Physiology-Lung Cellular and Molecular Physiology*, *280*(6), L1168–L1178. https://doi.org/10.1152/ajplung.2001.280.6.L1168

Piantadosi, C. A., & Schwartz, D. A. (2004). The acute respiratory distress syndrome. *Annals of Internal Medicine*, *141*(6), 460–470. Retrieved from http://www.ncbi.nlm.nih.gov/pubmed/15381520

Pichiule, P., Chavez, J. C., & LaManna, J. C. (2004). Hypoxic Regulation of Angiopoietin-2 Expression in Endothelial Cells. *Journal of Biological Chemistry*, *279*(13), 12171–12180. https://doi.org/10.1074/jbc.M305146200

Podell, S., Burrascano, C., Gaal, M., Golec, B., Maniquis, J., & Mehlhaff, P. (1999). Physical and biochemical stability of Optison, an injectable ultrasound contrast agent. *Biotechnology and Applied Biochemistry*, *30 (Pt 3)*, 213–223. Retrieved from http://www.ncbi.nlm.nih.gov/pubmed/10574690

Post, S., Heijink, I. H., Hesse, L., Koo, H. K., Shaheen, F., Fouadi, M., … Nawijn, M. C. (2018). Characterization of a lung epithelium specific E-cadherin knock-out model: Implications for obstructive lung pathology. *Scientific Reports*, *8*(1), 13275. https://doi.org/10.1038/s41598-018-31500-8

Poynter, M. E., Irvin, C. G., & Janssen-Heininger, Y. M. W. (2003). A prominent role for airway epithelial NF-kappa B activation in lipopolysaccharide-induced airway inflammation. *Journal of Immunology (Baltimore, Md. : 1950)*, *170*(12), 6257–6265. https://doi.org/10.4049/JIMMUNOL.170.12.6257

Prina, E., Ranzani, O. T., & Torres, A. (2015). Community-acquired pneumonia. *The Lancet*, *386*(9998), 1097–1108. https://doi.org/10.1016/S0140-6736(15)60733-4

Qin, P., Han, T., Yu, A. C. H., & Xu, L. (2018). Mechanistic understanding the bioeffects of ultrasound-driven microbubbles to enhance macromolecule delivery. https://doi.org/10.1016/j.jconrel.2018.01.001

Raghavendran, K., & Napolitano, L. M. (2011). Definition of ALI/ARDS. *Critical Care Clinics*, *27*(3), 429–437. https://doi.org/10.1016/j.ccc.2011.05.006

Rho, S.-S., Ando, K., & Fukuhara, S. (2017). *Dynamic Regulation of Vascular Permeability by Vascular Endothelial Cadherin-Mediated Endothelial Cell-Cell Junctions*. *J Nippon Med Sch* (Vol. 84). Retrieved from http://www2.nms.ac.jp/jnms/

Rice, T. W., Wheeler, A. P., Bernard, G. R., Hayden, D. L., Schoenfeld, D. A., Ware, L. B., & National Institutes of Health, National Heart, Lung, and Blood Institute ARDS Network. (2007). Comparison of the Sp o 2 /F io 2 Ratio and the Pa o 2 /F io 2 Ratio in Patients With Acute Lung Injury or ARDS. *Chest*, *132*(2), 410–417. https://doi.org/10.1378/chest.07-0617

Riley, R. L., & Cournand, A. (1949). *'Ideal' Alveolar Air and the Analysis of Ventilation-Perfusion Relationships in the Lungs*. *Journal of Applied Physiology*, *1*(12), 825–847. https://doi.org/10.1152/jappl.1949.1.12.825

Rokkam, D., Lafemina, M. J., Lee, J. W., Matthay, M. A., & Frank, J. A. (2011). Claudin-4 levels are associated with intact alveolar fluid clearance in human lungs. *The American Journal of Pathology*, *179*(3), 1081–1087. https://doi.org/10.1016/j.ajpath.2011.05.017

Ruan, S.-Y., Lin, H.-H., Huang, C.-T., Kuo, P.-H., Wu, H.-D., & Yu, C.-J. (2014). Exploring the heterogeneity of effects of corticosteroids on acute respiratory distress syndrome: a systematic review and meta-analysis. *Critical Care*, *18*(2), R63. https://doi.org/10.1186/cc13819

Rubenfeld, G. D., Caldwell, E., Granton, J., Hudson, L. D., & Matthay, M. A. (1999). Interobserver variability in applying a radiographic definition for ARDS. *Chest*, *116*(5), 1347–1353. Retrieved from http://www.ncbi.nlm.nih.gov/pubmed/10559098

Sagar KB, Rhyne TL, Myers GS, L. R. (1978). Characterization of normal and abnormal pulmonary surface by reflected ultrasound. *Chest*, *74*, 29–33.

Saharinen, P., Eklund, L., Miettinen, J., Wirkkala, R., Anisimov, A., Winderlich, M., … Alitalo, K. (2008). Angiopoietins assemble distinct Tie2 signalling complexes in endothelial cell–cell and cell–matrix contacts. *Nature Cell Biology*, *10*(5), 527–537. https://doi.org/10.1038/ncb1715

Sakula, A. (1981). R T H Laënnec 1781--1826 his life and work: a bicentenary appreciation. *Thorax*. https://doi.org/10.1136/thx.36.2.81

Schmitz, J., Owyang, A., Oldham, E., Song, Y., Murphy, E., McClanahan, T. K., … Kastelein, R. A. (2005). IL-33, an interleukin-1-like cytokine that signals via the IL-1 receptor-related protein ST2 and induces T helper type 2-associated cytokines. *Immunity*, *23*(5), 479–490. https://doi.org/10.1016/j.immuni.2005.09.015

Schober, A., Nazari-Jahantigh, M., Wei, Y., Bidzhekov, K., Gremse, F., Grommes, J., … Weber, C. (2014). MicroRNA-126-5p promotes endothelial proliferation and limits atherosclerosis by suppressing Dlk1. *Nature Medicine*, *20*(4), 368–376. https://doi.org/10.1038/nm.3487

Schulte, D., Küppers, V., Dartsch, N., Broermann, A., Li, H., Zarbock, A., … Vestweber, D. (2011). Stabilizing the VE-cadherin-catenin complex blocks leukocyte extravasation and vascular permeability. *The EMBO Journal*, *30*(20), 4157–4170. https://doi.org/10.1038/emboj.2011.304

Serpa Neto, A., Galvão, V., Pereira, M., Crepaldi Espósito, D., Cecília, M., Damasceno, T., & Schultz, M. J. (2012). *Neuromuscular blocking agents in patients with acute respiratory distress syndrome: a summary of the current evidence from three randomized controlled trials*. https://doi.org/10.1186/2110-5820-2-33

Sessa, R., Seano, G., di Blasio, L., Gagliardi, P. A., Isella, C., Medico, E., … Primo, L. (2012). The miR-126 regulates Angiopoietin-1 signaling and vessel maturation by targeting p85β. *Biochimica et Biophysica Acta (BBA) - Molecular Cell Research*, *1823*(10), 1925–1935. https://doi.org/10.1016/J.BBAMCR.2012.07.011

Shasby, D. M., Ries, D. R., Shasby, S. S., & Winter, M. C. (2002). Histamine stimulates phosphorylation of adherens junction proteins and alters their link to vimentin. *American Journal of Physiology-Lung Cellular and Molecular Physiology*, *282*(6), L1330–L1338. https://doi.org/10.1152/ajplung.00329.2001

Sheffield, P., Trehan, A., Boyd, B., & Wong, O. L. (2008). *Microbubbles as Ultrasound Contrast Agents and in Targeted Drug Delivery*. *Critical Reviews TM Biomedical Engineering* (Vol. 36). Retrieved from www.begellhouse.com

Shweiki, D., Itin, A., Soffer, D., & Keshet, E. (1992). Vascular endothelial growth factor induced by hypoxia may mediate hypoxia-initiated angiogenesis. *Nature*, *359*(6398), 843–845. https://doi.org/10.1038/359843a0

Smith, F. G., Perkins, G. D., Gates, S., Young, D., McAuley, D. F., Tunnicliffe, W., … BALTI-2 study investigators. (2012). Effect of intravenous β-2 agonist treatment on clinical outcomes in acute respiratory distress syndrome (BALTI-2): a multicentre, randomised controlled trial. *The Lancet*, *379*(9812), 229–235. https://doi.org/10.1016/S0140-6736(11)61623-1

Song, J., Lu, H., Zheng, X., & Huang, X. (2015). Effects of Vascular Endothelial Growth Factor in Recovery Phase of Acute Lung Injury in Mice. *Lung*, *193*(6), 1029–1036. https://doi.org/10.1007/s00408-015-9803-x

Soumelis, V., Reche, P. A., Kanzler, H., Yuan, W., Edward, G., Homey, B., … Liu, Y.-J. (2002). Human epithelial cells trigger dendritic cell–mediated allergic inflammation by producing TSLP. *Nature Immunology*, *3*(7), 673–680. https://doi.org/10.1038/ni805

Steinberg, K. P., Hudson, L. D., Goodman, R. B., Hough, C. L., Lanken, P. N., Hyzy, R., … National Heart, Lung, and Blood Institute Acute Respiratory Distress Syndrome (ARDS) Clinical Trials Network. (2006). Efficacy and Safety of Corticosteroids for Persistent Acute Respiratory Distress Syndrome. *New England Journal of Medicine*, *354*(16), 1671–1684. https://doi.org/10.1056/NEJMoa051693

Steinberg, K. P., Milberg, J. A., Martin, T. R., Maunder, R. J., Cockrill, B. A., & Hudson, L. D. (1994). Evolution of bronchoalveolar cell populations in the adult respiratory distress syndrome. *American Journal of Respiratory and Critical Care Medicine*, *150*(1), 113–122. https://doi.org/10.1164/ajrccm.150.1.8025736

Suffia, I., Reckling, S. K., Salay, G., & Belkaid, Y. (2005). A role for CD103 in the retention of CD4+CD25+ Treg and control of Leishmania major infection. *Journal of Immunology (Baltimore, Md. : 1950)*, *174*(9), 5444–5455. https://doi.org/10.4049/JIMMUNOL.174.9.5444

Sugiyama, M. G., Armstrong, S. M., Wang, C., Hwang, D., Leong-Poi, H., Advani, A., … Lee, W. L. (2015). The Tie2-agonist Vasculotide rescues mice from influenza virus infection. *Scientific Reports*, *5*(1), 11030. https://doi.org/10.1038/srep11030

Sugiyama, M. G., Gamage, A., Zyla, R., Armstrong, S. M., Advani, S., Advani, A., … Lee, W. L. (2016). Influenza Virus Infection Induces Platelet-Endothelial Adhesion Which Contributes to Lung Injury. *Journal of Virology*, *90*(4), 1812–1823. https://doi.org/10.1128/JVI.02599-15

Sugiyama, M. G., Mintsopoulos, V., Raheel, H., Goldenberg, N. M., Batt, J. E., Brochard, L., … Lee, W. L. (2018). Lung Ultrasound and Microbubbles Enhance Aminoglycoside Efficacy and Delivery to the Lung in *E. Coli* -induced Pneumonia and ARDS. *American Journal of Respiratory and Critical Care Medicine*, rccm.201711-2259LE. https://doi.org/10.1164/rccm.201711-2259LE

Sukriti, S., Tauseef, M., Yazbeck, P., & Mehta, D. (2014). Mechanisms regulating endothelial permeability. *Pulmonary Circulation*, *4*(4), 535–551. https://doi.org/10.1086/677356

Sureka, B., Bansal, K., & Arora, A. (2015). Pulmonary edema - cardiogenic or noncardiogenic? *Journal of Family Medicine and Primary Care*, *4*(2), 290. https://doi.org/10.4103/2249-4863.154684

Taddei, A., Giampietro, C., Conti, A., Orsenigo, F., Breviario, F., Pirazzoli, V., … Dejana, E. (2008). Endothelial adherens junctions control tight junctions by VE-cadherin-mediated upregulation of claudin-5. *Nature Cell Biology*, *10*(8), 923–934. https://doi.org/10.1038/ncb1752

Thakur, L., Kojicic, M., Thakur, S. J., Pieper, M. S., Kashyap, R., Trillo-Alvarez, C. A., … Gajic, O. (2009). Alcohol consumption and development of acute respiratory distress syndrome: a population-based study. *International Journal of Environmental Research and Public Health*, *6*(9), 2426–2435. https://doi.org/10.3390/ijerph6092426

Thickett, D. R., Armstrong, L., & Millar, A. B. (2002). A Role for Vascular Endothelial Growth Factor in Acute and Resolving Lung Injury. *American Journal of Respiratory and Critical Care Medicine*, *166*(10), 1332–1337. https://doi.org/10.1164/rccm.2105057

Tlaxca, J. L., Anderson, C. R., Klibanov, A. L., Lowrey, B., Hossack, J. A., Alexander, J. S., … Rychak,

J. J. (2010). Analysis of in vitro transfection by sonoporation using cationic and neutral microbubbles. *Ultrasound in Medicine & Biology*, *36*(11), 1907–1918. https://doi.org/10.1016/j.ultrasmedbio.2010.05.014

Tosi, M. F., Stark, J. M., Hamedani, A., Smith, C. W., Gruenert, D. C., & Huang, Y. T. (1992). Intercellular adhesion molecule-1 (ICAM-1)-dependent and ICAM-1-independent adhesive interactions between polymorphonuclear leukocytes and human airway epithelial cells infected with parainfluenza virus type 2. *Journal of Immunology (Baltimore, Md. : 1950)*, *149*(10), 3345–3349. Retrieved from http://www.ncbi.nlm.nih.gov/pubmed/1358969

Touw, H. R., Parlevliet, K. L., Beerepoot, M., Schober, P., Vonk, A., Twisk, J. W., … Tuinman, P. R. (2018). Lung ultrasound compared with chest X-ray in diagnosing postoperative pulmonary complications following cardiothoracic surgery: a prospective observational study. *Anaesthesia*, *73*(8), 946–954. https://doi.org/10.1111/anae.14243

Tsai, H.-C., Tsai, C.-H., Chen, W.-S., Inserra, C., Wei, K.-C., & Liu, H.-L. (2018). Safety evaluation of frequent application of microbubble-enhanced focused ultrasound blood-brain-barrier opening. *Scientific Reports*, *8*(1), 17720. https://doi.org/10.1038/s41598-018-35677-w

Ueno, H., Matsuda, T., Hashimoto, S., Amaya, F., Kitamura, Y., Tanaka, M., … Ishizaka, A. (2004). Contributions of High Mobility Group Box Protein in Experimental and Clinical Acute Lung Injury. *American Journal of Respiratory and Critical Care Medicine*, *170*(12), 1310–1316. https://doi.org/10.1164/rccm.200402-188OC

Ultrasound in Medicine and Biology. (2013). *Ultrasound in Medicine & Biology*, *39*(5), I–II. https://doi.org/10.1016/S0301-5629(13)00639-X

Umbrello, M., Formenti, P., Bolgiaghi, L., & Chiumello, D. (2016). Current Concepts of ARDS: A Narrative Review. *International Journal of Molecular Sciences*, *18*(1). https://doi.org/10.3390/ijms18010064

Uyeki, T. M., Bernstein, H. H., Bradley, J. S., Englund, J. A., File, T. M., Fry, A. M., … Pavia, A. T. (2018). Clinical Practice Guidelines by the Infectious Diseases Society of America: 2018 Update on Diagnosis, Treatment, Chemoprophylaxis, and Institutional Outbreak Management of Seasonal Influenza a I D S A G U I D E L I N E Clinical Infectious Diseases ® 2019;68(6):e1-47. *Clinical Infectious Diseases IDSA Influenza Clinical Guidelines*, *2019*, 68.

https://doi.org/10.1093/cid/ciy866

van der Flier, M., van Leeuwen, H. J., van Kessel, K. P., Kimpen, J. L., Hoepelman, A. I., & Geelen, S. P. (2005). Plasma vascular endothelial growth factor in severe sepsis. *Shock (Augusta, Ga.)*, *23*(1), 35–38. Retrieved from http://www.ncbi.nlm.nih.gov/pubmed/15614129

van Wamel, A., Kooiman, K., Harteveld, M., Emmer, M., ten Cate, F. J., Versluis, M., & de Jong, N. (2006). Vibrating microbubbles poking individual cells: Drug transfer into cells via sonoporation. *Journal of Controlled Release*, *112*(2), 149–155. https://doi.org/10.1016/J.JCONREL.2006.02.007

VanBavel, E. (2007). Effects of shear stress on endothelial cells: Possible relevance for ultrasound applications. *Progress in Biophysics and Molecular Biology*, *93*(1–3), 374–383. https://doi.org/10.1016/J.PBIOMOLBIO.2006.07.017

Venables, H. (2011). How does ultrasound work? *Ultrasound*, *19*(1), 44–49. https://doi.org/10.1258/ult.2010.010051

Venneri, M. A., Palma, M. D., Ponzoni, M., Pucci, F., Scielzo, C., Zonari, E., … Naldini, L. (2007). Identification of proangiogenic TIE2-expressing monocytes (TEMs) in human peripheral blood and cancer. *Blood*, *109*(12), 5276–5285. https://doi.org/10.1182/blood-2006-10-053504

Villar, J., Pérez-Méndez, L., & Kacmarek, R. M. (1999). Current definitions of acute lung injury and the acute respiratory distress syndrome do not reflect their true severity and outcome. *Intensive Care Medicine*, *25*(9), 930–935. Retrieved from http://www.ncbi.nlm.nih.gov/pubmed/10501747

Villar, J., Sulemanji, D., & Kacmarek, R. M. (2014). The acute respiratory distress syndrome. *Current Opinion in Critical Care*, *20*(1), 3–9. https://doi.org/10.1097/MCC.0000000000000057

Walkey, A. J., Del Sorbo, L., Hodgson, C. L., Adhikari, N. K. J., Wunsch, H., Meade, M. O., … Fan, E. (2017). Higher PEEP versus Lower PEEP Strategies for Patients with Acute Respiratory Distress Syndrome. A Systematic Review and Meta-Analysis. *Annals of the American Thoracic Society*, *14*(Supplement_4), S297–S303. https://doi.org/10.1513/AnnalsATS.201704-338OT

Wang, D. S., Panje, C., Pysz, M. A., Paulmurugan, R., Rosenberg, J., Gambhir, S. S., … Willmann, J. K. (2012). Cationic versus neutral microbubbles for ultrasound-mediated gene delivery in cancer. *Radiology*, *264*(3), 721–732. https://doi.org/10.1148/radiol.12112368

Wang, G., Ji, X., Xu, Y., & Xiang, X. (2016). Lung ultrasound: a promising tool to monitor ventilator-associated pneumonia in critically ill patients. https://doi.org/10.1186/s13054-016-1487-y

Wang, L., Tang, X., Xiang, X., Tang, Y., & Qiu, L. (2019). Experimental study of TNF-α receptor gene transfection by ultrasound-targeted microbubble destruction to treat collagen-induced arthritis in rats invivo. *Experimental and Therapeutic Medicine*, *17*(3), 1601–1610. https://doi.org/10.3892/etm.2019.7158

Wang, S., Aurora, A. B., Johnson, B. A., Qi, X., McAnally, J., Hill, J. A., … Olson, E. N. (2008). The endothelial-specific microRNA miR-126 governs vascular integrity and angiogenesis. *Developmental Cell*, *15*(2), 261–271. https://doi.org/10.1016/j.devcel.2008.07.002

Ware, L. B., Zhao, Z., Koyama, T., May, A. K., Matthay, M. A., Lurmann, F. W., … Calfee, C. S. (2016). Long-Term Ozone Exposure Increases the Risk of Developing the Acute Respiratory Distress Syndrome. *American Journal of Respiratory and Critical Care Medicine*, *193*(10), 1143–1150. https://doi.org/10.1164/rccm.201507-1418OC

Weibel, E. R. (2017). Lung morphometry: the link between structure and function. *Cell and Tissue Research*, *367*(3), 413–426. https://doi.org/10.1007/s00441-016-2541-4

Wessel, F., Winderlich, M., Holm, M., Frye, M., Rivera-Galdos, R., Vockel, M., … Vestweber, D. (2014). Leukocyte extravasation and vascular permeability are each controlled in vivo by different tyrosine residues of VE-cadherin. *Nature Immunology*, *15*(3), 223–230. https://doi.org/10.1038/ni.2824

Wever-Pinzon, O., Suma, V., Ahuja, A., Romero, J., Sareen, N., Henry, S. A., … Chaudhry, F. A. (2012). Safety of echocardiographic contrast in hospitalized patients with pulmonary hypertension: a multi-center study. *European Heart Journal Cardiovascular Imaging*, *13*(10), 857–862. https://doi.org/10.1093/ehjci/jes057

Williams, A. E., & Chambers, R. C. (2014). The mercurial nature of neutrophils: still an enigma in ARDS? *American Journal of Physiology. Lung Cellular and Molecular Physiology*, *306*(3),

L217-30. https://doi.org/10.1152/ajplung.00311.2013

Williams, A. E., José, R. J., Mercer, P. F., Brealey, D., Parekh, D., Thickett, D. R., … Chambers, R. C. (2017). Evidence for chemokine synergy during neutrophil migration in ARDS. *Thorax*, *72*(1), 66–73. https://doi.org/10.1136/thoraxjnl-2016-208597

Witzenbichler, B., Westermann, D., Knueppel, S., Schultheiss, H.-P., & Tschope, C. (2005). Protective Role of Angiopoietin-1 in Endotoxic Shock. *Circulation*, *111*(1), 97–105. https://doi.org/10.1161/01.CIR.0000151287.08202.8E

Yagi, T., & Takeichi, M. (2000). Cadherin superfamily genes: functions, genomic organization, and neurologic diversity. *Genes & Development*, *14*(10), 1169–1180. Retrieved from http://www.ncbi.nlm.nih.gov/pubmed/10817752

Ye, D., Zhang, X., Yue, Y., Raliya, R., Biswas, P., Taylor, S., … Chen, H. (2018). Focused ultrasound combined with microbubble-mediated intranasal delivery of gold nanoclusters to the brain. *Journal of Controlled Release*, *286*, 145–153. https://doi.org/10.1016/j.jconrel.2018.07.020

Zhang, Y., Jiang, G., Sauler, M., & Lee, P. J. (2013). Lung endothelial HO-1 targeting in vivo using lentiviral miRNA regulates apoptosis and autophagy during oxidant injury. *FASEB Journal : Official Publication of the Federation of American Societies for Experimental Biology*, *27*(10), 4041–4058. https://doi.org/10.1096/fj.13-231225

Zhao, R., Jiang, J., Li, H., Chen, M., Liu, R., Sun, S., … Wang, S. (2018). Phosphatidylserine-microbubble targeting-activated microglia/macrophage in inflammation combined with ultrasound for breaking through the blood–brain barrier. *Journal of Neuroinflammation*, *15*(1), 334. https://doi.org/10.1186/s12974-018-1368-1

Zhao, Y.-Z., Luo, Y.-K., Lu, C.-T., Xu, J.-F., Tang, J., Zhang, M., … Liang, H.-D. (2008). Phospholipids-based microbubbles sonoporation pore size and reseal of cell membrane cultured *in vitro*. *Journal of Drug Targeting*, *16*(1), 18–25. https://doi.org/10.1080/10611860701637792

Zhou, Y., Li, P., Goodwin, A. J., Cook, J. A., Halushka, P. V., Chang, E., & Fan, H. (2018). Exosomes from Endothelial Progenitor Cells Improve the Outcome of a Murine Model of Sepsis. *Molecular Therapy*, *26*(5), 1375–1384. https://doi.org/10.1016/j.ymthe.2018.02.020

Zhou, Y., Li, P., Goodwin, A. J., Cook, J. A., Halushka, P. V., Chang, E., … Fan, H. (2019). Exosomes from endothelial progenitor cells improve outcomes of the lipopolysaccharide-induced acute lung injury. *Critical Care*, *23*(1), 44. https://doi.org/10.1186/s13054-019-2339-3